University of Trento
University of Brescia
University of Padova
University of Trieste
University of Udine
University IUAV of Venezia

Ph.D. Student: eng. Valerio Mancini

RESPONSE OF FLUSH END-PLATE JOINTS UNDER COMBINED ACTIONS

eng. Nadia Baldassino (Tutor)
prof. eng. Riccardo Zandonini (Tutor)

April, 2012

UNIVERSITY OF TRENTO

Engineering of Civil and Mechanical Structural Systems (XXIV cycle)

Doctoral School Head: prof. Davide Bigoni

Final examination: 05/04/2012

Board of Examiners:

prof. Riccardo Zandonini	(Università degli Studi di Trento)
prof. Enrico Radi	(Università degli Studi di Modena e Reggio Emilia)
prof. Guido Magenes	(Università degli Studi di Pavia)
prof. Jan-Willem G. van de Kuilen	(Technische Universität München)

SUMMARY

In this work, aspects concerning the behaviour of steel joints under combined actions are investigated. Adopting the philosophy of the component method the attention focused on the analysis of a basic component of the connection: the T-stub. Research works carried out in the recent past extensively investigated the T-stub response under tension, while no data are available for the T-stub's response under combined tension (N) and shear force (V). In the thesis experimental, numerical and theoretical studies on this topic are presented.

The starting point is the experimental activity carried out at University of Trento on column T-stubs under different combinations of axial and shear force. The experimental outcomes strongly highlighted the influence of the loading conditions on the strength and deformation capacity of the T-stub. In a second phase 3D numerical models were developed and calibrated to reproduce the actual behaviour of the T-stubs. The numerical simulations were then extended to different specimen geometries to investigate the main geometrical parameters which could affect the T-stub response.

On the basis of experimental and numerical data a theoretical model based on limit analysis was then developed. It allows predicting a simplified load-displacement curve of the T-stub under a generic combination of N and V. The results obtained from the analytical model seem to reproduce with sufficient accuracy the complex behaviour of the T-stub, allowing to appraise the elastic stiffness and the yield load.

SOMMARIO

Nel presente lavoro viene analizzato il comportamento di giunti in acciaio soggetti a stati di sollecitazione composti. Adottando la filosofia del metodo per componenti l'attenzione si focalizza sull'analisi di una componente base della connessione: il T-stub. Studi e ricerche svolti nel recente passato si sono ampiamente occupati della risposta del T-stub in trazione, mentre non sono disponibili dati riguardo il comportamento del T-stub nel caso di azioni combinate di trazione (N) e taglio (V). Relativamente a quest'ultimo argomento nella tesi vengono presentati studi di carattere sperimentale, numerico ed analitico.

Il punto di partenza è l'attività sperimentale svolta presso l'Università di Trento su T-stub della colonna soggetti a diverse combinazioni di sforzo assiale e taglio. I risultati sperimentali hanno chiaramente evidenziato come la condizione di carico influenzi pesantemente sia la resistenza cha la capacità deformativa del T-stub. In una seconda fase sono stati sviluppati e calibrati modelli numerici 3D che hanno consentito di riprodurre l'effettivo comportamento dei T-stub. Le simulazioni numeriche sono poi state estese a campioni con diverse geometrie al fine di investigare quali siano i parametri che maggiormente influenzano la risposta dei T-stub.

Sulla base dei dati sperimentali e numerici è stato infine sviluppato un modello teorico basato sull'analisi limite. Il modello consente di stimare, seppur in via approssimata, la curva carico-spostamento del T-stub per una qualsiasi combinazione di N e V. I risultati ottenuti dal modello analitico sembrano riprodurre con sufficiente accuratezza il complesso comportamento del T-stub, consentendo di stimare la rigidezza elastica ed il carico associato allo snervamento del T-stub.

Doctoral School Head	Tutor	Tutor
prof. Davide Bigoni	*ing. Nadia Baldassino*	*prof. Riccardo Zandonini*

CONTENTS

NOTATIONS

In the document if not differently specified the following symbols are used:

P_f	probability of failure
M	bending moment acting on a joint
Φ	joint rotation
S_j	joint rotational stiffness
$S_{j,ini}$	initial joint rotational stiffness
k_i	elastic stiffness of a joint component
E	modulus of elasticity
E_b	bolts modulus of elasticity
$M_{j,Ed}$	joint design bending moment
$M_{j,Rd}$	joint design bending resistance
$F_{tr,Rd}$	design tension resistance per bolt row
B	bolt force
$B_{t,Rd}$	design bolt tension resistance
Bu	ultimate tensile load of a bolt
f_y	steel yield strength
f_u	steel ultimate strength
Q	prying force
M_{pl}	negative plastic moment (plastic hinge at the web line)
M'_{pl}	positive plastic moment (plastic hinge at the bolt line)
m_{pl}	plastic moment per unit length of a steel plate
t	flange thickness
m	distance from the location of M_{pl} to the bolt line
n	distance from the location of Q to the bolt line
L_{eff}	effective length of a T-stub

F	force acting on a T-stub
φ	inclination of the applied load F
N	axial component of F
V	shear component of F
ΔF	work associated to the external tensile load
ΔE	internal energy dissipation in a T-stub flange
ΔE_i	energy dissipated in a yield line
δ_v	transverse displacement of T-stub flange
n_i	axial force per unit length on a yield line
n_{Rd}	axial resistance per unit length of a steel plate

1. INTRODUCTION

1.1 Purpose of this study

The spreading of a localized damage in a structure can lead to its progressive collapse. Considering the strategies proposed by different standards it is clear that one crucial way to inhibit the progressive collapse is the design of redundant structures with sufficient ductile behaviour allowing deformations when local failures occur. Redundancy can be achieved by permitting force redistribution within the structural system. Therefore, members and joints have to be especially designed and optimised. However, the design codes currently adopted in different States (Great Britain, Italy, United States, Canada, etc.) in general do not provide detailed rules for the practical design of structural elements and connections against progressive collapse. Hence, further design guidance are needed in this area.

The aim of the present project is to define general requirements for ductile joints as part of a structural system subjected to exceptional unforeseen loading. By considering the simple case of the loss of a column due to accidental actions, the structure can experience redistribution of internal forces, large displacements and development of catenary actions. These events significantly affect the joints. Before the event, joints are subject mainly to bending moment and shear force. As soon as the column collapses, if the structural members and the connections posses adequate levels of strength and ductility, catenary action can develop in the floor system allowing the transfer to the rest of the structure of the axial load in the column located just over the lost one. This induces a tensile axial force in the beam. If the beams or the joints reach their full plastic resistance under combined internal forces, the response evolves with the activation of large inelastic displacements, resulting in an increment of the axial load and a decrement of the bending moment. At the end of the process internal forces in the beams and the joints are substantially different from the initial ones with the

prevalence of axial force. Assuming the joints being the weakest components, robustness implies that they should possess adequate ductility to allow for large displacements and resistance under different combinations of axial, shear force and bending moment. This allow the redistribution of the internal forces needed to reach the new equilibrium condition.
The developed research activity focused on the behaviour of steel bolted semi-rigid joints in the domain of large displacements. The case of combined action is considered. Joint ductility under combined action is one of the key issues to be mastered in order to develop reliable approaches for the design of robust structures.

1.2 Objectives

To better understand how a connection behave under a general loading condition which comprises bending moment, axial and shear forces the basic principles of the component method implemented in the EN 1993-1-8 [41] were adopted. This approach allows appraising the joint behaviour from the response of its elementary components, able to reproduce the complex connection behaviour. In case of bolted beam-to-column connections the response of the tension zone of the joint is modelled through equivalent T-stub elements.
The main objective was to obtain a simplified force-displacement relationship for the T-stub component able to take into account also the effect of the shear force which is disregarded in the current EN 1993-1-8 [41] approach. The study was performed from experimental, numerical and analytical points of view. Experimental tests were performed on T-stub elements under different combinations of axial and shear force in order to evaluate the influence of shear force on the collapse load and on the development of flange mechanisms. On the basis of the experimental results numerical and analytical models have been developed in order to reproduce, as close as possible, the behaviour of T-stubs under different loading conditions. The analytical model will be useful to understand if the component method, which considers only the case of joint in bending, could be extended also to a more general loading condition.

1.3 Thesis outline

The thesis consists of 8 chapters. The first chapter gives a general description of the research topic, the scope and the objectives of the thesis. The second chapter

introduces the prescriptions given by the European codes about structural design against accidental actions. In chapter three are present different methods available in literature to predict the behaviour of beam-to-column connections in bending and under combined bending and axial force. The fourth chapter describes the case of study, summarizing the outcomes of an European research project on robust structures. Additionally the results of experimental tests on T-stub elements subjected to different combination of axial (N) and shear force (V) are analyzed and discussed. In chapter five the numerical models of the T-stubs developed on the basis of the experimental results are presented. The results obtained from the numerical simulation are then compared with the experimental data. In the sixth chapter starting from the theoretical model based on the limit analysis for the prediction of the yield load of a T-stub under pure tension a new model is proposed. Adopting a similar approach the new formulation allows to predict the yield load also for T-stubs under combined axial and shear force. To validate the effectiveness of the proposed theoretical formulation in chapter seven parametrical analyses are performed changing the geometrical properties of the specimens. In chapter eight are summarized the main results of the presented work and possible developments are proposed.

2. STRUCTURAL ROBUSTNESS

2.1 Concept of robustness

Starting from the collapse of Ronan Point Building (London, 1968), in Europe, and especially in Great Britain, new design guidelines were developed to avoid progressive collapse of structures due to local damages. Recent events like the terrorist attacks at the Alfred P. Murrah Building (Oklahoma City, 1995) and the World Trade Centre (New York, 2001) highlighted once more the inadequacy of the traditional design rules in case of accidental actions. The English experience [1] together with the American one [2] and several research projects around the world led the design standards' approach to a new philosophy, in which a new safety requirement is considered: the structural robustness.

Figure 2.1 - Ronan Point Building and Alfred P. Murrah Building collapses

The concept of “robustness” is associated to the structural behaviour in case of accidental actions [3]. If the structure is not robust, localized failures caused by accidental actions can activate the so called progressive collapse, a sort of chain reaction which could result in the partial or total collapse of the structure. Therefore a structure is defined "robust" when the accidental actions result in damages not disproportioned to the event which caused them [3]. The aim of designing robust structures is hence not to prevent damages to structural elements but to limit the extent of failure which should remain localized in specific areas avoiding the spreading to the rest of the structure. In other words, design a structure that allows no damages may result in an extremely high complexity and consequently enormous realization costs.

2.2 Background of the design codes

2.2.1 British approach

Following the recommendations of the official inquiry after the gas explosion at the Ronan Point Building, in Great Britain the concept of robust structure was introduced in building design standards. This was initially issued through Circulars of the Ministry of Housing and Local Government in 1968 and later in 1970 by the Fifth Amendment to the Building Regulations [4]. These requirements were developed with respect to the hazard of an internal gas explosion for buildings with more than five storeys but they were also considered to be able to offer a minimum safety level against other accidental actions. In 1976 the Approved Document A [5] introduced general guidelines to achieve structural robustness, suggesting three different strategies to ensure a minimum structural safety level against accidental loading conditions. As first option it recommended the realization of horizontal and vertical ties between structural elements to allow the activation of alternative load path. When tying was not possible bridging represented a valid alternative, so the structure should be designed to bridge over a loss of an untied member. The last method, when also bridging was not applicable, consisted in the design and protection of key elements, defined as those structural members upon which depends the stability of the rest of the structure. In the following years these strategies were developed leading to the last version of the Approved Document A published in 2004 [1]. The methods for avoiding disproportionate collapse (tying, bridging and key element design) have also been included in various British

Standard Material Codes which nowadays provide a number of alternative or mixed solutions.

2.2.2 American approach

In the United States the general notions of global structural integrity were briefly introduced in 1972 in the ANSI A.58.1 document [6], published in a revised and extended version in 1982. The most significant improvement in the latter version of ANSI A.58.1 [7] was a more appropriate definition of structural integrity and the introduction of two different design approaches to achieve robustness. The first called "direct design", which considered explicit conditions for analysis, the second called "indirect design" which included implicit considerations aimed to avoid the progressive collapse through the provision of minimum levels of strength, continuity, and ductility. In the following years these guidelines were transposed into the so called ASCE-7/ANSI A.58 document without substantial changes from the previous versions. Only the versions of the document published after 2001 were deeply revised in order to collect the more advanced information and design strategies developed in the last years (redundancy, tying, compartmentalization, ductile detailing, development of catenary action in floor systems, load bearing interior partitions, different directions of spans in floor slabs, etc.). The reason of these improvements in the ASCE 7-02 [8] edition was related to the tragic events of 11th September 2001. These events highlighted the increased hazards associated to terrorism and the need to consider also this aspect that may not have been considered significant in the past, for a robust structural design. Numerous investigations and research projects on progressive collapse were carried out in the recent years leading to the publishing of a wide number of documents not only by researchers but also by regulatory authorities (ASCE [8], [2], DoD [9], [10], GSA [11], ISC [12], etc.).

2.2.3 Canadian approach

The National Building Code of Canada is among the codes that introduced the concept of progressive collapse several years ago. In the 1975 edition [13] structural integrity was assumed to be a basic requirement of the design process. To avoid progressive collapse buildings and other structural systems had to fulfil specific requirements which

were not requested for usual design situations. Structural integrity, strength or other defences against hazards associated with progressive collapse due to local failure caused by severe overloads or abnormal loads, had to reduce failure probability to a level commensurate with good engineering practice. The code provided also various preventive design requirements such as ductility in connections, design to prevent individual structural elements from being removed by an abnormal event and establishment of alternative load paths. The 1977 edition [14] gives some principles aimed mainly to the limitation of the spread of the damaged area. An attempt was done to quantify a limit of the damage spreading, identifying approximately an allowable damaged area which extents one storey above and below the location of the abnormal event and horizontally between the immediately adjacent load-carrying elements. In the 1980 edition [15] no direct references to the prevention of progressive collapse were adopted, only general principles were given. Furthermore, no design details were established, contrarily to previous editions. All the later editions, including the current one published in 1995 [16], comprise structural integrity in the design requirements. However, the enforce version is less specific, and more general in its approach to regulating design to prevent progressive collapse. It simply defines structural integrity as “the ability of the structure to absorb local failure without widespread collapse". It also assumes that structures designed in accordance with the prescriptions for normal design situations possess an adequate degree of structural integrity, achieved generally through detailing requirements. However, the code defines specific circumstances in which additional evaluations are required (medium/high rise building systems made of components of different materials, whose interconnection is not covered by design standards, buildings outside the scope of the code, and buildings exposed to severe accidental loads such as vehicle impact or explosion).

2.2.4 Italian approach

In Italy only in recent years the concept of robust structural design has been introduced with the D.M. 14/01/2008 [17]. The general principles about robustness are very similar to the ones proposed by the EN 1991-1-7 [3], even if not so detailed as in the European code. The accidental actions described in the D.M. 14/01/2008 [17] comprise fire, explosions and impacts. From an operative point of view the Italian code suggests to verify the robustness of a structure introducing in the design conventional nominal

actions in addition to other loads acting on the structure. The conventional actions are represented by two forces with a magnitude of 1% of the other applied loads. These forces have to be applied horizontally along two perpendicular directions, in order to check the global structural response. Otherwise, specific damage scenarios have to be analyzed in order to ensure adequate safety levels. In these analyses depending on the materials adopted in the design of the structures specific values of the materials partial safety factors are suggested. The D.M. 14/01/2008 [17] provides also specific simplified load models to simulate the effects of the different accidental actions. However, joints and members design rules prescribed for normal design situations are considered in general able to fulfil robustness requirements and no detailing prescription are given for robust design.

2.2.5 The Eurocodes

Studies and design standards on progressive collapse developed in Great Britain represented the basis for the developing of several design codes that are currently in use. Among them in the European Community this issue is covered also by EN 1991-1-7 [3], which provides basic principles for achieving robustness. Despite EN 1991-1-7 [3] and the Approved Document A [1] adopt the same approach, the European standard offers wider information about the accidental actions and the related structural analysis methods. In September 2004, CEN TC250 Subcommittee approved the first draft of prEN 1991-1-7 "Accidental Actions". The draft after few improvements have been transposed into the final version and receipted by the European member states in 2006. EN 1991-1-7 [3] deals mainly with impacts and explosions, fire and earthquake are covered in specific parts of the Eurocodes system. The document gives also general rules to deal with identified and unidentified accidental actions with proper analysis methods. These aspects will be discussed in detail in the next paragraph.

2.3 Design strategies in EN1991-1-7

The code describes the principles and application rules for the assessment of accidental actions on buildings and bridges. The basic principle is that a local damage is acceptable, provided that it will not endanger the structure and that the overall load-bearing capacity is maintained during an appropriate length of time to allow necessary

emergency measures to be taken [3]. In order to reduce the risk of disproportioned collapse different strategies are proposed like prevention of actions, physical protection of the structure and provision of sufficient structural redundancy and ductility.
In the following the approaches proposed by EN 1991-1-7 [3] to evaluate the accidental action and adopt adequate analysis methods to ensure a sufficient safety level against them are presented.

2.3.1 Accidental Actions

EN 1990 [18] defines an accidental action as: "an action, usually of short duration but of significant magnitude that is unlikely to occur on a given structure during the design working life". Typical examples are earthquakes, fires, explosions, impacts, floods, landslides, extreme climatic actions etc. These are classified as “identified” accidental actions, but damages can be caused also by a variety of not identifiable reasons like human errors, improper use of the structure, exposure to aggressive agents and terrorist attacks.
The general principles about safety against accidental actions given by EN 1991-1-7 [3] refer to the same basic design requirements provided by EN 1990 [18]. It states that a structure should be designed and executed in such a way that it will not be damaged by events such as explosions, impacts and the consequences of human errors to an extent disproportionate to the original causes. This means to limit the failure probability of the structure to an acceptable level adopting appropriate measures that should be economically acceptable.
To reduce the susceptibility to progressive collapse it is possible in general to identify three different operative levels:

- events control;
- direct design methods;
- indirect design methods.

The event control provides measures to prevent or reduce the entity of the action or its probability of occurrence to acceptable levels. This method is used when it is not possible to limit the damage due to the characteristics of the accidental action. This method not necessarily involves directly the properties of the structure, it could be applied for example by preventive measures like regular inspections, structural maintenance, etc. Direct methods are based on strength checks of structural elements

(members, connections, etc.) against accidental actions and on the ability of the structure to transfer loads after the “removal” of specific structural elements. In other words they are based on the redundancy of the structure and its capability to activate alternative load paths. Indirect methods operate in terms of inhibition of progressive collapse assuring minimum levels of strength, ductility and structural continuity through the realization of structures with low sensitivity to damages and adequate requirements of local resistance.

2.3.1.1 Consequence classes

A key issue in structural engineering is to define when is necessary to take into account also accidental action in the design process. An useful parameter is the estimation of the consequences that the collapse of the structure or of a part of it induces on the society (casualties, economic losses, damage to the environment, etc.).
EN 1991-1-7 [3], accordingly with EN 1990 [18], classifies the structures in three “consequences classes” (Table 2.1), depending on whether they are characterized by low (class CC1), medium (class CC2) or high consequences (class CC3).

Consequences class	**Description**	**Examples of buildings and civil engineering works**
CC1	Low consequence for loss of human life, *and* economic, social or environmental consequences small or negligible	Agricultural buildings where people do not normally enter (e.g. storage buildings), greenhouses
CC2	Medium consequence for loss of human life, economic, social or environmental consequences considerable	Residential and office buildings, public buildings where consequences of failure are medium (e.g. an office building)
CC3	High consequence for loss of human life, or economic, social or environmental consequences very great	Grandstands, public buildings where consequences of failure are high (e.g. a concert hall)

Table 2.1 - Consequence classes [18]

To each class are associated different types of buildings, with specific destination of use, building dimensions (number of storey, area of each floor), specific analysis

methods and differentiated prevention strategies (Table 2.2). They are subdivided in two different categories: structural strategies (design of structure and its elements for adequate strength levels, alternative load paths, etc.) and non-structural strategies (reduction of probability of occurrence of the action, of its magnitude, of the consequences of a collapse, etc.).

Consequences class	Example of categorization of building type and occupancy
CC1	Single occupancy houses not exceeding 4 storeys. Agricultural buildings. Buildings into which people rarely go, provided no part of the building is closer to another building, or area where people do go, than a distance of 1.5 times the building height.
CC2a Lower Risk Group	5 storey single occupancy houses. Hotels not exceeding 4 storeys. Flats, apartments and other residential buildings not exceeding 4 storeys. Offices not exceeding 4 storeys. Industrial buildings not exceeding 3 storeys. Retailing premises not exceeding 3 storeys of less than 1000 m² floor area in each storey. Single storey educational buildings. All buildings not exceeding two storeys to which the public are admitted and which contain floor areas not exceeding 2000 m² at each storey.
CC2b Upper Risk Group	Hotels, flats, apartments and other residential buildings greater than 4 storeys but not exceeding 15 storeys. Educational buildings greater than single storey but not exceeding 15 storeys. Retailing premises greater than 3 storeys but not exceeding 15 storeys. Hospitals not exceeding 3 storeys. Offices greater than 4 storeys but not exceeding 15 storeys. All buildings to which the public are admitted and which contain floor areas exceeding 2000 m² but not exceeding 5000 m² at each storey. Car parking not exceeding 6 storeys.
CC3	All buildings defined above as Class 2 Lower and Upper Consequences Class that exceed the limits on area and/or number of storeys. All buildings to which members of the public are admitted in significant numbers. Stadia accommodating more than 5000 spectators. Buildings containing hazardous substances and /or processes.

Table 2.2 - Categorization of consequences classes [3]

2.3.1.2 Analysis methods

Different analysis methods are defined on the basis of the consequences classes and the properties of the accidental action. For each consequences class EN 1991-1-7 [3] provides that:

- for CC1 no specific consideration is necessary for accidental actions except to ensure that the robustness and stability rules given in the Eurocodes are met;
- for CC2, depending upon the specific circumstances of the structure, a simplified analysis by static equivalent action models may be adopted or prescriptive design/detailing rules may be applied;
- for CC3 an examination of the specific case should be carried out to determine the level of reliability and the complexity of structural analyses required. This may need a risk analysis to be carried out and the use of refined methods such as dynamic analyses, non-linear models and interaction between the load and the structure.

2.3.1.3 Risk mitigation measures

Non-structural strategies are essentially based on the events control. This could be carried out by preventive measures with the main aim to allow the evacuation of the damaged structure.

To mitigate the risk related to the occurrence of the accidental action, together with the already mentioned strategies (inspection and maintenance of the structure), EN 1991-1-7 [3] suggests to operate as in the following:

- elimination or reduction of the hazard for example by, making an adequate design, modifying the design concept and providing the countermeasures to mitigate the hazard, etc.;
- by-passing the hazard by changing the design concepts or occupancy, for example through the protection of the structure, provision of sprinkler system, etc.
- controlling the hazard, for example, by controlled checks, warning systems or monitoring.

Otherwise it is possible to:

- overcome the hazard by providing, for example, increased reserves of strength or robustness, availability of alternative load paths through structural redundancy, or resistance to degradation, etc.;
- allowing controlled collapse of a structure where the probability of injury may be reduced, for example for impact on lighting columns or signal posts.

2.3.1.4 Structural measures

Together with the analysis method EN 1991-1-7 [3] defines for each consequence class also different risk mitigation strategies. They can provide simple design prescriptions or specific strength requirements. In detail:

- for CC1: building has to be designed and constructed in accordance with the rules given in the Eurocodes for satisfying stability in normal use, no further specific consideration is necessary with regard to accidental actions from unidentified causes.
- for CC2a: in addition to the recommended strategies for CC1, the provision of effective horizontal ties, or effective anchorage of suspended floors to walls, respectively for framed and load-bearing wall construction should be provided.
- for CC2b: in addition to the recommended strategies for CC1, the provision of horizontal ties together with vertical ties in all supporting columns and walls should be provided. Alternatively the building should be checked to ensure that upon the notional removal of each supporting column and each beam supporting a column, or any nominal section of load-bearing wall the building remains stable and that any local damage does not exceed a certain limit. Where the notional removal of such columns and sections of walls would result in an extent of damage in excess of the agreed limit, or other specified limits, then such elements should be designed as a "key element". In the case of buildings of load-bearing wall construction, the notional removal of a section of wall, one at a time, is likely to be the most practical strategy to adopt.
- for CC3: systematic risk assessment of the building should be undertaken accounting for both foreseeable and unforeseeable hazards.

From the design point of view it is important to underline that specific design criteria are given only for CC2a and CC2b. The aim of those prescriptions is to ensure a minimum strength level of the structure, allowing the activation of alternative load paths in case of sudden collapse of a column. For CC3 only possible strategies to develop for each specific case depending on the considered problem are given. For this class risk analyses should be carried out at a qualitative or, if the relevance of the problem is high, at quantitative level. In the qualitative risk analysis all the hazards and the corresponding scenarios should be identified. The identification of hazards and hazard scenarios is a crucial task to perform a risk analysis. It requires a detailed examination

and understanding of the problem. In the quantitative risk analysis probabilities should be estimated for all undesired events and their subsequent consequences. The probability estimations are usually at least partly based on judgement and may for that reason differ substantially from actual failure frequencies. If failure can be expressed numerically the risk may be presented as the mathematical expectation of the consequences of an undesired event.

2.3.1.5 Choice of the design strategy with respect to action type

An alternative to the classification of the design strategies by consequences classes is the one based on the type of action (Figure 2.2). The accidental actions are subdivided in identified and unidentified (if it is no possible to foresee all possible hazard scenarios).

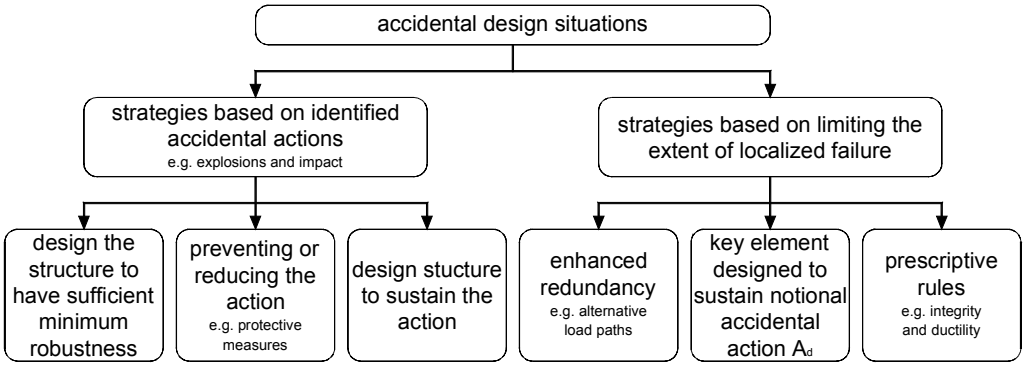

Figure 2.2 - Strategies for Accidental Design Situations

Identified actions are defined considering their occurrence probability, their consequences, the possible preventive measures that could be adopted and the definition of acceptable risk. As briefly introduced in paragraph 2.2.5, EN 1991-1-7 [3] considers as identified actions impacts and explosion, for fire and heartquake (that are also considered as identified actions) the code refers to the relative prescriptions and design rules given by the other Eurocodes.
Both for impact and explosions the code proposes reference values of accidental loads, models for representing them and risk analysis methods.

2.3.1.6 Strategies against identified actions

The proposed measures to mitigate the risk of accidental actions include one or more of the following strategies:

- preventing the action from occurring (e.g., in the case of bridges, by providing adequate clearances between the trafficked lanes and the structure) or reducing the probability and/or magnitude of the action to an acceptable level through the structural design process (e.g., in the case of buildings providing sacrificial venting components with low mass and strength to reduce the effect of explosions);
- protecting the structure against the effects of an accidental action by reducing the effects of the action on the structure (e.g. by protective bollards or safety barriers);
- ensuring that the structure has sufficient robustness by adopting one or more of the following approaches:
    - by designing certain components of the structure upon which stability depends as key elements to increase the likelihood of the structure's survival following an accidental event;
    - designing structural members, and selecting materials, to have sufficient ductility to absorb significant strain energy without rupture;
    - incorporating sufficient redundancy in the structure to facilitate the transfer of actions to alternative load paths in case of an accidental event.

2.3.1.7 Strategies against unidentified actions

Strategies based on unidentified accidental actions cover a wide range of possible events and are related to strategies based on limiting the extent of localised failure. The risk mitigation should be achieved by adopting one or more of the following approaches:

- designing key elements, on which the stability of the structure depends, to sustain the effects of a model of accidental action A_d;
- designing the structure so that in the case of a localised failure (e.g. failure of a single member) the stability of the whole structure or of a significant part of it would not be endangered;

- applying prescriptive design/detailing rules providing acceptable robustness for the structure (e.g. three-dimensional tying for additional integrity, or a minimum level of ductility of structural members subject to impact).

2.4 Reliability differentiation

2.4.1 Differentiation by β values

Once established the consequence class (CC) of a structure (Table 2.3), it is possible to relate it to a reliability class (RC), identified by the reliability index β. Consequence classes CC1, CC2 and CC3 are hence associated with reliability classes RC1, RC2 and RC3 respectively.

Frequency of use	**Consequence of failure**		
	Low	**Medium**	**High**
Low	CC1	CC2	CC3
Medium	CC2	CC2	CC3
High	Not applicable	CC3	CC3

Table 2.3 - Consequence classes matrix

The reliability index β is a function of the probability of failure P_f, as shown in Table 2.4.

$\mathbf{P_f}$	10^{-1}	10^{-2}	10^{-3}	10^{-4}	10^{-5}	10^{-6}	10^{-7}
β	1.28	2.32	3.09	3.72	4.27	4.75	5.20

Table 2.4 - β-P_f relationship

In Table 2.5 the relationships between the consequence classes, the reliability classes and the minimum recommended (target) values of β for different limit states are summarized.

The design of a structure performed with the partial factors given in the Eurocodes is generally expected to result in a structure with a β value greater than 3.8 for a 50 year reference period at ultimate limit states and greater than 1.5 at serviceability limit states (which correspond to CC2 or RC2).

The probability of failure and its corresponding β index are only notional values that do not necessarily represent actual failure rates (which depend mainly on human errors). They are used as operational values for code calibration purposes and comparison of reliability levels of structures [19].
The determination of β is a very complex topic, due to the need to relate it with actual data about actions and resistances.

Consequence class	Reliability class	Values for β			
		Ultimate limit states		Serviceability limit states	
		1 year reference period	50 year reference period	1 year reference period	50 year reference period
CC3	RC3	5.2	4.3	2.9	1.5
CC2	RC2	4.7	3.8		
CC1	RC1	4.2	3.3		

Table 2.5 - Consequence classes, reliability classes and reliability index β

These values in general show a significant dispersion depending from the variability both of the magnitude of the actions and the values of resistances. A comparable scatter would probably be found using the Eurocodes models. This is due to the fact that all codified models are unavoidably approximate in order to simplify the design in the most common cases and be more or less appropriate for each particular case [19].

2.4.2 Differentiation by measures relating to partial factors

An alternative way to achieve the reliability evaluation is by distinguishing classes of γ_F factors to be used in fundamental combinations for persistent design situations. This approach provides a multiplication factor K_{FI} to be applied to the partial factors of unfavourable actions (Table 2.6). The value of K_{FI} depends from the reliability class of the structure.

K_{FI} factors for actions	Reliability class		
	RC1	RC2	RC3
K_{FI}	0.9	1.0	1.1

Table 2.6 - K_{FI} factors for actions

Often, especially for CC3 (or RC3) instead of applying the K_{FI} factor it is normally preferable to apply alternative measures as higher levels of quality control.
Reliability differentiation can be also applied to the partial factors on resistance γ_M. However, this method is not normally used.

3. JOINTS IN STRUCTURAL ANALYSIS

The aim of structural analysis is to evaluate the behaviour (in terms of stresses, deformations, resultant forces, displacements, etc.) of structures under certain loads and boundary conditions. From the structural analysis results is possible to check if the designed structure fulfil in an adequate way all the requirements prescribed by the design standards.

As explained in the previous chapter a correct evaluation of the effects E of the actions, whom a structural system is subjected to, is directly related to an accurate appraisal of its reliability level. Furthermore, a realistic evaluation of the structure resistance against failure conditions can be reached only by analyses that take into account its real behaviour. The correct representation of the response of joints plays a fundamental role in the evaluation of the actual behaviour of a structure. Conventional analysis of steel frames assumes simplified models of joints like fully rigid or ideally pinned connections. The first hypothesis implies that the no rotations occurs within the connection, resulting in the assumption that the rotational stiffness of the joint tends to infinity. Otherwise, the second hypothesis results in the condition that no moment is transmitted and hence joint rotational stiffness tends to zero. These two idealized models are widely used in the design of several types of structures but they not always allow to have a suitable evaluation of the frame response.

The most types of connections behave between the two extremes: this induce, in some cases, to model the behaviour of the joint as a semi-rigid one. Several experimental tests have demonstrated that connections are in general in an intermediate level between rigid and ideally pinned conditions. This means that the joints exhibit a finite degree of flexibility. Moreover, they have a nonlinear behaviour that can be one of the most significant sources of nonlinearity in the structural behaviour both under static or dynamic loading conditions. Therefore, an accurate modelling of the joints behaviour in steel framed structures allow to have a better prediction of their overall response

(distribution of internal actions, stability of the members, etc.) with obviously a more accurate evaluation of the structural reliability level. This is the reason why the interest for understanding (and introduce in structural analysis) the actual behaviour of connections assumes a key role.
From robustness point of view, the design strategies against progressive collapse are frequently based on the development of alternative load paths. This doesn't mean that only structural member should be designed very carefully but also the connections between them. Especially the beam-to-column ones are fundamental to inhibit the spreading of a local damage. A good connections design should ensure not only a reserve of strength but also sufficient ductility to allow the structure to reach a new equilibrium condition without fail.

3.1 Beam-to-column joints in bending

Several research projects were carried out adopting different approaches leading to the development of a wide number of methodologies to analyze and define prediction methods of joints behaviour in term of moment-rotation curve (M-Φ). In the next pages some of these methods are briefly discussed.

3.1.1 Connection data bases

An efficient prediction of the joint flexural response is not easy to perform. Several researchers in the last decades worked on different prediction methods of beam-to-column connections M-Φ curves. Among the first approaches to the problem there was the experimental one, with the aim to build a sort of database to help researchers and designers to understand the actual behaviour of the connections.
In 1917, Wilson and Moore [20] were among the firsts to carry out full scale experimental tests on steel riveted connections to assess mainly their stiffness. The results were summarized graphically by M-Φ curves.
Further series of experimental and analytical researches followed in order to increase the knowledge about the behaviour of different type of joints. In the following years by means of the experimental results available in the literature, Jones et al. [21] reviewed and collected a total of 323 tests from 29 separate studies. Nethercot [22] examined and evaluated more than 800 individual tests from open literature, including 12 different

types of beam-to-column connections. In the 80's Goverdhan [23] collected a total of 230 experimental M-Φ curves and digitalized them to form a database of connections' behaviour. Kishi and Chen [24], [25] extended Goverdhan's work to a total of 303 tests and created a computerized data bank system.
The experimental evidence showed that the M-Φ curve were always strongly non linear. From the collected data it was clear that it was impossible to get experimental characterization curves for the entire range of possible connection types. Furthermore, experimental characterization was a possible strategy only for research purposes but not for design practice. The need to analytically describe the joint response became essential.

3.1.2 Analytical models

From the analytical point of view a great work was done by numerous researchers. The availability in the literature of test results databases for different types of connections led progressively to develop mathematical tools aimed at predicting the joints M-Φ relationship. The response of the connection were evaluated on the basis of the geometrical and mechanical joint properties.
These methods can be subdivided into four main classes: linear models, polynomial models, power models and exponential models. In the following a brief overview of the different methods is presented.

3.1.2.1 Linear models

Rathbun [26] was among the first to propose an analytical approach to the connection modelling. Starting from several experimental test on riveted connections he introduced the concept of semirigid behaviour of joints in frame analysis. Rathbun's linear model through a calibration process based on experimental evidence, represented the connection behaviour by the initial rotational stiffness S_i for the whole range of loading:

$$S_j = \frac{M}{\Phi} \tag{3.1}$$

where:

- M is the applied moment;
- Φ is the relative rotation between the beam and the column.

A very similar approach was adopted by Monforton and Wu [27]. They modified frame members stiffness matrices to take into account the connections' linear behaviour. It is clear that these simplified models were very simple to use but they were not applicable to describe the post-yielding behaviour of the connection.

Together with simple linear model proposed by Rathbun and Monforton and Wu, different improvements and alternative formulations were proposed. The limit of the linear model, which is not able to represent the plastic joint behaviour, were solved by approximating the M-Φ curve with bilinear models (Figure 3.1 - b). This allowed to obtain a better estimation of the joint behaviour without increasing in a disproportionate way the complexity of the model. Keeping in mind this philosophy additional formulations led to obtain multilinear models (Figure 3.1 - c).

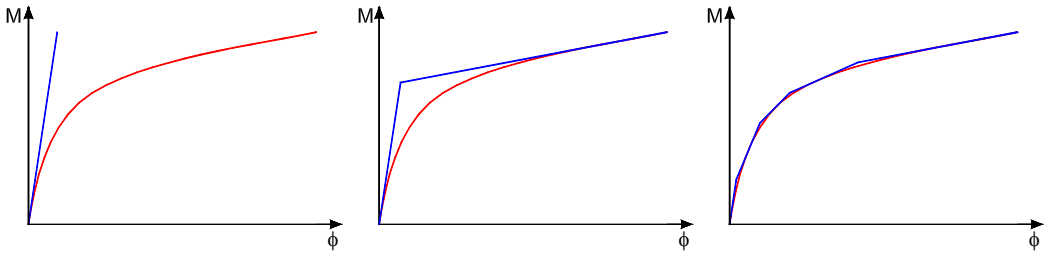

(a) linear (b) bilinear (c) multilinear

Figure 3.1 - Different types of linear models

3.1.2.2 Polynomial models

An alternative to linear models were represented by the so called polynomial models developed by Frye and Morris [28]. The prediction of the M-Φ curve was based on odd-power polynomials as:

$$\Phi = C_1 \cdot (K \cdot M)^1 + C_2 \cdot (K \cdot M)^3 + C_3 \cdot (K \cdot M)^5 \qquad (3.2)$$

where:

- K is a parameter depending on connection geometry;
- C_i are curve fitting constants to determine by least square method.

The M-Φ curve were well represented by these models. However, in some cases, they may give negative stiffness (first derivative of the function) that may be unacceptable [29] [30].
An alternative to an odd-power polynomial function was the adoption of cubic B-spline curves [31], able to better fit test data. The higher precision requires a wide number of experimental tests in the curve-fitting process [32] [33] that are not always available. In these models the experimental M-Φ data were divided into a number of subsets. Each subset was fitted through a cubic B-spline curve. This model avoided the problem of negative stiffness and was able to represent the non linear M-Φ behaviour very well [34].

3.1.2.3 Power models

Power models can characterize reasonably well the non linear M-Φ behaviour of different connection types. Several formulations are available depending from the number of parameters involved in the evaluation of the rotation as function of the moment. The simplest models like the one proposed by Krishnamurthy, Huang and Jeffrey [35] considers only two parameters, thus the function became:

$$\Phi = a \cdot M^b \tag{3.3}$$

where the two parameters a and b are used to fit the curve and have to satisfy the conditions a > 0 and b >1.
Figure 3.2 and Figure 3.3 show the sensibility of the M-Φ curve to the variations of a and b respectively. Is possible to observe that for limited variations of both a and b the predicted joint behaviour results strongly influenced.
This type of model generally does not represent the moment-rotation curve adequately [34] hence three parameter models were developed in order to obtain better results. Different formulations are available like [36] [37]:

$$\Phi = \frac{M}{K_i \cdot \left[1 - \left(M/M_u\right)^n\right]^{1/n}} \tag{3.4}$$

where:

- K_i is the initial connection stiffness;
- M_u is the ultimate moment capacity;
- n is the shape parameter of the M-Φ curve.

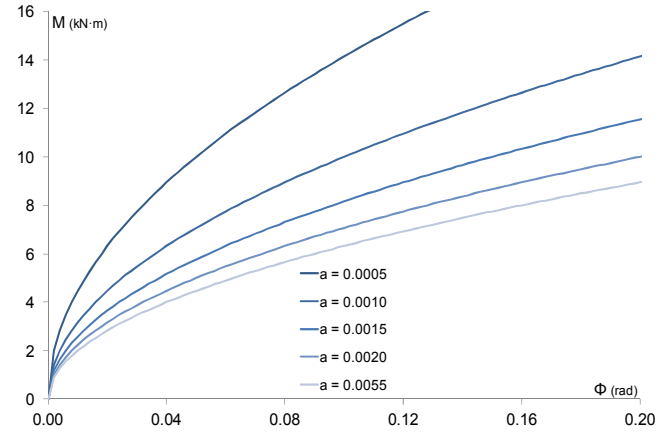

Figure 3.2 - Two parameters power model (b = 2.00)

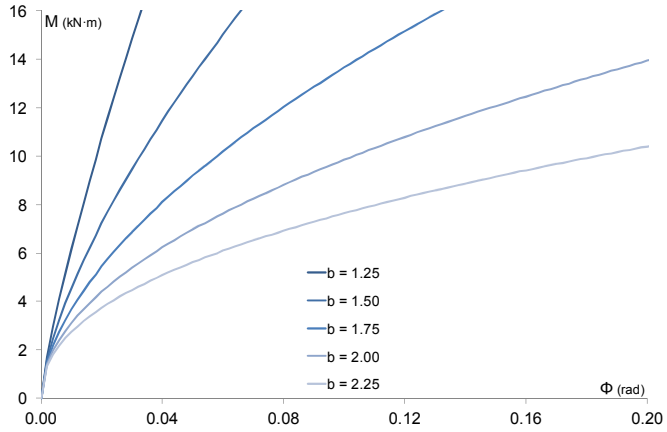

Figure 3.3 - Two parameters power model (a = 0.0010)

These models were not as accurate as the B-spline model however, the amount of required data for the model calibration in this case was drastically reduced. Nevertheless, these models may not be suitable for experimental curves that exhibit a strong hardening behaviour in their final part, near the collapse load [34].

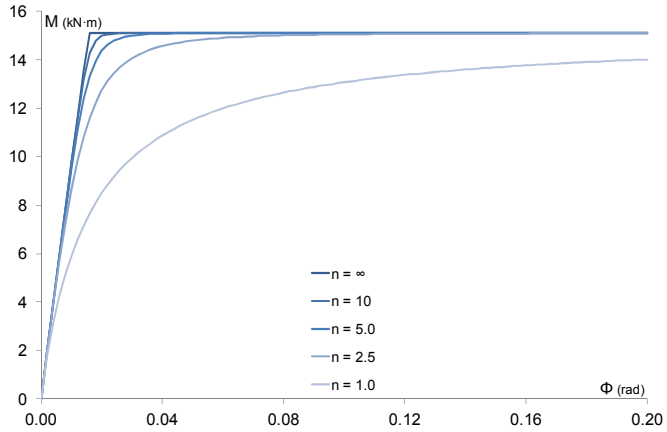

Figure 3.4 - Three parameters power model

3.1.2.4 Exponential models

Several models based on the exponential form are available in literature. They present similar formulations but with different complexity levels. The simplest, based on only two parameters [38] is:

$$M = M_u \cdot \left[1 - e^{-\frac{\beta \cdot \Phi}{M_u}} \right] \tag{3.5}$$

where:

- M_u is the ultimate moment;
- α and β are constant parameters.

As for the power models in Figure 3.5 and Figure 3.6 the response of the exponential model is presented in function of different values of α and β. In general exponential models are able to fit sufficiently well the experimental curves.

Further improvements were proposed in order to obtain a better representation also of the hardening part of the M-Φ curves [39] [34]. These formulations are based on multi-parameter exponential models, which assume the form:

$$M = \sum_{j=1}^{m} C_j \cdot \left[1 - e^{-\frac{|\Phi_r|}{2 \cdot j \cdot \alpha}} \right] + M_0 + R_{kf} \cdot |\Phi_r| \tag{3.6}$$

where:

- M_0 is the starting value of connection moment;
- R_{kf} is the strain hardening stiffness;
- α is a scaling factor (for numerical stability);
- C_j are curve fitting constants.

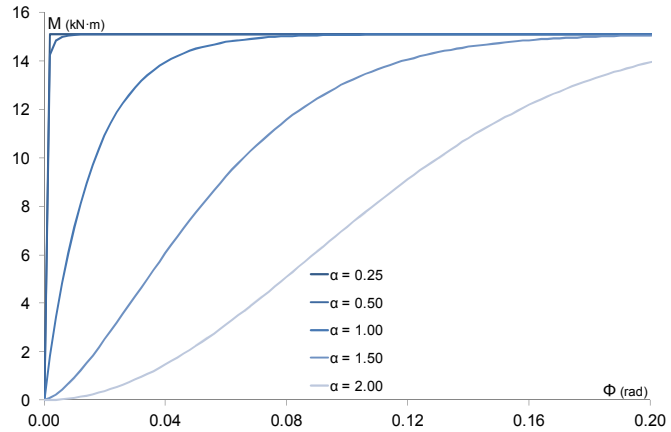

Figure 3.5 - Exponential model (β = 970)

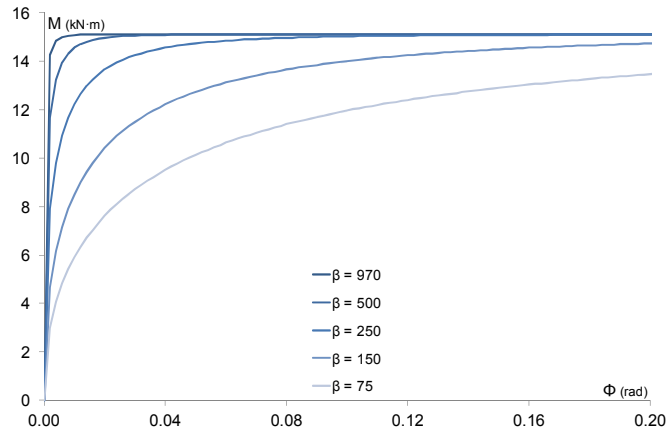

Figure 3.6 - Exponential model (α = 0.50)

This model is as good as the B-spline ones however, if there is a sharp change in the slope of the M-Φ curve it is not able to represent it effectively. For this reason the model was modified to include any sharp change in the slope of M-Φ curve [34] [39]:

$$M = M_0 + \sum_{j=1}^{m} C_j \cdot \left[1 - e^{-\frac{|\Phi_r|}{2 \cdot j \cdot \alpha}} \right] + \sum_{j=1}^{m} D_k \cdot (\Phi_r - \Phi_k) \cdot H[\Phi_r - \Phi_k] \tag{3.7}$$

where:

- D_k is a constant parameter for the linear function;
- Φ_k is the starting rotations of linear components;
- H[Φ] is the Heaviside step function (H[Φ] = 1 if Φ ≥ 0 and H[Φ] = 0 if Φ < 0);
- C_j and D_k are curve-fitting constants.

An alternative four parameters exponential model [40] in which all the involved parameters have a physical meaning is:

$$M = M_p \cdot \left(1 - e^{-\frac{(K_i - K_p + C \cdot \Phi) \cdot \Phi}{M_p}} \right) + K_p \cdot \Phi \tag{3.8}$$

where:

- M_p is the plastic moment capacity;
- K_i is the initial elastic stiffness;
- K_p is the strain hardening stiffness;
- C is an empirically determined constant for controlling the slope of the curve.

In Figure 3.7 curves associated to different values of the parameter C are compared.

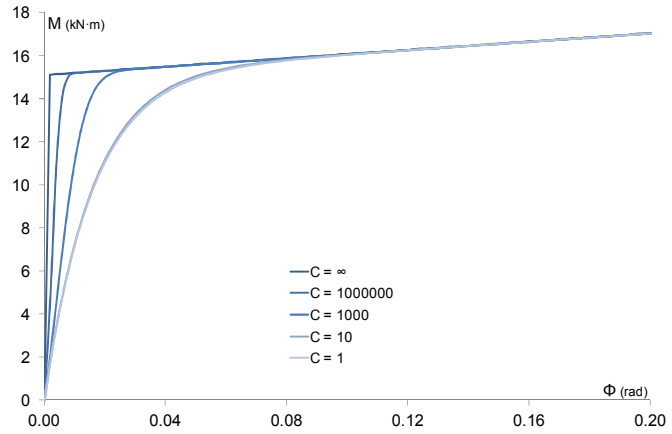

Figure 3.7 - Multi-parameter exponential model

3.1.2.5 Mechanical models

Numerous analytical methods for predicting the joints behaviour are available. Every model has his own advantages and disadvantages. However, all of them are related to a consistent experimental database.

Difficulties to perform and collect experimental data suggested to move towards different methods to determine the M-Φ curve. At this aim a new class of modelling techniques was developed: the mechanical methods.

The basic principle of these procedures is the approximation of the connection with different axial or rotational springs connected to each other in series or in parallel. Each spring has a simplified load-displacement constitutive law (typically a bilinear or a trilinear curve). To this class of models belongs for example the component method and the Krawinkler model, in which the joint is modelled respectively trough axial springs (Figure 3.8 - a) or rotational springs (Figure 3.8 - b). The component method is a general procedure, able to reproduce with a good approximation joints M-Φ curve, while Krawinkler model is specific for the description of panel zone of beam-to-column connections. For the purposes of this work the attention focused on the component method, which is described in a more detailed way in paragraph 3.2.

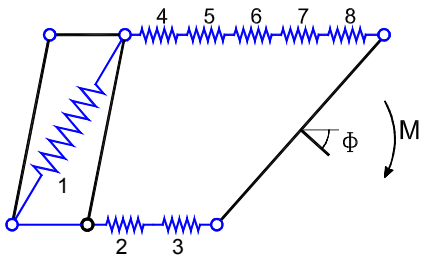

a) Component method

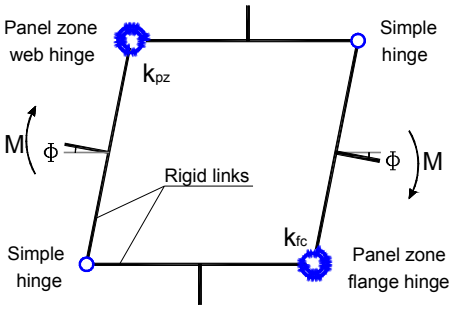

b) Krawinkler model

Figure 3.8 - Joint mechanical models

3.2 The component method

In the previous sections the importance of characterizing the type of joint for the global analysis of the structure was highlighted. Therefore a good approximation of the moment-rotation relationship (M-Φ) is necessary to describe the "actual" behaviour of the connections and hence of the whole structure.

The rotational capacity of a steel connection depends mainly on the deformation of its less ductile components. In flanged beam-to-column bolted connection a significant part of the plastic rotation is given by the column flange and the beam end-plate deformation. The behaviour of these components can be analyzed through equivalent T-stub elements. The "T-stub approach" is at the basis of the so called "component method" (EN 1993-1-8 [41]), a general procedure for the analytical evaluation of the mechanical properties of the connections (strength and stiffness) considering the characteristics of its every single component. The main steps of the "component method" can be summarized as:

- identification of the components of the joint subjected respectively to tension, compression or shear;
- determination of the mechanical behaviour of individual parts;
- "Assembly" of components for the calculation of the mechanical properties of the entire connection.

This "decomposition" of the joint into its basic components is particularly efficient. It allows to determine the overall characteristics of the connection trough the evaluation of the mechanical properties of its active components. Each basic component is described by its own load-displacement curve which represents the constitutive law of the associated equivalent spring.

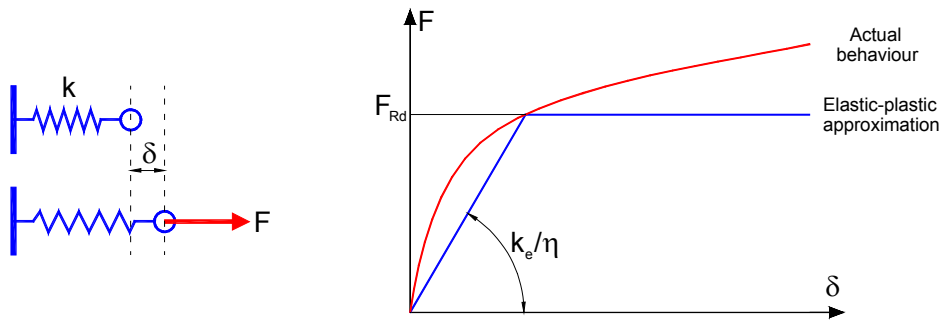

Figure 3.9 - Generic basic component idealization

The actual behaviour of a component is in general approximated with a simplified elastic-plastic curve, described by its design resistance $F_{Rd,i}$, and elastic stiffness k_i, depending on the type of action to which the component is subject (shear, tension, or compression). The mechanical model of the connection is hence composed by a set of

rigid links and springs coupled in an appropriate way in order to simulate the interaction between the different joint deformation sources.
According to the information contained in EN 1993-1-8 [41], the rotational stiffness of the connection can be calculated as:

$$S_j = \frac{E \cdot z^2}{\mu \cdot \sum_i \frac{1}{k_i}} \tag{3.9}$$

where:

- E is the elastic modulus of the material;
- z is the lever arm;
- k_i is the stiffness coefficient for basic joint component i;
- μ is the stiffness ratio $S_{j,ini}$/ S_j evaluated as follows:
  - if $M_{j,Ed} \leq \frac{2}{3} \cdot M_{j,Rd} \rightarrow \mu = 1.00$;
  - if $\frac{2}{3} \cdot M_{j,Rd} \leq M_{j,Ed} \leq M_{j,Rd} \rightarrow \mu = \left(1.50 \cdot \frac{M_{j,Ed}}{M_{j,Rd}}\right)^{\Psi}$

    in which the coefficient Ψ depends from the connection type as shown in Table 3.1.

Type of connection	Ψ
welded	2.70
bolted end-plate	2.70
bolted angle flange cleats	3.10
base plate connections	2.70

Table 3.1 - Ψ coefficients [41]

The coefficients k_i are given for each individual component according to the type of joint and to the loading conditions.
The design moment of the joint can be evaluated as follows:

$$M_{j,Rd} = \sum_r h_r \cdot F_{tr,Rd} \tag{3.10}$$

where:

- $F_{tr,Rd}$ is the effective design tension resistance of bolt row r;
- h_r is the distance from bolt row r to the centre of compression;
- r is the bolt row number.

$F_{tr,Rd}$ is the tensile resistance of the weakest component or in other words, it represents the smallest value of the tensile strengths of all the component of the bolt row r.

3.2.1 The equivalent T-stub approach

Some basic joint components, generally the ones which represent the tension region of the connection, can be approximated by equivalent T-stubs elements. The philosophy of "equivalent T-stub approach" is based on the concept that a joint component response can be simulated trough a T bolted element with a specific length l_{eff}, which depends from:

- joint geometry;
- joint loading conditions;
- T-stub loading condition (tension, compression, etc.).

3.2.1.1 Douty & McGuire

This method was initially investigated by Douty & McGuire [42] only for T-stub connections. However, they recognized the similarity between the behaviour of this type of connections and the extended end-plate ones. They developed a T-stub model which allows to compute prying forces at "working load" or at "ultimate load". This analytical model was derived from the assumption that the T-stub flange behaves as a simply supported elastic beam, with a span equal to the flange width, as shown in Figure 3.10.
Once the prying forces were obtained, the total bolt forces could be checked to ensure that bolt fracture does not govern the failure.
The maximum connection load would occur when at the bolt line and at the weld line the plastic moment M_p is reached. Douty & McGuire [42] pointed out that higher end-plate moments than M_p were experimentally observed. This was due to strain hardening which was neglected in their model.

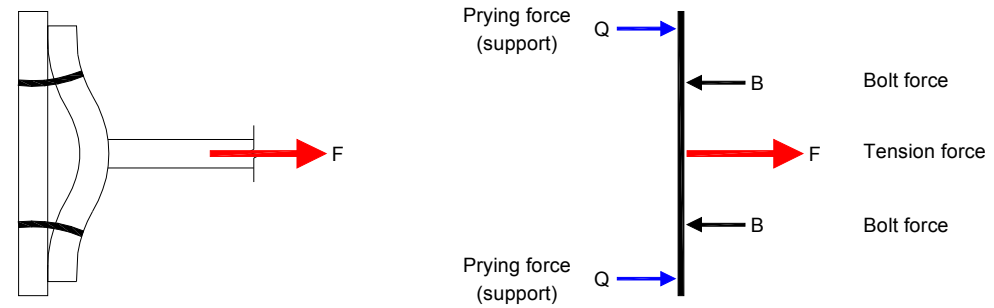

Figure 3.10 - Douty & McGuireT-stub idealization

They also clearly distinguished between two failure modes in the T-stub flange one in which two T-stubs separated before the flange yielding, and a second where yielding took place before the T-stubs separated. These are shown in Figure 3.11.

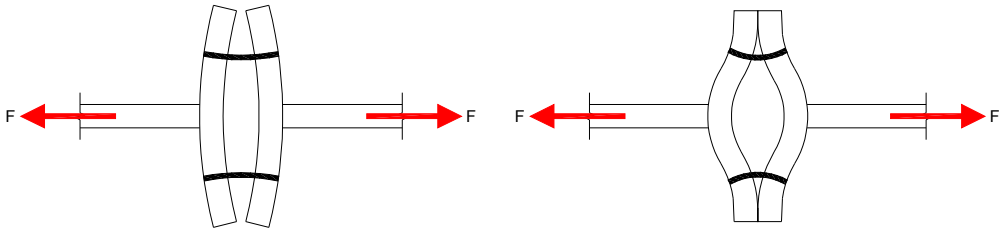

Figure 3.11 - Douty & McGuireT-stub failure mechanisms

They considered the first as a condition to be avoided as it led to brittle failure mechanisms while their aim was to ensure a ductile one.

3.2.1.2 Agerskov

Agerskov [43] investigated the response of T-stubs and beam-to-beam end-plate connections, in which the theory presented by Douty & McGuire [42] was used as a starting point. By measuring the bolt forces in experimental tests, Agerskov [43] evaluated the moments at the bolt line and at the weld line. He came to the conclusion that after an initial yielding of the end-plate at the weld line, the moment increases there due to strain hardening, but the moment at the bolt line does not increase due to a

decreasing of the prying forces (as a result of the reduced stiffness of the yielded end-plate).

Agerskov [43] considered a third failure mode, different from and intermediate between the two considered by Douty & McGuire [42]. This intermediate mode occurs if the bolts are not strong enough to restrain the end-plate sufficiently to form a plastic hinge at the bolt line. However, the bolts are too strong for the T-stubs to separate before both the weld line and bolt line yielded. This lead to a failure mode characterized by the development of a plasticized area only at the web line with a subsequent fracture of the bolts.

3.2.1.3 Zoetmeijer

Zoetemeijer [44] carried out a detailed experimental investigation on T-stub bolted connections. Starting from experimental results he developed a first theoretical one-dimensional model of the T-stub flange, based on an idealized collapse analysis. The T-stub is considered as a simply supported beam with two plastic hinges regions in which the moments reach a magnitude of M_{pl}. One region is located in proximity of the T-stub web and the other at the bolt line. He considered two possible failure mechanisms (Figure 3.12):

- mechanism A, in which the determining factor is the fracture of the bolts. Two cases are associated to this mechanism:
    - case "a", similar to Agerskov's failure mode, in which only the plastic hinge at the weld line develops while at bolt line the moment remains lower than M_{pl};
    - case "b", analogous to Douty & McGuire's first mode, in which the end-plate is so thick that the T-stub flanges separate before any flange yielding;
- mechanism B in which both plastic hinges at the bolt line and at the weld line develop and the failure is related to excessive deformation of the T-stub flange.

The static equilibrium of the forces on the T-stub, when the prying forces are zero (collapse Mechanism A - sub case b), gives:

$$F_u \cdot m = M_p \rightarrow t = 2 \cdot \sqrt{\frac{F_u \cdot m}{b \cdot f_y}} \tag{3.11}$$

with:

- F_u ultimate tension load on half of the T-stub;
- m = p/2 (half the bolt pitch);
- t flange thickness of the T-stub;
- b width of the T-stub;
- f_y yield stress of the material.

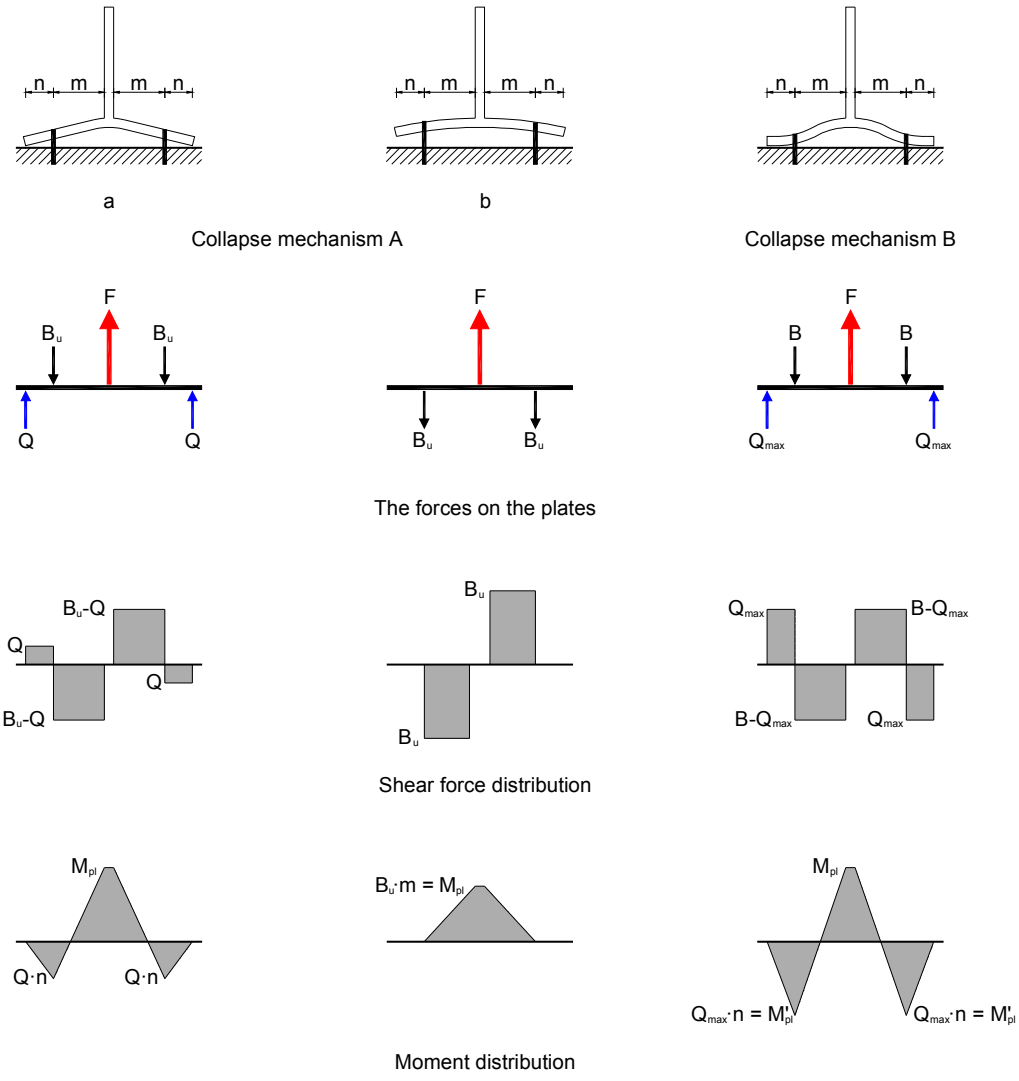

Figure 3.12 - Zoetmeijer's T-stub collapse modes

On the opposite side, when the prying force is at a maximum (collapse Mechanism B):

$$F_u \cdot m = M_p + M_p' \rightarrow t = \sqrt{\frac{2 \cdot F_u \cdot m}{b \cdot f_y}} \tag{3.12}$$

Where M_p and M_p' are plastic moments at the weld and bolt lines respectively. Equation (3.11) corresponds to the minimum plate thickness for the smallest bolt size, while Equation (3.12) corresponds to the maximum plate thickness to ensure plate failure, but using the largest bolt diameter.
In the first case the bolt diameter can be obtained as:

$$\sum B_u \leq F \tag{3.13}$$

while in the second case it can be evaluated as:

$$\sum B_u \geq F + \frac{M_p}{e} \tag{3.14}$$

where:

- B_u is the ultimate capacity of a bolt
- e is the distance to the edge about which prying took place (Figure 3.13).

Thus, Zoetemeijer demonstrated that the designer can control the failure mode quite easily by varying the plate thickness and bolt size for a given plate and beam geometry. For cases where the prying force is between these extremes, the two conditions to be satisfied are:

$$F_u \cdot m - \left(\sum B_u - F\right) \cdot n \leq M_p \tag{3.15}$$

if the bolt fracture is the determining factor, while if the excessive plate deformation is the determining factor:

$$F_u \cdot m \leq M_p + M_p' \tag{3.16}$$

When a T-stub is connected to a column flange however, the connection may be idealized as two T-stubs connected to each other and rotated of 90° as shown in Figure 3.13.

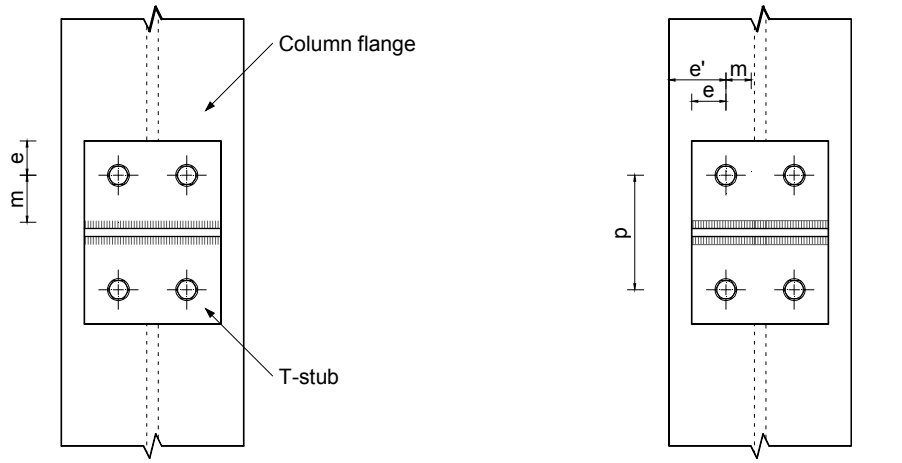

a) T-stub parameters

b) Column flange parameters

Figure 3.13 - Zoetmeijer's T-stub geometrical parameters

The above equations could be applied to the column flange and the T-stub independently, to obtain the respective values of F_u. Of course the collapse mechanism forms first in the component which has the weakest (thinner) flange. Thus, the flange with the lower value of F_u would be the critical component for the connection failure.

To apply Equation (3.15) and Equation (3.16) to column flange, Zoetemeijer [44] needed to calculate the related plastic moment M_p. This required a decision about the length of the column involved in the yielding process. He used the concept of participating or "effective length" of column flange, which was evaluated through energy considerations studying the yield lines collapse mechanism.

Two collapse mechanisms were considered for the column flange: Mechanism I and II. Mechanism I was analogous to Mechanism A for the T-stub and resulted in bolts fracture. Mechanism II was analogous to Mechanism B for the T-stub and resulted in an excessive deformation of the column flange. The proposed expressions for the participating column length respectively for Mechanism I and Mechanism II were:

$$L_{eff,I} = p + 5.5 \cdot m + 4 \cdot e' \tag{3.17}$$

$$L_{eff,II} = p + 4 \cdot m + 1.25 \cdot e' \quad (3.18)$$

where p is the bolt pitch (Figure 3.13). To obtain the collapse load the participating length has to be multiplied by the plastic moment per unit length M_p. The prediction of the collapse load obtained from this equation showed a good agreement with the experimental outcomes.

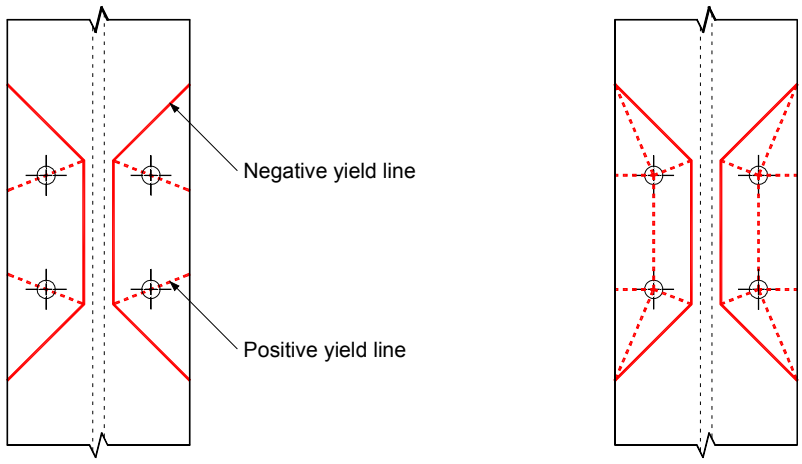

a) Mechanism I b) Mechanism II

Figure 3.14 - Zoetmeijer's T-stub failure mechanisms

3.2.1.4 Packer & Morris

Packer & Morris [45] applied a similar approach to Zoetemeijer [44] and concentrated the attention on the column flange deformation. They assumed that shear deformations were negligible. Their Mechanism A was for thick T-stubs where no flange yielding phenomena occurs and the bolts fail. Mechanism B was then related to the yielding of the T-stub flange only at the weld line and to the bolts fracture. Finally, the case in which the T-stub collapses due to the yielding of the flange at the weld line and at the bolt line identifies Mechanism C.

In applying the equations for Mechanisms B and C to column flanges (Zoetemeijer's Mechanisms I and II respectively), Packer & Morris adopted circular yield lines in the corners of the patterns rather than the straight lines investigated by Zoetemeijer. The basis for this approach was related to their experimental observations that showed circular rather than straight yield line patterns. Hence, analyzing the residual

deformations of the tested specimens Packer & Morris considered several yield lines configurations as further refinement to Zoetemeijer's proposals (Figure 3.15).

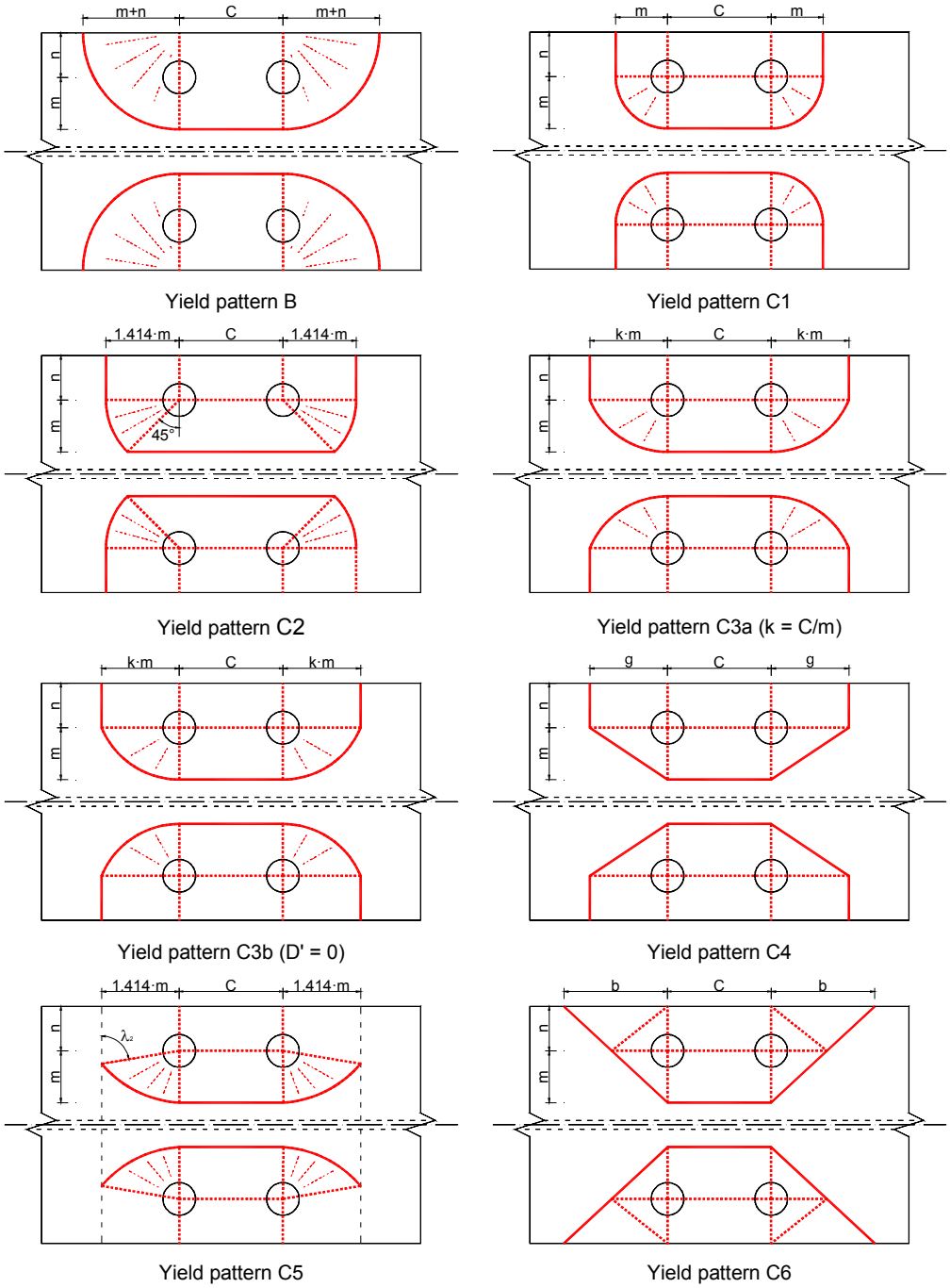

Figure 3.15 - Packer & Morris' T-stub failure mechanisms

Summarizing Zoetemeijer [44] introduced the very important concept of effective length for the column flange yield lines, and showed how this could be used in practical design. He also showed that the end-plate and the column flange could be analysed separately using the same principles.

Packer & Morris [45] extended this study analysing several yield line patterns for column flanges and defining the effective lengths associated to each plastic mechanism configuration. Their use of Zoetemeijer's equations on different yield lines patterns led to a consistent overestimation of the connection strength and to a consistent underestimation for the T-stubs one. Thus, they concluded that thin end-plate behaviour is not quite analogous to T-stub behaviour, through Zoetemeijer's equation led to better predictions than any of the other available models.

A second major contribution by Zoetemeijer is that he showed the importance of the interaction between the end-plate and the column flange, by demonstrating that the location and magnitude of the prying forces depends on the relative "thickness" of the end-plate compared to the column flange.

The literature review shows clearly that three failure modes can be identified for the end-plate or the column flange:

- "thin" behaviour with two yielded "zones";
- "thick" behaviour with bolt fracture prior to yielding;
- "intermediate" with bolt fracture after plate yielding.

The last two mechanisms are undesirable if joint ductility is required since they involve the brittle failure of bolts. It is also clear that the concept of "thin" end-plate (or column flange) is related not only to its own thickness, but also to the bolts size and strength.

3.3 Joint classification by EN 1993-1-8

The accuracy of the structural analysis of a framed structure is directly associated to the one adopted for modelling the joint behaviour. A higher accuracy in the representation of the joints response is related to a better estimation of the structural behaviour but also to a more complex analysis. Hence is necessary to select the most appropriate connection model to use depending on the adopted analysis type. The EN 1993-1-8 [41] classifies the beam-to-column connections considering three different methods of structural analysis:

- elastic analysis, based on a linear M-Φ relationship, in which the criterion for classifying the connection depends only on the rotational stiffness;

- rigid-plastic analysis, based on the connection design moment, provided that the joint is able to develop sufficient plastic rotation;
- elastic-plastic analysis based on a nonlinear M-Φ relationship. In this case, the classification of the joint depends on both stiffness and strength, considering also the rotational capacity.

Connections are hence classified in three different categories:

- simple joints, in which the joint may be assumed not to transmit bending moments;
- continuous joint, in which the behaviour of the joint may does not affect the analysis;
- semi-continuous joints, in which the behaviour of the joint needs to be taken into account in the analysis.

Method of global analysis	**Classification of joint**		
elastic	nominally pinned	rigid	semi-rigid
rigid-plastic	nominally pinned	full-strength	partial-strength
elastic-plastic	nominally pinned	rigid and full-strength	semi-rigid and partial-strength semi-rigid and full-strength rigid and partial-strength
Type of joint model	simple	continuous	semi-continuous

Table 3.2 - Type of joint model

3.3.1 Joint classification by rotational stiffness

The joint classification based on rotational stiffness S_j is mainly related to linear elastic analysis. S_j represents the slope of M-Φ curve. In the case of semi-rigid connection the

rotational stiffness $S_{j,ini}$ corresponding to the moment $M_{j,Ed}$ can be used for the entire analysis if the value of $M_{j,Ed}$ does not exceed $⅔ \cdot M_{j,Rd}$.

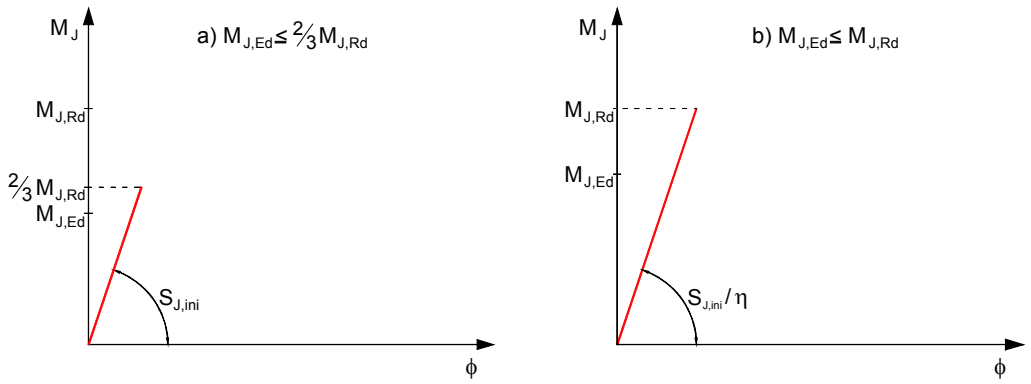

Figure 3.16 - Evaluation of rotational stiffness [41]

Alternatively, in a simplified way, it is possible to assume $S_{j,ini}/\eta$ as the value of initial stiffness, regardless of the value of $M_{j,Ed}$. The values of coefficient η depends on the type of joint as shown in Table 3.3.

Type of connection	**Beam-to-column joints**	**Other types of joints**
welded	2.00	3.00
bolted end-plates	2.00	3.00
bolted flange cleats	2.00	3.50
Base plates	---	3.00

Table 3.3 - Stiffness modification coefficient η

The EN 1993-1-8 [41] also gives limit values of $S_{j,ini}$ on the basis of which it is possible to classify the connection. Considering Figure 3.17 in a M-Φ diagram three different areas can be identified:

- zone 1: "rigid" if $S_{j,ini} \geq k_b \cdot \frac{E \cdot I_b}{L_b}$

  where:

  - k_b = 8 for frames where the bracing system reduces the horizontal displacement of at least 80%;
  - k_b = 25 for other frames, provided that in every storey $K_b/K_c \geq 0.10$. For frames where $K_b/K_c < 0.10$, the joints should be classified as semi-rigid;
- Zone 2: "Semi-rigid", includes all the nodes that do not belong to zones 1 and 3;
- Zone 3: "nominally pinned" if $S_{j,ini} \leq 0.50 \cdot \frac{E \cdot I_b}{L_b}$.

with:

- K_b mean value of I_b/L_b for all the beams at the top of that storey;
- K_c mean value of I_c/L_c for all columns in that storey;
- I_b second moment of area of the beam;
- I_c second moment of area of the column;
- L_b span of the beam;
- L_c storey height of a column.

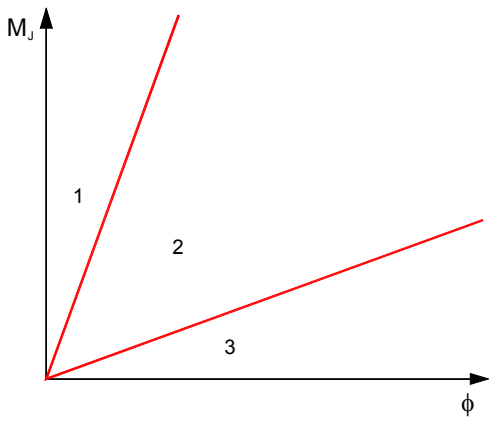

Figure 3.17 - Joint classification by rotational stiffness [41]

3.3.2 Joint classification by strength

The classification according to resistance is conventionally associated to rigid-plastic structural analysis. The classification criterion compares the design moment of the joint

$M_{j,Rd}$ with the design moment of the connected member. A joint can be classified as a "hinge" if $M_{j,Rd}$ is less than 25% of the design moment resistance required for a full-strength connection, provided that it has sufficient rotational capacity.

Joints are defined instead as full-strength ones if:

- at the top of the column $M_{j,Rd} \geq M_{b,pl,Rd}$ or $M_{j,Rd} \geq M_{c,pl,Rd}$;
- within column height $M_{j,Rd} \geq M_{b,pl,Rd}$ or $M_{j,Rd} \geq 2 \cdot M_{c,pl,Rd}$;

where $M_{b,pl,Rd}$ and $M_{c,pl,Rd}$ are respectively the design plastic moment of the beam and the column.

The connections which do not meet the criteria of hinge or full-strength connection are classified as partial-strength, provided that the plastic rotation Φ_{Cd} is adequate.

3.3.3 Joint classification by stiffness and strength

The "combined" classification procedure is usually adopted for elastic-plastic analysis. The M-Φ curve is described by a simplified bilinear diagram in which the elastic branch is described by the initial elastic stiffness $S_{j,ini}/\eta$ while the horizontal plastic branch is characterized by the value of plastic design moment $M_{j,Rd}$ (Figure 3.18).

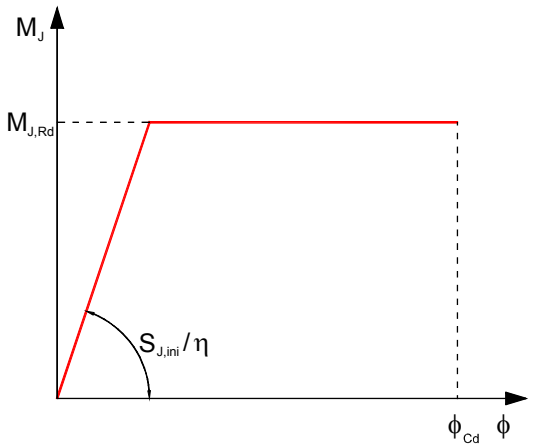

Figure 3.18 - Joint bilinear M-Φ curve [41]

As results of combining the two classification criteria previously described is possible to subdivide the M-Φ plane as reported in Figure 3.19. In this case the M-Φ curves are approximated with trilinear relationships described by the parameters $S_{j,ini}$, $S_{j,ini}/\eta$, $M_{j,Rd}$ and $\frac{2}{3} \cdot M_{j,Rd}$.

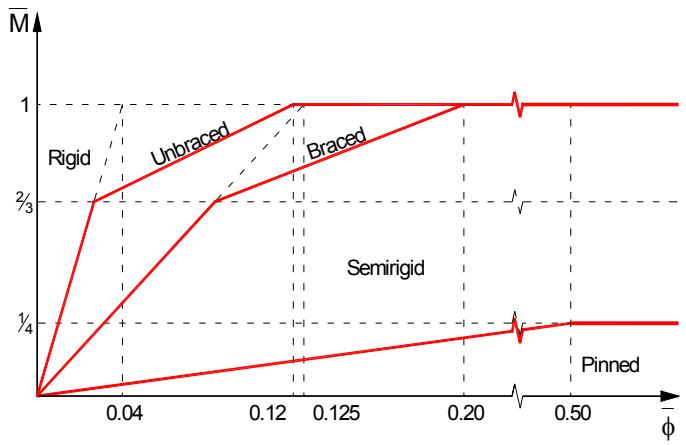

Figure 3.19 - Joint classification by stiffness and strength

3.4 Beam-to-column joints under combined actions

The component method is basically developed only for the evaluation of the bending moment's influence on the joint, but in general steel joints (especially in case of accidental actions) are subjected to bending moments, axial and shear forces. The influence of the loading condition on the joint behaviour is not negligible and may strongly affect the response of the connection, especially in terms of rotational stiffness S_j and strength $M_{j,Rd}$.

Currently, no specific criteria are given by the design standards like the EN 1993-1-8 [41] for the analysis of beam-to-column joints under combined forces. Only a limitation on the applied axial force in the beam is given, the axial force N_{Ed} should not exceed 5% of the member design resistance $N_{pl,Rd}$. This limitation usually covers the most common cases of structures under "normal" loading conditions, where steel frames are "coupled" with concrete slabs or metal steel sheeting decks which can be assumed able to behave like a rigid diaphragm. In other cases when the floor system is not sufficiently rigid this limit does not allow to apply the component method.

If $N_{Ed} > 0.05 \cdot N_{pl,Rd}$ it is recommended in the EN 1993-1-8 [41] to consider that the interaction resistance domain is defined by the polygon linking the four points corresponding respectively to the hogging and sagging bending resistances in absence of axial force and to the tension and compression axial resistances in absence of bending (Figure 3.20). In other words the connections subjected to combined bending moment and axial force have to fulfil the following condition:

$$\frac{M_{Ed}}{M_{j,Rd}} + \frac{N_{Ed}}{N_{j,Rd}} \leq 1 \qquad (3.19)$$

Several studies were recently developed to understand if the general philosophy of the component method could cover the situation of joint subjected to bending moment and significant axial force.

When the connection is subjected not only to bending moment any component should be characterized independently from the joint loading condition. The behaviour of any single component could be described by its own force-displacement curve that only depends on the level of the axial force to which is directly subjected [46], [47].

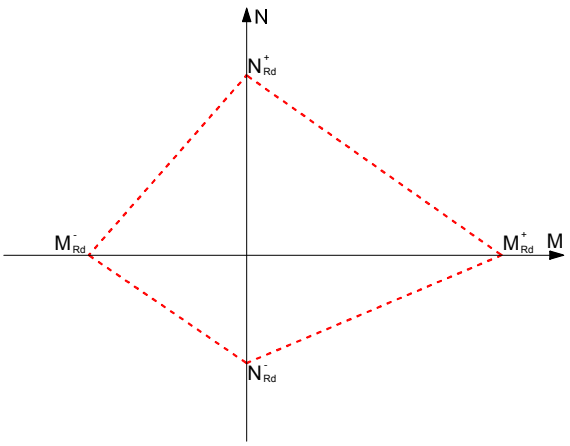

Figure 3.20 - EN 1993-1-8 simplified joint M-N domain

Due to the dependence of the mechanical model of the joint from the value and the direction of acting forces, some researchers are trying to extend the component method to a more general situation, taking into account the case of joint under bending moment and axial force.

3.4.1 Jaspart and Cerfontaine

Recently, some analytical studies were developed with the aim to predict the M-N interaction domain for beam-to-column joints. Jaspart [48] and Cerfontaine [49], [50] applied the basic principles of the component method to evaluate the M-N interaction on extended end-plate bolted joints.

The limit domain, outside which the joint collapse is reached, can be analytically defined considering the equilibrium equations at the connection level:

$$N = \sum_{i=1}^{n} F_i \tag{3.20}$$

$$M = \sum_{i=1}^{n} h_i \cdot F_i \tag{3.21}$$

where F_i and h_i are respectively the i-th line resistance and lever arm. The acting joint forces M_{Ed} and N_{Ed} are supposed to be located at the mid-height of beam and they are related by the definition of an eccentricity:

$$e = \frac{M}{N} \tag{3.22}$$

This model assumes the hypothesis that all the components of the joint possess an infinite ductility. This lead to consider a perfectly plastic analysis, based on the principles of the static theorem [49].This means that a distribution of internal forces which is in equilibrium whit M_{Ed} and N_{Ed} should be defined and of course it should also satisfy the collapse criteria:

$$\sum_{i=m}^{p} F_i \le F_{mp}^{Rd,\alpha} \quad m = 1,...,p \quad \text{and} \quad p = m, m+1,...,n \tag{3.23}$$

where $F_{mp}^{Rd,\alpha}$ is the group resistance including the m to p rows for the α component. When m is equal to p, $F_{mp}^{Rd,\alpha}$ represent the m-line individual resistance for the α component.

As stated in [49], considering all the equilibrium equations and the collapse criteria, a step by step application of the static theorem generates: "the interaction criterion between the bending moment (M) and the axial force (N) at collapse is described by a group of 2·n straight line parallel segments, two by two, whose inclination angle is respectively the n-rows lever arm (h_k). Along these segments, the force (F_k) varies between zero and the maximum row resistance, defining two segment points".

This means that the previous equations should be rewrite as:

$$M = h_k \cdot N + \sum_{i=1}^{n} (h_i - h_k) \cdot F_i^c \quad k = 1,...,n \tag{3.24}$$

that means:

$$F_i^c = \max\left(F_i^{Rd+};0\right) \text{ if } i < k \tag{3.25}$$

$$F_i^c = \min\left(F_i^{Rd+};0\right) \text{ if } i > k \tag{3.26}$$

or:

$$F_i^c = \min\left(F_i^{Rd-};0\right) \text{ if } i < k \tag{3.27}$$

$$F_i^c = \max\left(F_i^{Rd-};0\right) \text{ if } i > k \tag{3.28}$$

with:

$$F_i^{Rd+} = \min\left(F_{mi}^{Rd} - \sum_{\substack{j=m \\ \neq sup,inf}}^{i-1} F_j^{Rd+}, m = 1,...,i\right) \quad i < k \tag{3.29}$$

$$F_i^{Rd-} = \min\left(F_{im}^{Rd} - \sum_{\substack{j=i+1 \\ \neq sup,inf}}^{m} F_j^{Rd-}, m = i...,n\right) \quad i > k \tag{3.30}$$

It can be noticed that the resistances of the rows (F_i^{Rd+} and F_i^{Rd-}) are differently defined according to the i index that can be lower (F_i^{Rd+}) or greater (F_i^{Rd-}) than k index. These equations define the value of the axial force acting in each row and permit to obtain the design moment and axial force resistance in equilibrium and in according with the collapse criteria. This gives also the possibility to define analytically, trough the application of the component method, a M-N interaction domain for the connection, as reported in Figure 3.21.

In Figure 3.21, the approximated domain suggested by the EN 1993-1-8 [41] (red dashed line) is compared with the one obtained by Jaspart and Cerfontaine (blue continuous line) for a joint with two bolt rows in tension.

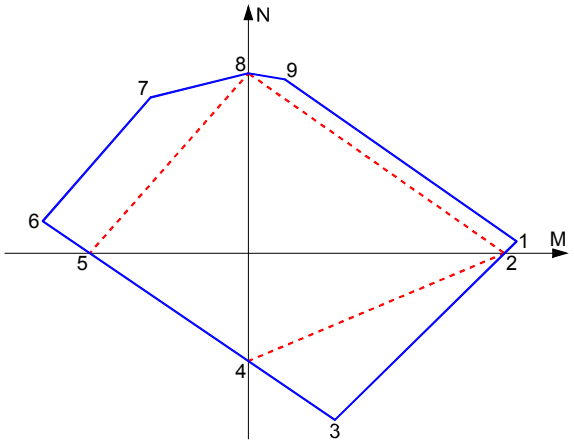

Figure 3.21 - M-N domain obtained with the component method

The Jaspart and Cerfontaine domain is defined by the following points:

1. maximum positive bending resistance;
2. positive bending resistance for $N_{Ed} = 0$;
3. maximum compression resistance;
4. compression resistance for $M_{Ed} = 0$;
5. negative bending resistance for $N_{Ed} = 0$;
6. maximum negative bending resistance;
7. point of activation of second bolt row ($M_{Ed} < 0$);
8. maximum tension resistance;
9. point of activation of second bolt row ($M_{Ed} > 0$).

The method presented above is well defined from the theoretical point of view, but currently only very few experimental data are available in literature to validate it. Among these recent experimental and numerical studies were carried out by da Silva et al. [51], [52], [46], [47], Urbonas and Daniunas [53], [54] and František and Švarc [56].

However this model doesn't give any information about the ductility related to the failure mechanism of the joint. It should of course be derived looking at the weakest component of each row and analyzing its own failure mode, but no information can be obtained directly from the M-N diagram.

3.4.2 Da Silva et al.

Jaspart and Cerfontaine [48] applied the principles of the component method with the aim of predicting the M-N interaction domain and the initial stiffness of bolted beam-to-column joints. Adopting the same general principles, da Silva et al. [51], [52] proposed analytical expressions for the full evaluation of the M-Φ curves of joints under combined bending and axial force. To provide a firm basis for further theoretical developments, an experimental program [46] was carried out at the University of Coimbra on flush and extended end-plate beam-to-column connections. The test program included 16 specimens: 9 flush end-plate joints and 7 extended end-plate joints. The comparison between the analytical and the experimental results was made in terms of M-Φ curves. Small differences in the initial stiffness were observed but in general their theoretical model well approximated the experimental results.
Parametrical analyses [47] were carried out in order to evaluate the sensitivity of the M-N interaction domain to different joint configurations. The results showed that beam section changes did not produce significant modifications on the interaction diagram inferior point, this happened because the compression component that controlled the joint behaviour was the column web in compression. The increase in the joint flexural capacity was proportional to the increase of the beam section due to the correspondent increase of the lever arm of the internal forces in the tension bolt rows. Column section changes pointed out that the controlling joint design component was the column web in compression for the smaller column profile and the beam flange in compression component for the bigger one.

3.4.3 Urbonas and Daniunas

The extension of the component method for evaluating the influence of bending moment and axial force on the rotational stiffness and moment resistance of a joint was investigated also by Urbonas and Daniunas [53] [54]. Their numerical investigations showed that the axial force influences the rotational stiffness and the moment resistance of joints. Tension axial force decreases the rotational stiffness of the joints and compression axial force increases it. For tension axial forces of 10% and 25% of axial load-bearing capacity of the joint the stiffness decreases approximately of 15% and 50% respectively.

3.4.4 Nethercot et al

Nethercot et al. [55] aimed at developing a consistent and simple approach to determine any moment versus rotation curve from experimental tests including the axial versus bending moment interaction. The proposed theoretical approach is exclusively based on the use of M-N-Φ curves and it can be easily incorporated into a nonlinear semi-rigid joint finite element formulation. The method was validated assuming as reference the experimental tests carried out by Lima, da Silva et al. [46] on flush end-plate joints. A good agreement with the experimental results was obtained.

3.4.5 František and Švarc

František and Švarc [56] carried out five experimental tests as basis for further theoretical analyses. The experimental activity focused mainly on the evaluation of M-N-Φ interaction curves and also on the end-plate failure modes (deformations, contact areas, etc.) both for beam-to-beam and beam-to-column joints. The measured M-N-Φ curves were incorporated into the European databank of M-Φ curves. The experimental collapse loads were in accordance with the prediction based on component method. Further analytical analyses are currently under preparation.

4. EXPERIMENTAL TESTS

4.1 Case of study

The increasing interest on structural robustness and the difficulty to deal with accidental loading conditions highlighted the need to deeper investigate the structural behaviour after such events. The usual design methods are not able to ensure an optimized design of the structure against such severe loading conditions.

The European Community with the introduction of EN 1991-1-7 [3] has provided new methodologies to prevent the progressive collapse which could lead to the partial or total collapse of the structure. However, the code does not define detailing rules for robust design. The cause can be found in the very limited available background data related to this problem. Events like the gas explosion at Ronan Point Building, the bomb at Alfred P. Murrah Building and the terrorist attacks at the World Trade Centre present a low probability of occurrence, wide differences in terms of loading condition and evolution of the phenomena. From these facts it is apparent the difficulty of defining specific design rules.

The European Community few years ago financed a research project called “Robust Structures by Joint Ductility” promoted by the Research Fund for Coal and Steel. The partners of the research project were:

- Département Mécanique des Matériaux et Structures, Université de Liège, Belgium;
- Institut für Konstruktion und Entwurf, Universität Stuttgart, Germany;
- Dipartimento di Ingegneria Meccanica e Strutturale, Università degli Studi di Trento, Italy;
- PROFILARBED - Research (PARE), Luxembourg;
- PSP - Prof. Sedlacek & Partner, Technologien im Bauwesen GmbH, Germany;

The research focused on the behaviour of steel and steel-concrete composite framed buildings. Among the considered scenarios the research mainly focuses on the sudden

collapse of an inner column of a building due to an accidental action. As briefly introduced in paragraph 1.1 the project assumes as progressive collapse prevention strategy the structural redundancy, to allow for alternative load paths. The development of alternative load paths allows the redistribution of internal forces to the undamaged part of the structure. This could be achieved by the activation of membrane effects within the structural members (catenary action in the floor system) with the transition from pure bending to tension and shear loading condition in beam-to-column connections. The possibility to activate alternative load paths is strictly related not only to the ductility of members but also to the beam-to-column connections one, necessary for the development of large displacements and the activation of catenary load transfer mechanism. This requires that all the structural elements and connections have to possess a high degree of plastic deformability (ductility) under combined bending, shear, and axial forces.

4.1.1 Reference building

As previously introduced the research activity focuses on a specific case of study. The investigated scenario considers the collapse of an inner column in a multi-storey building. In detail, the structure assumed as reference within the research project is a three storey framed office building designed in accordance with the Eurocodes for "normal" loading conditions. The building is composed of three main frames (3 m spaced). Each main frame has four bays with a span of 4.0 m and three storeys with an height of 3.5 m. Hence the building has a total width of 16 m and a total height of 10.5 m. The main frames are assumed to be braced and the column bases to be perfect hinges.

All the columns are HE A 160 hot rolled sections while the beams are made with IPE 140 profiles. To ensure a full connection between the IPE 140 beams and the upper concrete slab Nelson studs with a diameter of 16 mm and a height of 75 mm are welded on the upper beam flanges. The floor slab is in C25/30 reinforced concrete and has a thickness of 120 mm. The reinforcement is composed by two layers, one placed at the top (B450C Ø10/200 mm rebars) and one placed at the bottom (B450C Ø10/150 mm rebars). The beam to column connection is made by a flush end-plate 8 mm thick, welded to the beam and bolted to the column flange by four M20 8.8 bolts, preloaded with a torque moment of 350 N·m. The grade of all steel component is S355.

The joints are classified as semi rigid and partial strength ones. In Table 4.1 are summarized the main properties of steel and composite connections in terms of stiffness and strength.

Joint type	$M_{el,Rd}$ (kN·m)	$M_{pl,Rd}$ (kN·m)	$V_{pl,Rd}$ (kN)	$S_{j,ini}$ (kN·m/rad)
External (steel joint)	10.1	15.1	134.4	970
Internal (composite joint)	26.5	39.8	134.4	7541

Table 4.1 - Mechanical properties of joints

The loads considered for the design of the structural elements are:

- the self-weight;
- a permanent load G_k = 2.0 kN/m²;
- an imposed load Q_k = 3.0 kN/m².

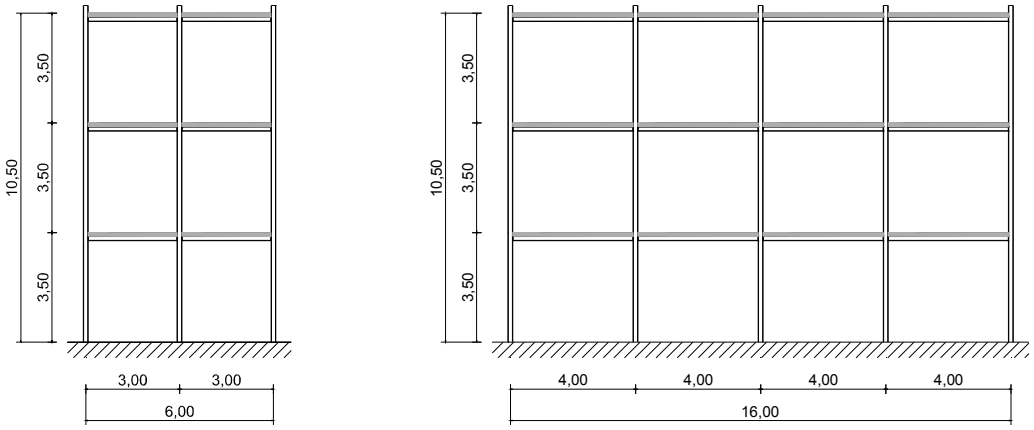

Figure 4.1 - Reference building

4.1.2 The activity carried out within the Robustness project

In the first stage of the research project experimental tests were carried out respectively on a full-scale substructure, on complete joints and also on their components in order to perform an accurate evaluation of the joints response.

The component tests carried out at the University of Trento investigated the behaviour of each single (steel and concrete) component of the joint under uniaxial or combined loading conditions. The joint tests performed at University of Stuttgart aimed at analyzing the M-Φ curves and the M-N interaction of the composite joint specimens for hogging and sagging moment. The substructure tested at University of Liege reproduced the behaviour of a complete structural system when loss of a column occurs.

4.1.2.1 Substructure test

Firstly a substructure test was performed at the University of Liege (Figure 4.2). The substructure layout was defined in order to reproduce as close as possible the actual frame behaviour.

Figure 4.2 - Substructure experimental tests

The isolation of the substructure from the composite frame, the reduction of the external spans and the restrain conditions at the external joints acting as perfect hinges modified a key element: the lateral elastic restraint “K”. The lateral restrain is given by the “undamaged” part of the structure (Figure 4.3). Hence for the test, specific lateral restraints were placed at each side of the substructure so as to restore the actual boundary conditions altered by the substructure layout modifications [57].

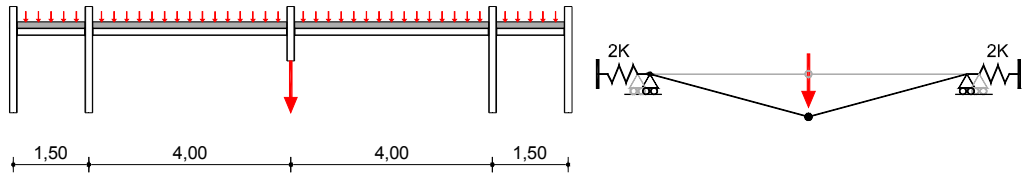

Figure 4.3 - Substructure configuration

During the test on the substructure an uniformly distributed load was firstly applied on the internal beams. In this phase, two locked jacks were placed at the middle of the substructure to simulate the presence of the column. In the following step, the support offered by the jacks was removed allowing the free deflection of the system. In the last step a vertical force was applied in correspondence of the damaged column up to collapse. In Figure 4.4 the load-displacement curve of the tested substructure is reported.

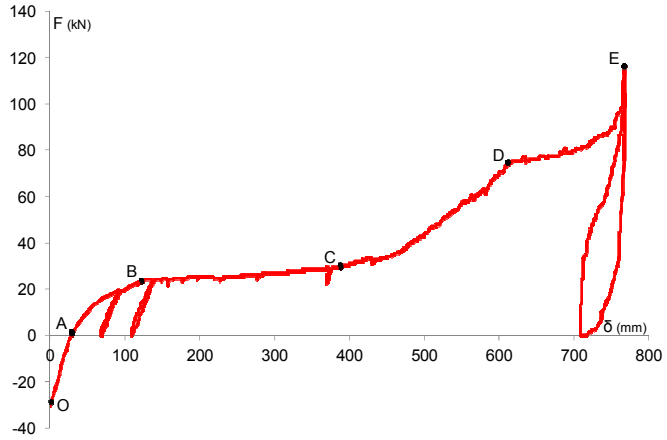

Figure 4.4 - Substructure load-displacement curve (at mid-span)

The vertical reaction associated to the uniformly distributed load and to the self-weight of the structure was equal to -33.5 kN (point “O” in Figure 4.4). In the O-A branch the structure exhibited an elastic behaviour. Then, as previously mentioned, a vertical load was progressively applied until collapse of the specimen. In the A-B segment the structure entered in the yielding stage to finally form plastic hinges at the joint level (point B). During this stage, remarkable cracks in the slab in the proximity of the external composite joints are detected and yielding of some steel components of the joints was observed (column web and beam flange in compression). From point B to point C the vertical displacement increased for an approximately constant vertical

applied load. During this stage, the concrete cracks in the vicinity of the external composite joints continued to develop and yielding spread in the steel components. One important observation is that the concrete in the vicinity of the internal composite joint split in compression [57]. Starting from point C significant membrane forces began to develop, while at point D the longitudinal rebars near the external composite joints completely collapsed and the external joints started working as steel ones with a consequent loss of stiffness, which affected the development of the membrane forces. However, it can be observed that the loss of the slab rebars did not affect the loading capacity of the substructure [57].After point D the substructure was still able to support additional vertical loads, due to the reduction of the membrane forces associated to the drop of beams axial stiffness. At the end of the test, a maximum vertical displacement of 775 mm was reached for an applied vertical load of 114 kN. The maximum horizontal displacement at each side of the structure was equal to 45 mm for a horizontal load of 147 kN.

4.1.2.2 Joints tests

The joint tests realized at the University of Stuttgart were subdivided into two series (Figure 4.5):

- 5 tests on composite joints related to the substructure tested in Liege;
- 6 bending tests on pure steel joints.

Figure 4.5 - Composite and steel joints experimental tests

Trough the M-Φ curves and the M-N interaction curves of the joints their strength and ductility were analyzed in order to evaluate their ability to activate membrane forces, achieving additional bearing capacity.

In Figure 4.6 M-Φ curves for the different composite joint tests are reported. For hogging (negative) bending moment, joints exhibited an initial elastic behaviour up to approximately $M_j \approx 18$ kN·m. Cracks started to develop at the lower surface of the concrete slab resulting in a stiffness reduction with a consequent changing in the slope of the M-Φ curves. Then the curves became approximately linear up to $M_j \approx 40$ kN·m [57]. From this point some components started yielding and the curves became flat.

The joints tested under sagging (positive) moment showed an initial stiffness a bit greater than for hogging moment. The M-Φ curves for sagging moment started with an initial elastic branch up to $M_j \approx 28$ kN·m [57]. At this point small cracks appeared at the lower surface of the concrete slab and the next part of the M-Φ -curve became curvilinear. Summarizing the joint rotation for hogging moment was mainly influenced by the steel components (including the rebars) for sagging moment it was associated to the effect of the concrete crumbling at the upper surface of the slab. Just before reaching a horizontal tangent of the curve the concrete at the upper surface began spalling and that was also the reason for the limitation of the bearing capacity [57].

The M-N interaction of the joints (Figure 4.7) during the test procedure was evaluated as follows:

- in the first step specimens were subjected to pure bending;
- in the second step the vertical jack was arrested with a certain deflection and the axial load was applied by the horizontal jack.

The horizontal tension force caused an additional joint moment which counteracted the moment produced by the vertical jack. The M-N curves for positive moment changed at the end into negative moment and met the M-N curves for negative moment at the same level [57].

Both composite joint tests and substructure test showed the ability of the connections to develop large rotations and to change the internal load combination from pure bending state to a combined bending and tension exposure.

In steel joints tests two main parameters were investigated:

- the variation of the end-plate thickness, to get all possible failure modes of the component end-plate in bending (from mode I to mode III);
- the arrangement of the bolts which greatly influences the deformation and the bearing capacity of the joints.

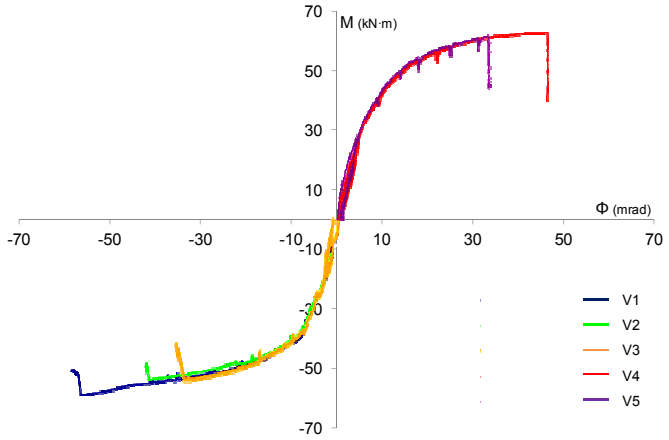

Figure 4.6 - Joints M-Φ curves

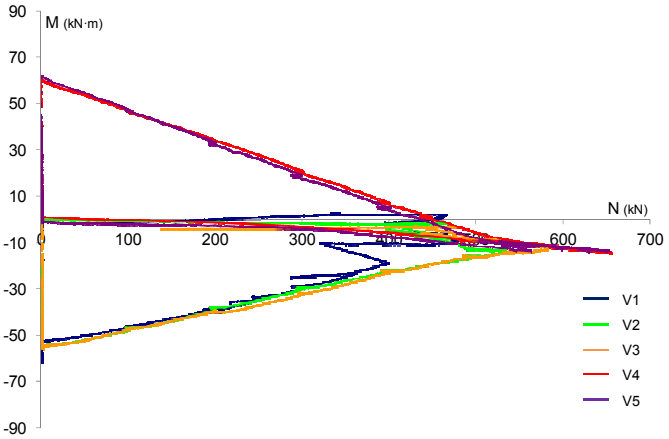

Figure 4.7 - Joints M-N interaction

A crucial finding of these tests was that due to an increase of the end-plate deformation additional membrane forces in the end-plate could be activated leading to much more bearing resistance as calculated according to the component method. These membrane effects could only be activated completely if the resistance of the bolts was sufficient. Therefore the bolts have to be oversized in comparison to the design according to the component method. The deformability of the end-plate caused even an additional effect to the bolts. Due to the highly deformed end-plate the bolts were additionally stressed by bending.

Furthermore by increasing both the vertical distance between the beam flange and the bolts and the horizontal distance between the beam web and the bolts the end-plate becomes more deformable [57].

4.1.2.3 Components tests

The contribution of University of Trento to the project was mainly related to the analysis of the behaviour of on steel and concrete joint basic components in the large displacements field. In detail, the study comprises tests on:

- reinforced concrete specimens;
- unstiffened and stiffened T-stub specimens;
- connections.

All specimens configuration is consistent with both substructure and joint tests.

The tensile tests on reinforced concrete specimens aimed to appraise of the influence of tension stiffening on the deformation capacity of the reference composite joints (Figure 4.8). Eleven tests were performed considering two different specimen layouts with different geometries and rebars layouts. The comparison between the deformation capacity of the specimens and of the bare rebars allows in fact evaluating the stiffening effect of the concrete in between the cracks.

Tests results highlighted the remarkable stiffening effects of concrete: the response at the ultimate conditions showed that the concrete can reduce the deformation capacity of steel from 57% up to 83% [57].

Figure 4.8 - Tests on reinforced concrete specimens

Tensile tests on T-stubs allowed to investigate different key aspects of their behaviour such as the influence of the presence of stiffeners (and their position), the end-plate thickness, the bolts preload and the loading conditions (Figure 4.9).

To deeper understand the complex response of the joints tested is Stuttgart (both composite and steel joints) the behaviour of their steel components elements was analyzed. The experimental study included:

- unstiffened T-stub (column flange and end-plate components), subdivided in:
    - 39 tests under pure tension on T-stubs with different lengths;
    - 16 tests under different combinations of axial (N) and shear force (V).
- stiffened T-stub under tension (40 tests).

The experimental response confirmed the remarkable deformation capacity of the specimens consequent to the hardening of the material and the activation of a membrane action within the T-stub flange [57]. The simplified “T-stub” approach which is the basis of the component method neglects this important contributions, which can represent a not negligible reserve of strength. In fact the experimental values of the collapse loads are higher than the ones evaluated by the EN 1993-1-8 [41] procedure. Furthermore the flange yielding condition cannot be accurately identified, and the definition of a criterion for its evaluation is required.

The collapses of stiffened T-stubs occurred by premature failure of the bolts due to significant bending caused by the local deformation of the flange. The activation of the expected mode I was hence not detected and collapse mode III was instead observed [57]. However, the stiffeners allowed increasing the collapse load between 16.9% and 30.8%. respect to unstiffened specimens. As to the T-stub ductility, results showed a negative effect of stiffeners when they are located close to the bolt [57].

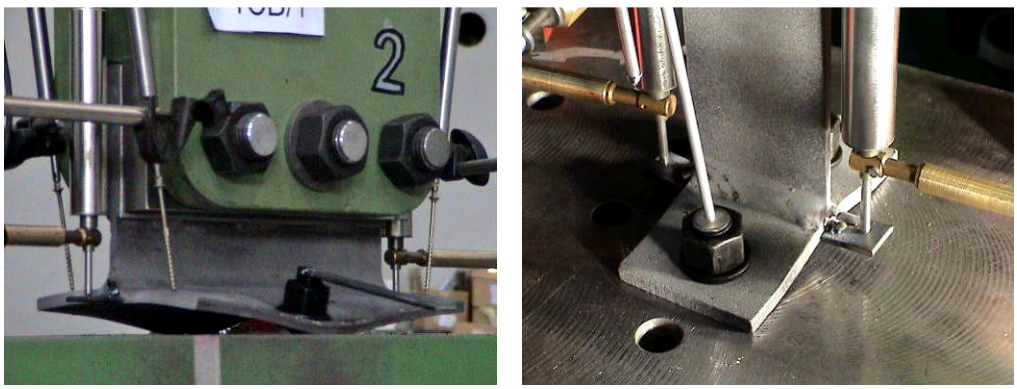

Figure 4.9 - Tests on T-stub specimens

Further tests aimed to analyze the response of the steel joint configuration of the reference composite frame. Three different test configurations were selected:

- end-plate T-stub connected to the column (3 tests);
- full steel connection on rigid support (5 tests);
- full steel connection on the column (6 tests).

For the first configuration, only tests under pure tension were performed, while for the other configurations tests under different combinations of bending moment (M), axial (N) and shear force (V) were carried out. The different loading conditions were obtained through an initial relative inclination between the beam and the actuator. The selected inclinations are 0° (pure tension), 11° and 20°.

For the T-stubs bolted on the column the collapse was associated to bolts fracture, which were subject to significant bending due to the high deformation of both the column and the T-stub flanges. Respect to the condition of rigid support the collapse load for T-stub bolted to the column was reduced of about 10% [57].

The behaviour of the connection on rigid support was remarkably affected by the loading conditions. Assuming the tension tests as reference, an initial inclination angle of 11° led to a reduction the ultimate load of 16.2%. For an inclination angle of 20°, the reduction increased to 43.7%. The experimental response in all the tests was characterised by significant deformations of the end-plate. As for the T-stub bolted to the column, the bolts were subject to significant bending [57].

For the complete joint (connection on column), large deformations of both the column and the end-plate developed before collapse which was also in this case caused by bolt fracturing. Negligible differences in term of collapse loads were detected comparing the case of pure tension with the one with an inclination of 11°. For an initial inclination of the applied load of 20° a reduction of 21.5% of the collapse load was instead observed.

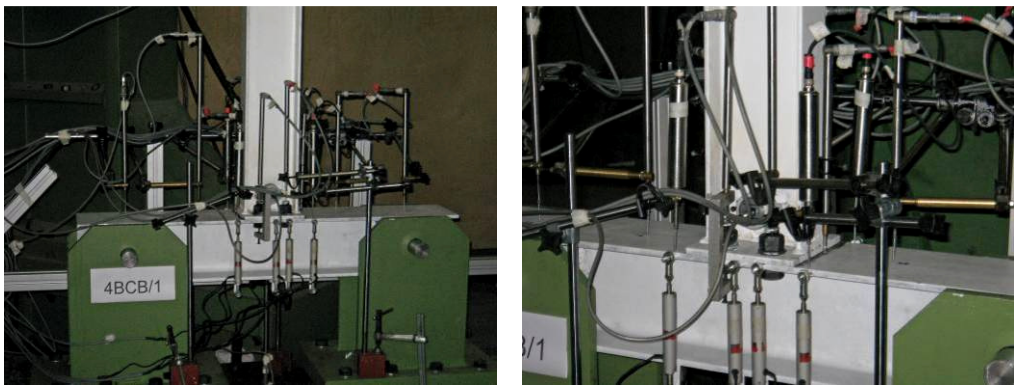

Figure 4.10 - Tests on reference steel connection

Summarizing assuming the rigid support condition as reference the collapse load of the complete joint decreases of 15.5% up to 29%, depending on the load conditions [57]. Stiffness and ductility were also significantly influenced as shown in Figure 4.11

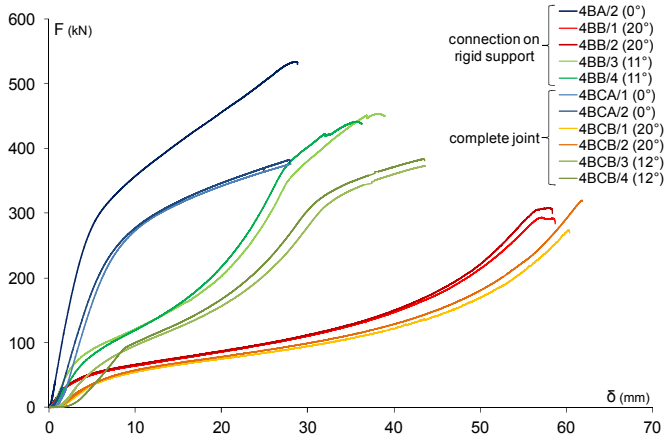

Figure 4.11 - Steel joint and connection load-displacement curves

From the outcomes of the whole experimental activity carried out in Liege, Stuttgart and Trento some guidelines for a robust design of connection were derived (Table 4.2).
These principles represent a first step in the definition of detailing rules to be adopted to ensure an adequate structural safety level against also accidental actions and the associated phenomena of potential progressive collapse of the structure.

Component	Requirements
reinforcement in tension (RFT)	• the ductility of the tension bar in the concrete slab can be improved by extending the tension bar due to an increase of the distance of the first shear stud to the end-plate • the ductility of the reinforcement can be improved by choosing B450C (f_u/f_y > 1.3) instead of BSt500S(B) (f_u/f_y > 1.08)
end-plate in bending (EPB) + column flange in bending (CFB)	• it is advantageous when both components have nearly the same resistance acc. the definition in EN 1993-1-8, that means in usual cases the same steel grade as well as the same thickness, so both may contribute similarly to the joint deformation • the resistance of these components have to be smaller than the resistance of the bolts (considering over-strength and membrane effects for both components) • the ductility may be improved by increasing the vertical distance from the bolts to the beam flange and horizontal distance from the bolts to the beam web • for composite joints the deformability of both components have to be sufficient to activate the tension bar in the concrete slab completely
bolts in tension (BT)	• the bolts have to be oversized in such a way that all over-strength effects as well as membrane effects in all designed ductile components are covered
beam flange in compression (BFC)	• the beam flange in compression tends to be designed as weakest component of the joint due to the fact that buckling of the flange is a quite ductile failure and under biaxial loading the stress changed into tension so for additional normal tension force the beam flange is still fully functional
concrete slab in compression (CC)	• the concrete slab in compression for joints under sagging moment fails due to the sharp bend from the joint rotation and the resulting high compressive strain at the upper concrete surface • the crushing of the concrete is important to enable also a ductile behaviour for sagging moment but the influence of the concrete compressive strength to the crushing effect seems to be of minor importance

Table 4.2 - Requirements for joint components to ensure a ductile joint behaviour [57]

4.2 Tests on T-stub elements under combined actions

The present work focuses on the response T-stub elements under different combination of axial and shear force. In the following the results of the experimental tests carried out on column T-stub specimens under different combination of N and V are presented and discussed.

4.2.1 Specimens layout

The specimen was obtained from a portion of HE A 160 profile which comprised part of the column flange and the column web. The specimen measured 256 x 152 x 160 mm. The flange had two holes with a diameter d_0 = 22 mm, to allow the insertion of two M20 bolts. The web of the specimen was appropriately reinforced by welding on both sides a 100 x 256 x 5 mm steel plate (Figure 4.12). The stiffness of the web was designed to inhibit undesired collapse mechanisms that were not significant for the purposes of testing.

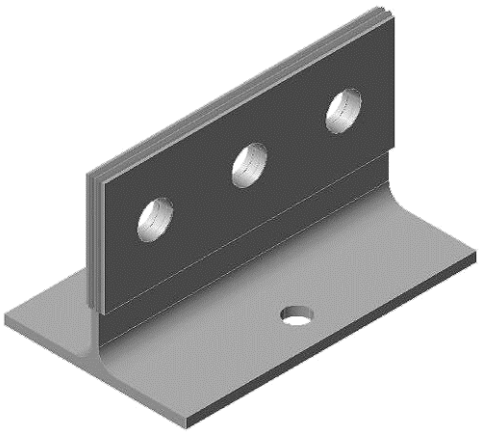

Figure 4.12 - Column T-stub specimen

4.2.2 Tests set-up and procedures

In order to analyze the response of the T-stub under different combinations of axial and shear forces a specific test apparatus was designed.

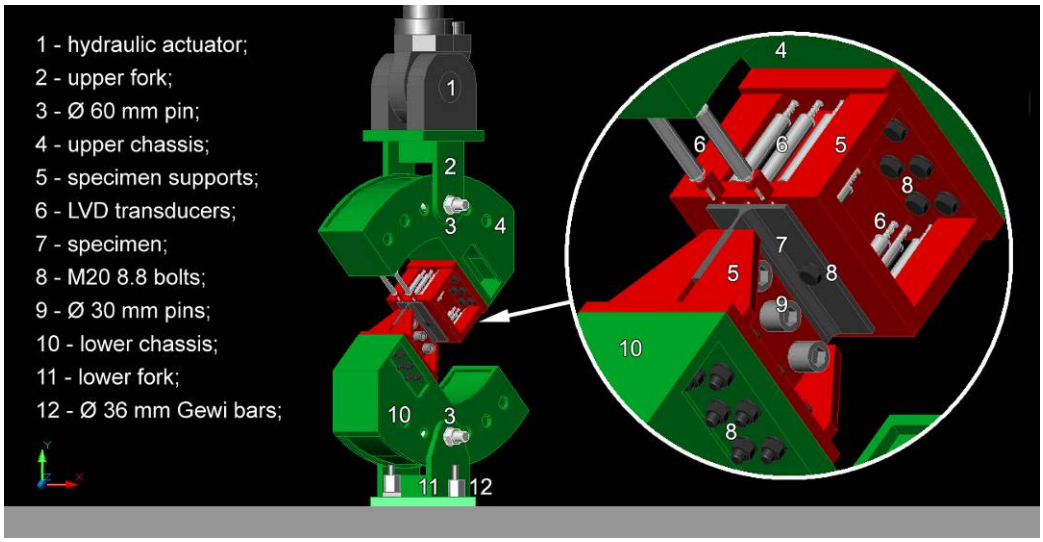

Figure 4.13 - T-stub tests device

The test device consisted of two curved box-section chassis. The connection between the top and bottom parts of the device was achieved through the specimen. In particular the flange of the specimen was connected to the upper part of the test set-up by means of two M20 class 8.8 bolts, while the connection with the lower part and the specimen web was made by three pins Ø 30 mm. To obtain different loading conditions was sufficient to rotate the device changing the position of the pin which connects the box-section chassis with the lower and upper forks, connected respectively to the laboratory floor and to the hydraulic actuator. The inclination angle φ of the device was defined as:

$$\varphi = \arctan\left(\frac{N}{V}\right) \tag{4.1}$$

where N and V are respectively the axial and the shear components of the external applied load F. The angle φ = 0° corresponded to the condition of pure shear, while an increasing value of φ led to obtain loading conditions in which the axial force is greater and greater.

The test device was designed in order to have no bending moment acting on the specimen.

Before proceeding with the tests T-stub specimen and bolts geometry were checked for any scatter between the nominal and actual sizes. All the tests were performed under displacement control.

Figure 4.14 - Different T-stub tests configurations

The loading process was characterized by an initial preloading cycle (up to 30 kN) and a final loading cycle up to specimen collapse. To evaluate the specimens' deformations a total of fourteen transducers were used (Figure 4.15), two for the measurement of displacements associated to shear force (parallel to T-stub flange) and twelve for the displacements associated to tension force evaluation (perpendicular to T-stub flange).

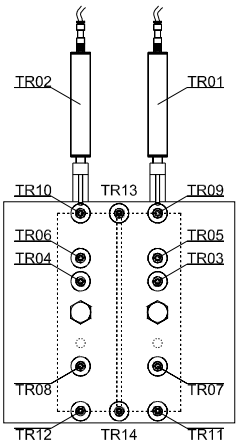

Figure 4.15 - T-stub tests instrumentation

4.2.3 Tests results

All sixteen column T-stub (1CC specimens) were successfully tested. The collapse in all tests occurred, as expected, due to bolts failure. Figure 4.16 shows two typical deformations of the bolts at collapse. In particular, the picture on the left refers to a pure

shear test (1CC_00°), while the one on the right is related to test with an inclination angle φ of 60° (1CC_60°). The comparison between the two figures shows the significant effect of bending due to the combination of axial and shear forces. As a result of the bolts deformation at the collapse there was a remarkable bearing of the holes in the T-stub flange (Figure 4.17).

With the exception of test with φ < 45°, significant deformations were observed, associated to the development of flange mechanisms. This effect can be observed in Figure 4.18, which shows a comparison between the flange deformation at failure for specimen tested at 45° and 75°.

The displacements perpendicular to the flange, confirmed the experimental evidence. Considering the load displacement curves acquired from the different transducers it was possible to appraise further information about the evolution of the flange deformation with the inclination angle φ. Figure 4.19 and Figure 4.20 show the load-displacement curves of the T-stub flange associated with φ = 15° (specimen 1CC_15°/2), while Figure 4.21 and Figure 4.22 are related to φ = 60° (specimen 1CC_60°/3). As expected the maximum deformation were recorded at the flange ends, while smaller ones are measured in the area around the bolts.

The comparison between the displacements acquired by transducers placed symmetrically with respect to the bolts showed an asymmetry in the behaviour of the specimens. This phenomena may be associated to the effect of the shear force, in fact the lower is the value of φ the greater is the asymmetry detected. The presence of the shear force induced a modification in the "deformation mode" of the T-stub flange, with higher displacements in the "upper" part of the flange (transducers TR09, TR10 and TR13).

Figure 4.16 - Bolts deformation at collapse

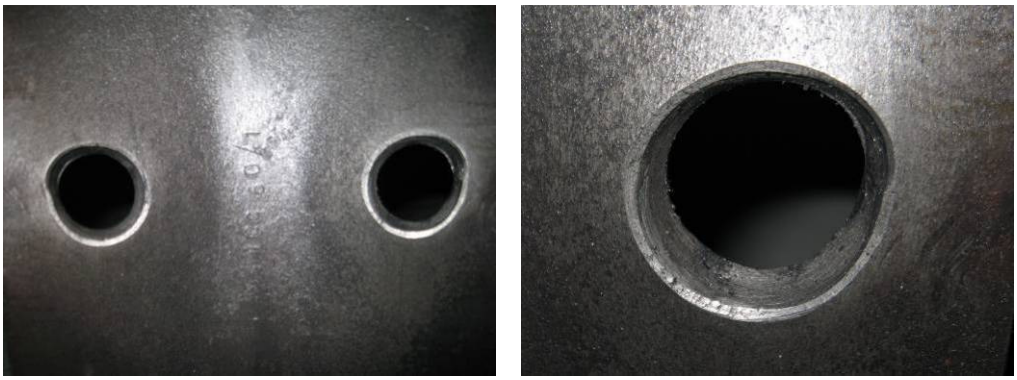

Figure 4.17 - Bolt's holes deformation at collapse

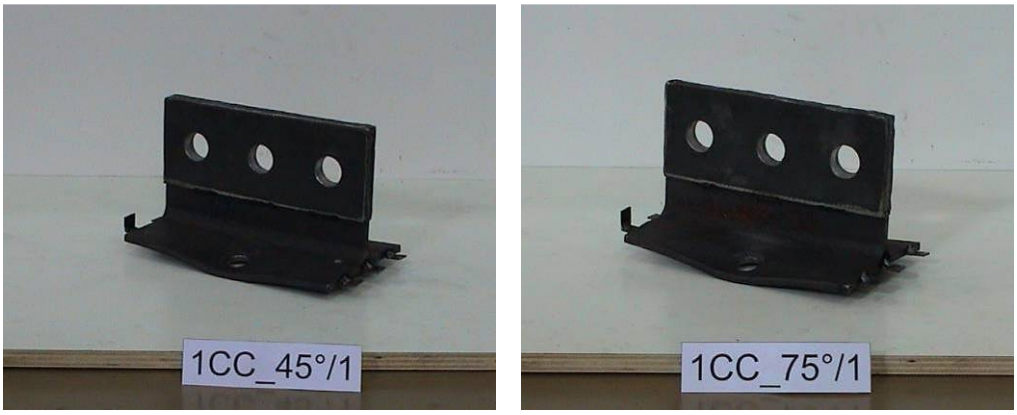

Figure 4.18 - Specimen flanges deformation at collapse

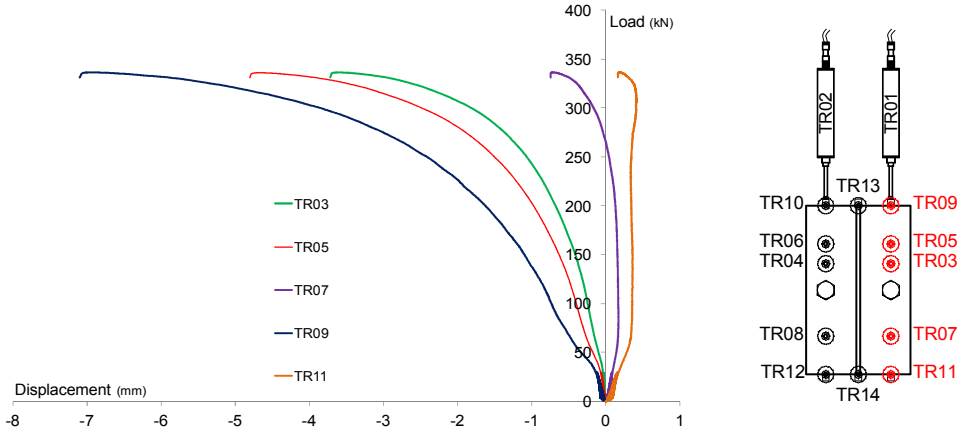

Figure 4.19 - 1CC_15°/2 load-displacement curves (right side)

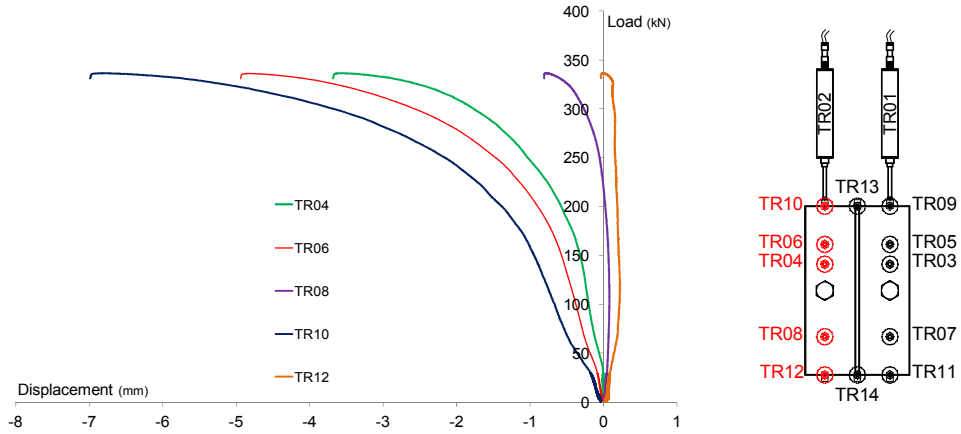

Figure 4.20 - 1CC_15°/2 load-displacement curves (left side)

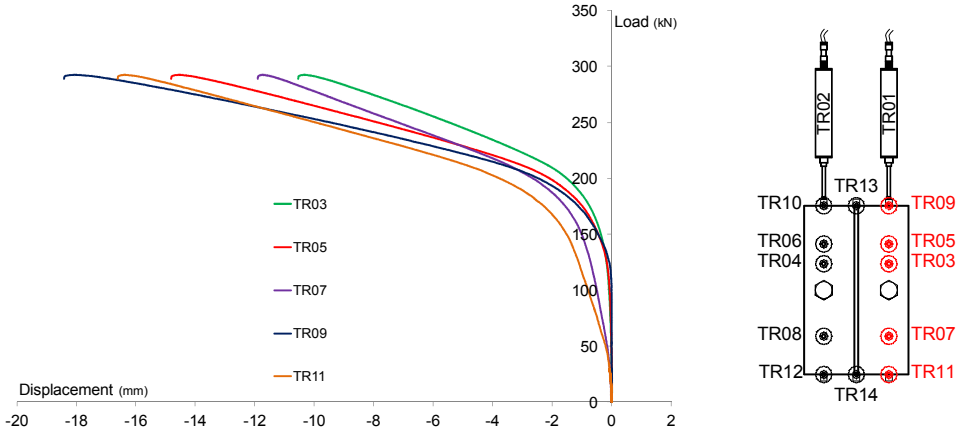

Figure 4.21 - 1CC_60°/3 load-displacement curves (right side)

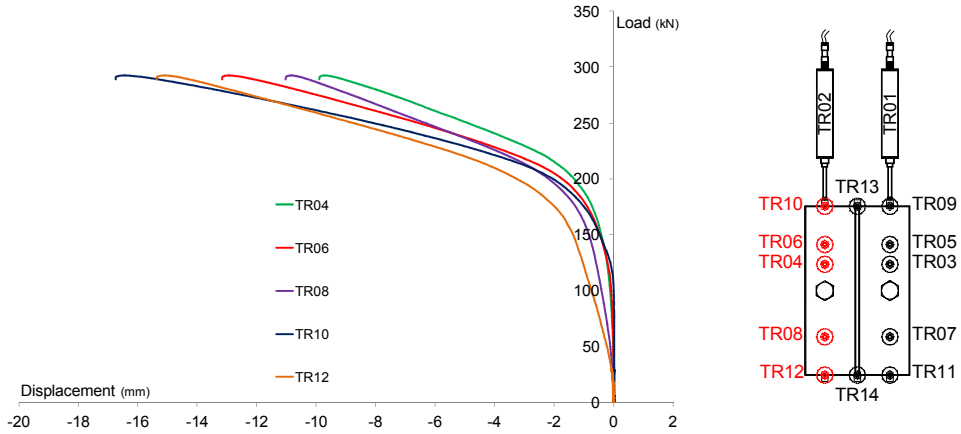

Figure 4.22 - 1CC_60°/3 load-displacement curves (left side)

In Figure 4.23 are presented the load-displacement curves of transducers TR13 and TR14, positioned at the opposite extremes of the T-stub flange. In detail, the dotted lines refer to TR13 while the continuous ones represent the transducer TR14. The difference between the displacement recorded by TR13 and the one relative to TR14 tends to decrease with the increasing of the inclination angle φ. For φ = 75° the flange behaviour is almost symmetric.

Differences in measured displacements can be observed also in tests with an inclination angles of 0° in which no tension force is present and hence no transverse flange displacements were expected. This phenomena may be associated with parasitic bending moments, caused by the progressive deformation of the bolts and T-stub flange which led to a small "shift" of the position of resultant of the applied load. However, comparing for example the curves related to φ = 0° with the ones associated to 15° < φ < 45° is possible to notice that the effect of parasitic bending is small if compared with the asymmetry associated to the shear force. In fact for φ = 0° the average difference between the displacement measured by TR13 and TR14 at collapse is lower than 2 mm while for 15° < φ < 45° the gap is approximately of 5 mm. Starting from φ = 60° this difference decreases, due to the prevalence of the axial force with respect to the shear one.

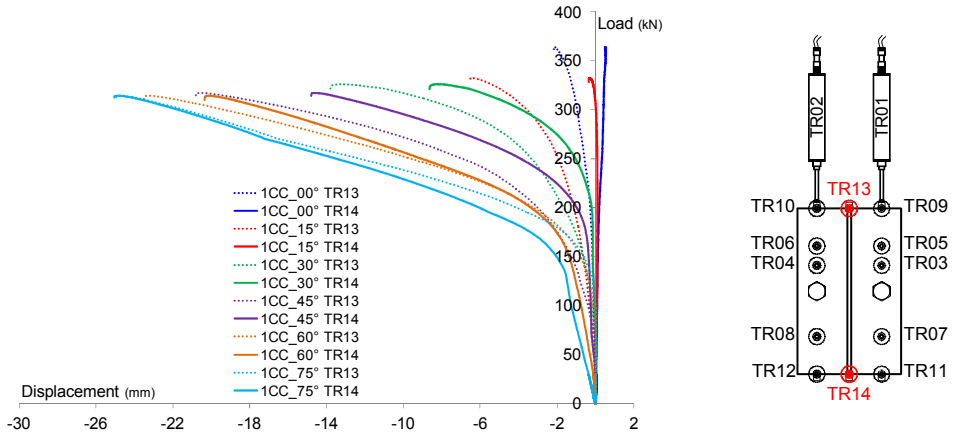

Figure 4.23 - TR13 and TR14 load-displacements curves for different values of φ

A very similar behaviour, can be observed in Figure 4.24, where the transducers positioned in proximity of the bolts (TR05, TR06 and TR07, TR08) are compared. The average curves of the transducers placed in the upper part of the plate are represented

by a continuous line, while the dotted ones are associated to the average displacements recorded by the transducers in the lower part of the T-stub flange.

Comparing Figure 4.23 and Figure 4.24 it is possible to appraise that in general the difference between the displacement measured by TR13 and TR14 is practically the same evaluated between the average curves for transducers TR05-TR06 and TR07-TR08. This allows considering negligible the effect of the parasitic bending moment. In fact a significant effect of the bending moment should results in wider differences between TR13 and TR14 than for the inner transducers due to the fact that they are positioned farther from the bolt, which represent the "centre of rotation" of the specimen.

Observing the load-displacement curves related to transducers TR01 and TR02 (Figure 4.25) is possible to notice that in general to a progressive increasing of φ corresponds a reduction of stiffness, associated to the changing of the load transfer mode.

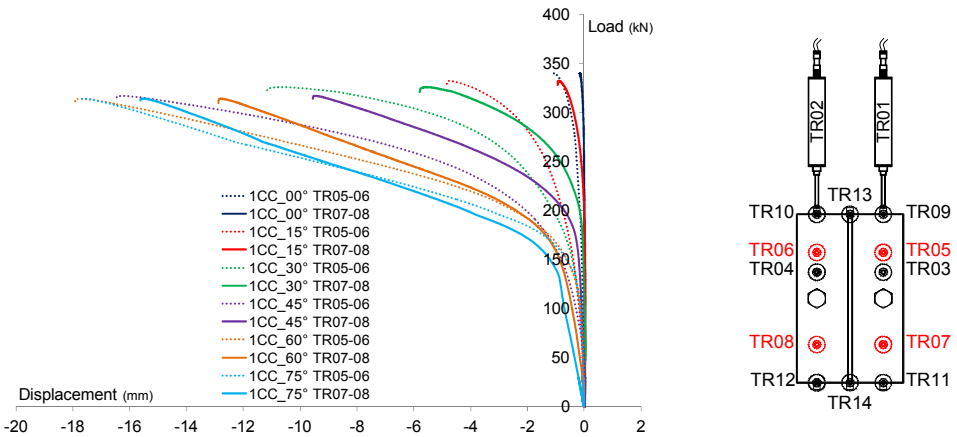

Figure 4.24 - TR05÷TR06 and TR07÷TR08 average load-displacements

For 0° ≤ φ ≤ 30°, where the shear component of the external load is greater than the axial one, the initial stiffness of the different curves is very similar. In all these tests the failure is governed mainly by bearing phenomena with fracture in shear of the bolt shanks. In the curves associated to inclination angles greater than 45° it is possible to observe a stiffer behaviour, due to the limited displacements that occur in the longitudinal direction of the T-stub flange in the first part of the tests. Is also possible to observe that at collapse the maximum displacements are associated to the tests with 30° < φ < 75°. For tests with φ ≥ 60° the load-displacement curves are characterized by a very slow increment of the longitudinal displacement in the initial part, with a sudden

increment for an applied load of about 200 kN. This phenomena is related to the formation of a flange plastic mechanism which causes a rapid increment of the transverse displacements of the T-stub flange and to the particular acquisition conditions of the longitudinal displacements.

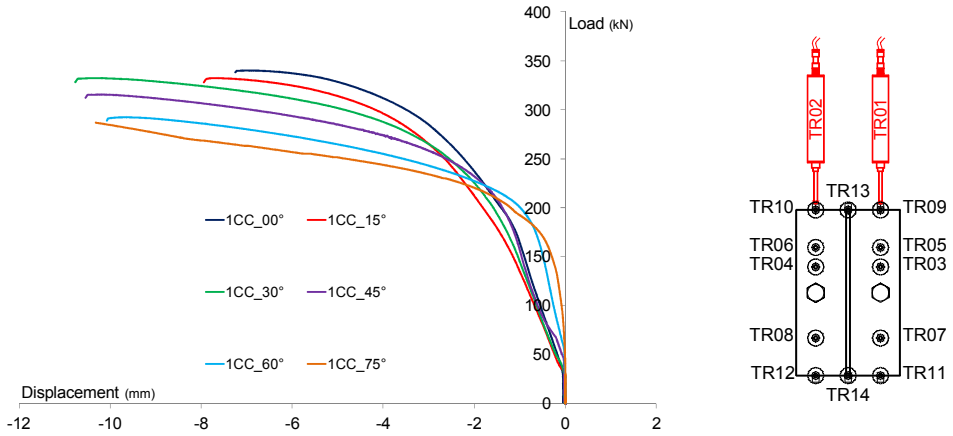

Figure 4.25 - TR01 and TR02 average load-displacements curves for different values of φ

In fact, as highlighted in Figure 4.26, to avoid damage to the instrumentation due to the sudden collapse of bolts (and the consequent instantaneous unload of the T-stub flange), between the two vertical transducers and the specimen was inserted a screw.

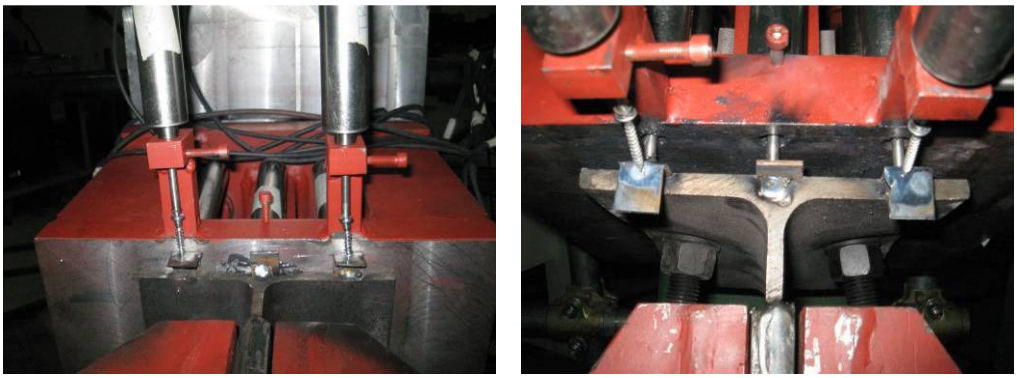

Figure 4.26 - Transducers TR01 and TR02

Figure 4.27 shows the influence of the presence of the screw on the acquired displacements. The screw follows the deformation of the T-stub flange not only in the longitudinal direction, but also in the transverse one. This cause a progressive rotation of the screw and a consequent deviation between the real displacement (named as "d"

in Figure 4.27) and the acquired one (named as "TR01-02"). Hence, knowing the length of the screw (30 mm) and the displacements recorded by the transducers TR09 and TR10 is possible to recalculate "d" and "TR01-02" displacement values.

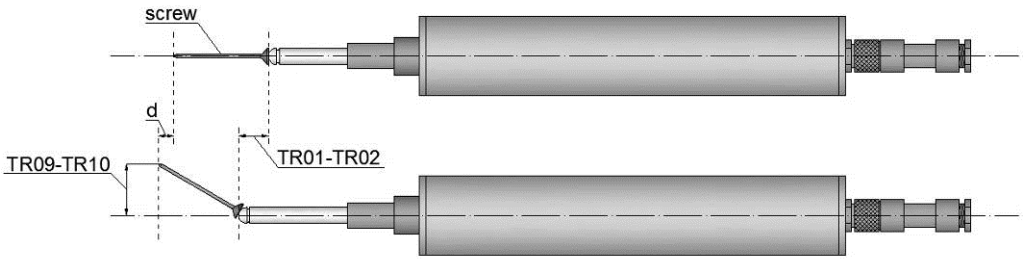

Figure 4.27 - TR01 and TR02 measured vs. real displacement

The "corrected" values of the longitudinal displacements of the T-stub flanges are shown in Figure 4.28, Figure 4.29 and Figure 4.30 with a dotted line, while with a continuous one is plotted the average experimental curve.

Obviously the gap between the experimental curve and the "corrected" one tends to decrease with the decreasing of φ. For φ = 0° the two curves are practically coincident (Figure 4.28), due to the negligible displacements related to transducers TR09 and TR10. Comparing the corrected values of the longitudinal displacements of the T-stubs evaluated for different inclination angles (Figure 4.31) it is now possible to see that the greater displacements are clearly associated to the tests where an higher shear force is applied.

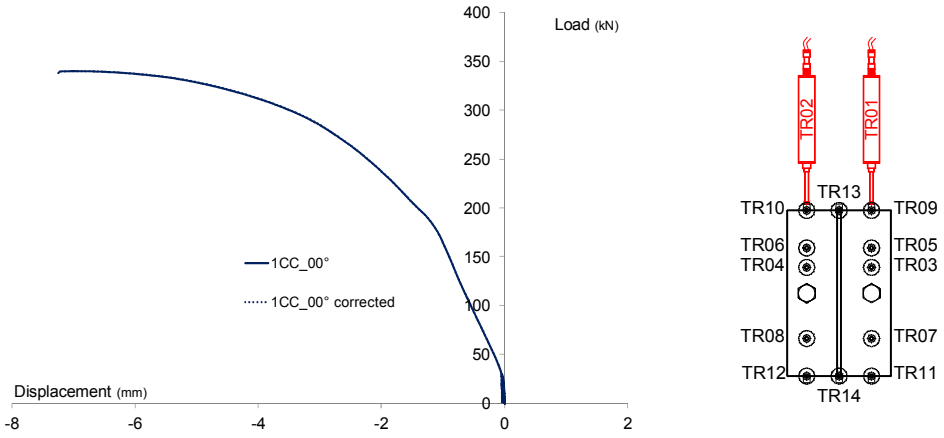

Figure 4.28 - Corrected values of TR01 and TR02 for φ = 0°

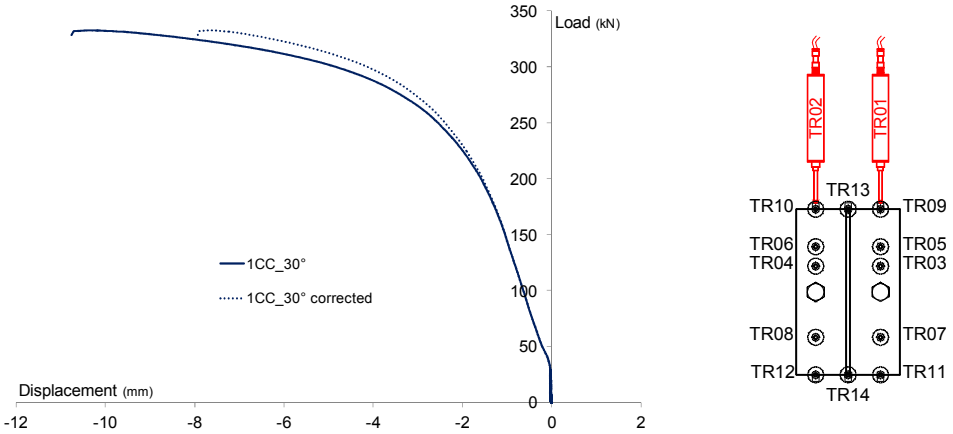

Figure 4.29 - Corrected values of TR01 and TR02 for φ = 30°

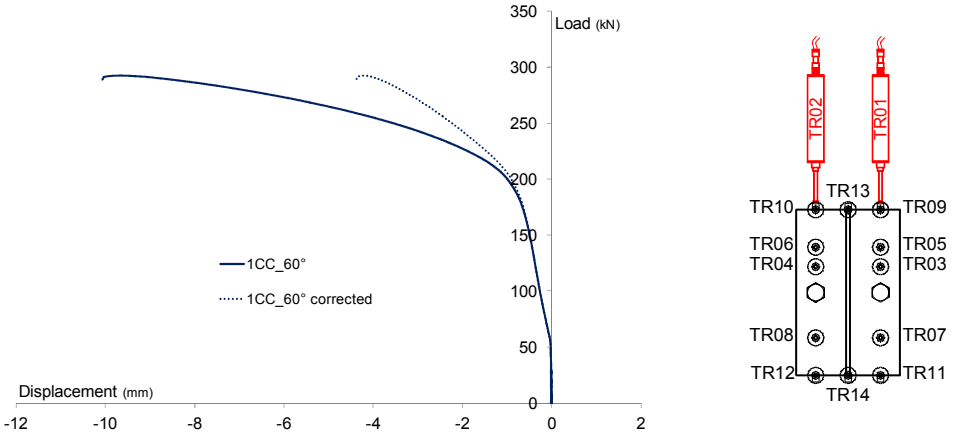

Figure 4.30 - Corrected values of TR01 and TR02 for φ = 60°

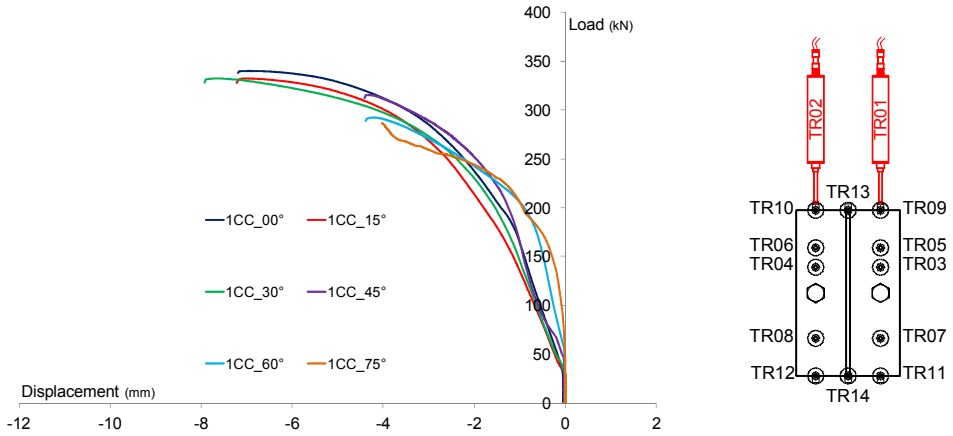

Figure 4.31 - Corrected TR01 and TR02 load-displacements curves for different values of φ

Once obtained the actual value of the longitudinal displacements of the specimens a further analysis, in order to evaluate the global load-displacement curves of the T-stub is done. Through a vector sum of the average longitudinal and transverse displacements of the T-stub flange the load-displacement curves for different inclination angles are evaluated (in red) and compared with the ones obtained directly from the actuator (in blue) in Figure 4.32 and Figure 4.33 respectively for φ = 30° and φ = 60°. From the comparison is possible to observe quite similar behaviours. The curves obtained from the specimens' transducers show however, a stiffer behaviour. This is due to the fact that the curve obtained from the actuator comprises also the deformation of the specimen web and of the different parts of the test devices.

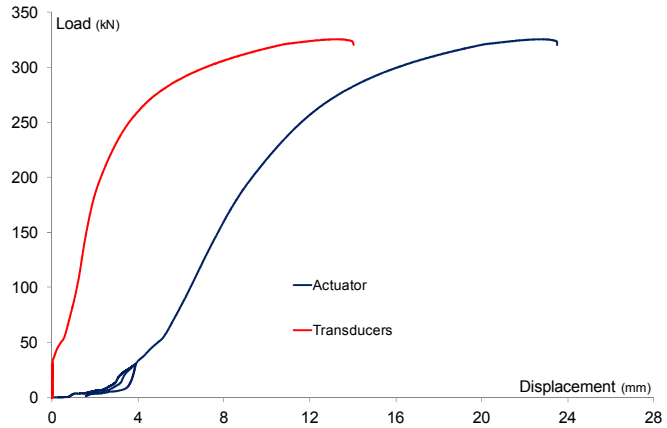

Figure 4.32 - Actuator load-displacements curves for φ = 30°

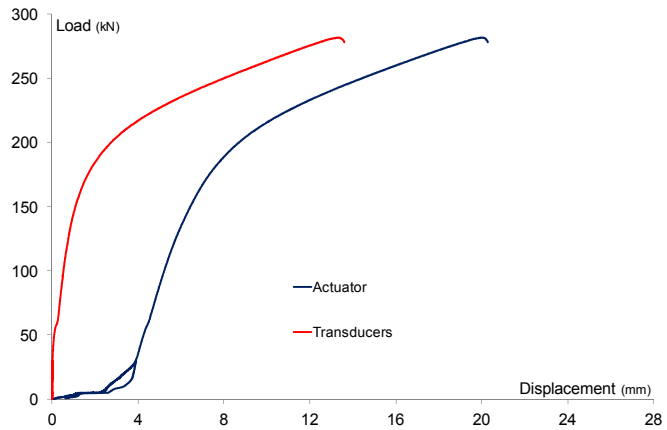

Figure 4.33 - Actuator load-displacements curves for φ = 60°

Test results in terms of average collapse loads are given in Table 4.3. Figure 4.34 and Figure 4.35 provides a graphical representation of the results of Table 4.3. In particular, Figure 4.34 describes the relationship between the total load at failure (F) and the inclination angle φ of the applied load. Figure 4.35 instead shows the relationship between axial component (N) and shear component (V) of the force F.

Test angle (deg)	**Collapse load** (kN)	**Axial component** (kN)	**Shear component** (kN)
0	352.55	0.00	352.55
15	334.40	86.55	323.01
30	329.20	164.60	285.10
45	316.08	223.50	223.50
60	314.44	272.31	157.22
75	305.00	294.61	78.94
90	285.728	285.728	0.00

Table 4.3 - T-stub experimental collapse loads

In both graphs the red dots represent the experimental results, while the blue curves represent the average trend of the relationship between values on the abscissa and on the ordinate.

The results appear to identify a significant interaction between the axial and shear force. From the graph of Figure 4.34 is possible to see that the collapse load of the specimens tends to decrease linearly (of about 11 kN every 15°).

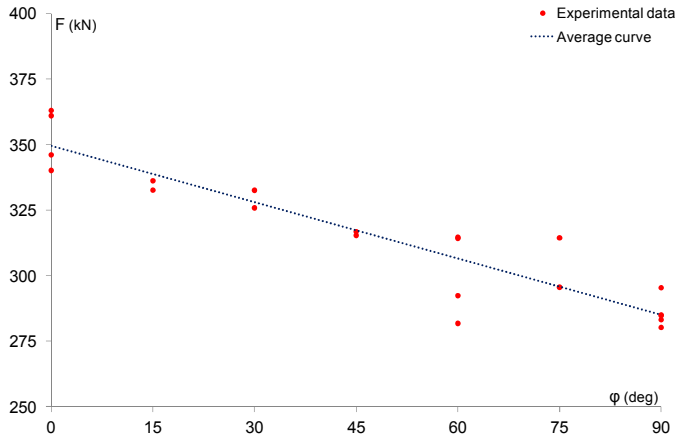

Figure 4.34 - Collapse loads vs. inclination angles φ

The average curve of Figure 4.35 allows instead identifying a strong of N-V interaction domain for column T-stubs.

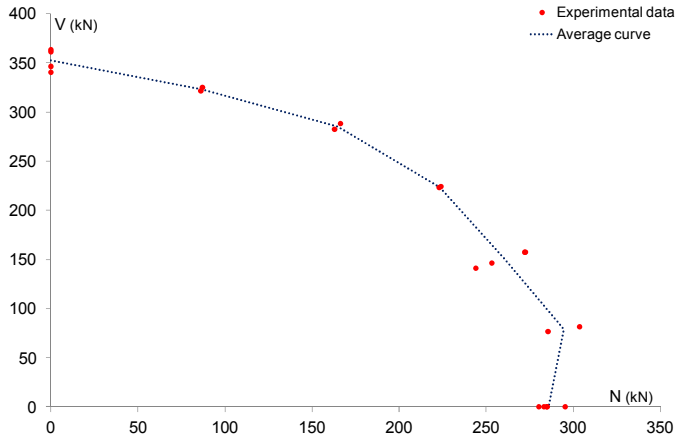

Figure 4.35 - Axial vs. shear component of collapse loads

4.3 Evaluation of specimens' residual deformations

In order to get a better evaluation of the T-stubs failure mechanisms after the test the specimens' residual deformations were acquired by a laser system MEL M5L/200 (Figure 4.36) in order to obtain the deformed shape of the T-stubs flanges.

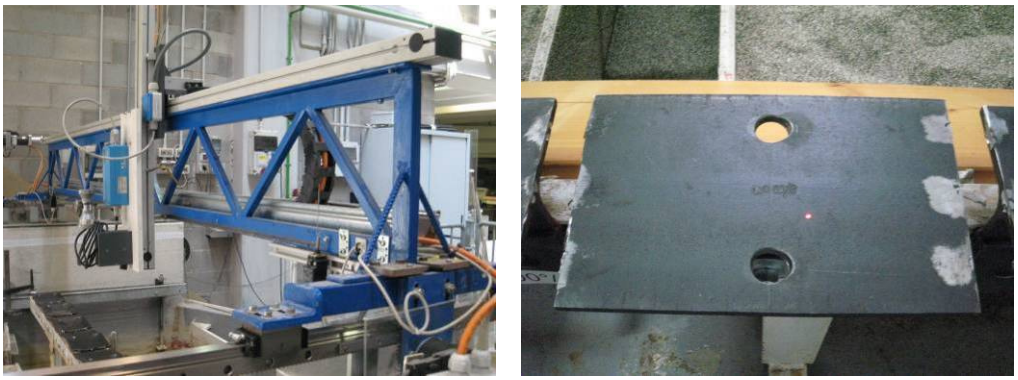

Figure 4.36 - Laser scanning procedure

This technique was originally developed for topography and hydraulic engineering purposes, in order to examine for example the variation in the morphology of river beds in hydraulic experimental models. Through several data acquisition at fixed times during

the experimental activity was possible to evaluate the effects of the water running (bed erosion, meanders development, etc.).

The laser acquisition system offers the possibility to acquire and digitalize the shape of complex surfaces with a very good precision. This aspect suggested to use this technique for evaluating the residual deformation of the T-stub flanges.

The laser system allows to acquire digital data to obtain 2D and 3D models of the scanned object. The "shape" of the scanned object is captured through a grid of points, which density depends from the resolution chosen for the scanning operation, or rather by the horizontal spatial increments Δx and Δy of the grid points. For each point the laser measures the value of the vertical coordinate z. In this case was chosen a grid with square cells with $\Delta x = \Delta y = 2$ mm that allow to acquire a great amount of data, adequate to "evaluate" the residual deformations (the z coordinate) of the specimens (Figure 4.37).

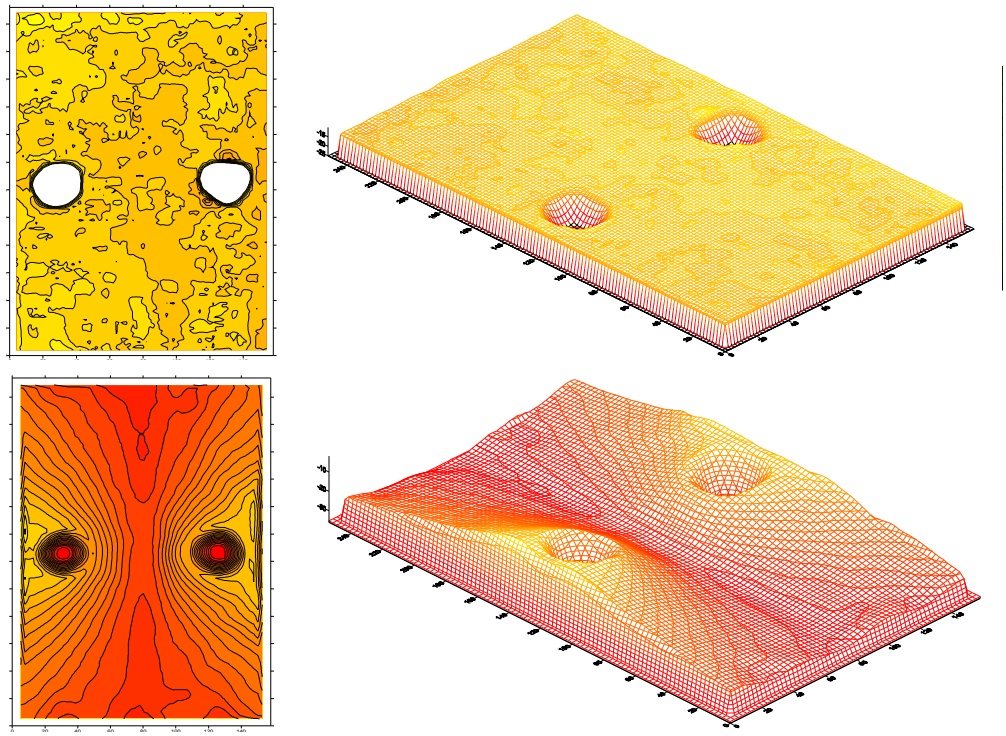

Figure 4.37 - 2D and 3D models from laser acquisition for φ = 0° and φ = 75°

After the scanning procedure the obtained data were elaborated by a specific surfaces mapping software (Surfer 7.0) which allowed to obtain 2D and 3D models of the specimens.

The first step was to perform the "smoothing" of the matrix which contains the data obtained from the scanning. This function allowed to calculate new values of the z coordinate of the grid's points as a sort of weighted average based on the z values of the adjacent points. The "smoothing" operation was necessary to eliminate the "noise" (due to the local variability of the reflecting properties), the local defects of the scanned surfaces and some erroneous z values due to the difficulties to scan in proximity of the plates' borders and holes. The smoothing was performed using the Kriging method, which was one of the most effective algorithm among the ones available in the software.

From the new matrix obtained by the smoothing operation was possible to trace for example contour maps with level lines, contour maps with slope lines and of course 3D models. In these representations the yellow colour indicates negligible displacements, while when the colour turns to red the displacements increase as shown in Figure 4.37.

The software provided some useful tools to analyze the surface geometry, allowing to interpret the grid files. The "grid calculus" options helped to define and quantify characteristics in the grid file that might not be obvious by simple looking at a contour map of the surfaces. Through the "terrain slope" module Surfer automatically determined, for each grid point of the surface, the magnitude and direction of the steepest slope. This elaboration was based on the derivatives calculus by central difference method. The first and second order derivatives in the generic point P of coordinates (x_n, y_n) were evaluated as:

$$\left.\frac{dz}{dx}\right|_{(x=x_n)} \approx \frac{z(x_{n+1}) - z(x_{n-1})}{2 \cdot \Delta x} \tag{4.2}$$

$$\left.\frac{dz}{dy}\right|_{(y=y_n)} \approx \frac{z(y_{n+1}) - z(y_{n-1})}{2 \cdot \Delta y} \tag{4.3}$$

$$\left.\frac{d^2z}{dx^2}\right|_{(x=x_n)} \approx \frac{z(x_{n+1}) - 2 \cdot z(x_n) + z(x_{n-1})}{\Delta x^2} \tag{4.4}$$

$$\left.\frac{d^2z}{dy^2}\right|_{(x=x_n)} \approx \frac{z(y_{n+1}) - 2 \cdot z(y_n) + z(y_{n-1})}{\Delta y^2} \tag{4.5}$$

$$\left.\frac{d^2z}{dx \cdot dy}\right|_{(x=x_n, y=y_n)} \approx \frac{z(x_{n+1}, y_{n+1}) - z(x_{n-1}, y_{n+1}) - z(x_{n+1}, y_{n-1}) + z(x_{n-1}, y_{n-1})}{4 \cdot \Delta x \cdot \Delta y} \tag{4.6}$$

The terrain slope module produced contour maps representing the isolines of constant steepest slope. The slope S at the generic point P is the magnitude of the gradient in that point:

$$S = \sqrt{\left(\frac{\partial z}{\partial x}\right)^2 + \left(\frac{\partial z}{\partial y}\right)^2} \approx \sqrt{\left(\frac{z(x_{n+1}) - z(x_{n-1})}{2 \cdot \Delta x}\right)^2 + \left(\frac{z(y_{n+1}) - z(y_{n-1})}{2 \cdot \Delta y}\right)^2} \tag{4.7}$$

The slope was reported in degrees, from 0 (horizontal) to 90 (vertical), the conversion of the slope in degrees was simply made adopting the following relationship:

$$S_T \approx \frac{360}{2 \cdot \pi} \cdot \arctan\left(\sqrt{\left(\frac{z(x_{n+1}) - z(x_{n-1})}{2 \cdot \Delta x}\right)^2 + \left(\frac{z(y_{n+1}) - z(y_{n-1})}{2 \cdot \Delta y}\right)^2}\right) \tag{4.8}$$

The slope isoline maps were used to highlight the maximum slope line that allow to identify the collapse mechanisms of the steel plates (yield lines).

The results for column T-stubs (Figure 4.38) showed a progressive spread of the area involved in the flange plastic mechanism. The evaluation of the residual deformations of T-stub flanges confirmed the behaviour observed in the load-displacement curves: to a decreasing of the inclination angle φ is associated an increasing asymmetry of the flange deformations. Figure 4.38 offers an overview of the evolution of the residual deformations and the yield mechanisms of the T-stub flange in function of the angle φ. It is necessary to point out that in the range $0° < \varphi \leq 30°$ no appreciable flange mechanisms were detected. For these values of φ the collapse was associated to bolts failure with only local bearing phenomena around the bolts' holes, as highlighted from the slope contour lines.

Starting from the slope isolines maps it was possible to identify simplified failure mechanisms as shown in Figure 4.39. The best approximation was attained through the so called "non circular" patterns. Assuming as reference the dashed horizontal lines, referred to the extension of the mechanism for the case $\varphi = 30°$, it was possible to have a qualitative comparison between the different failure mechanisms.

Together with an increasing symmetry, to an increment of the inclination angle φ (and hence of the axial component of the applied load) was associated also a growth of the portion of the T-stub flange involved by the formation of the plastic mechanism.

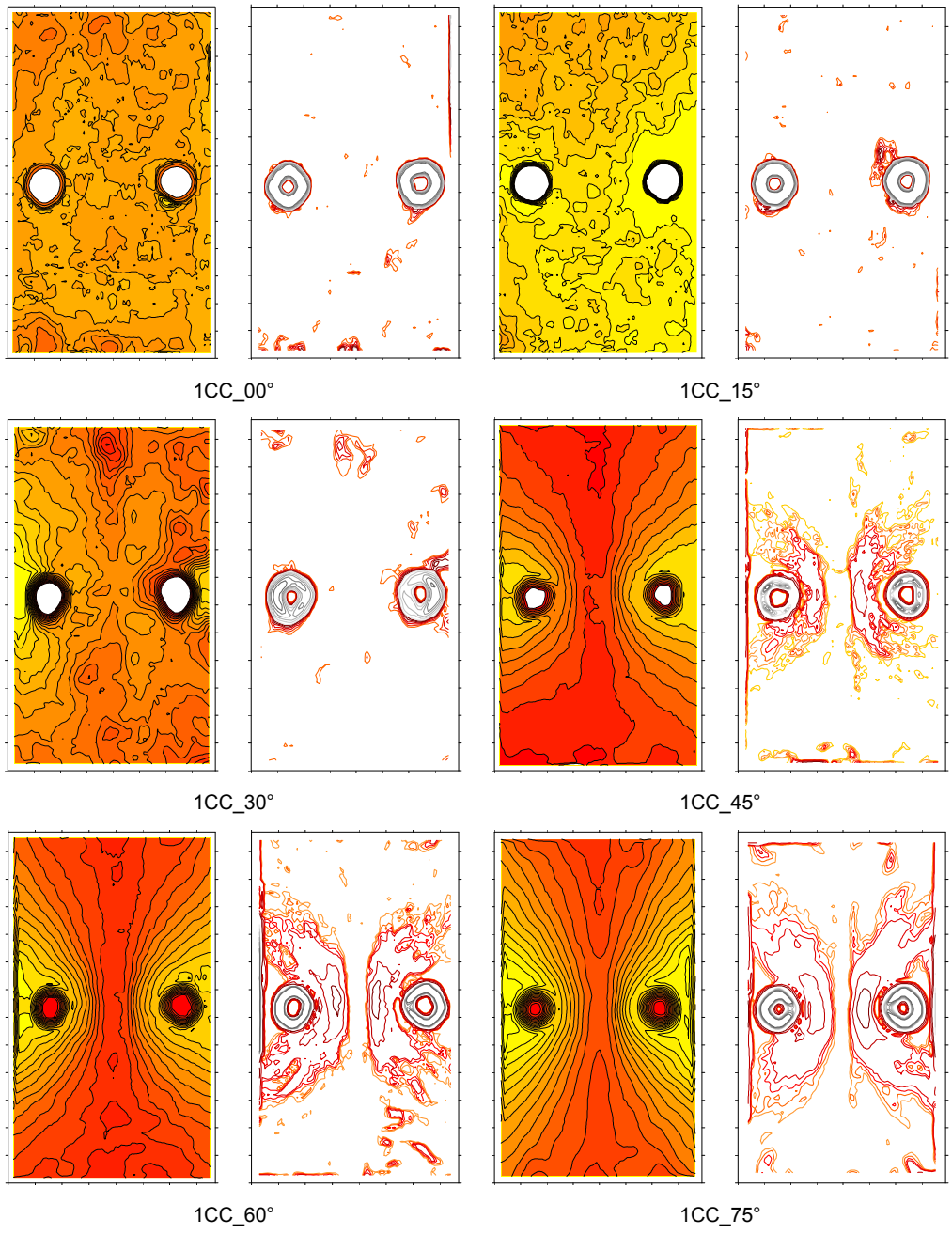

Figure 4.38 - T-stub flange residual deformations

Thus, is possible to state that a progressive increasing of the overall length of the yield lines can be observed with approximately a proportional relationship to the axial component of the load.

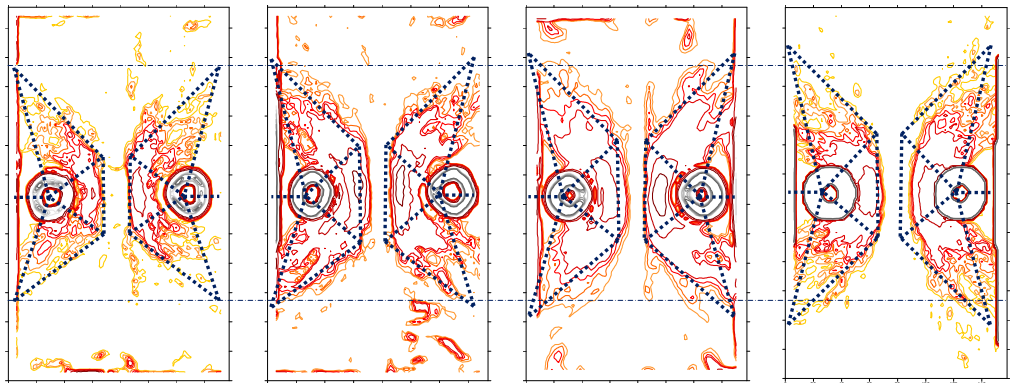

Figure 4.39 - T-stub flange mechanisms

Further analyses and considerations about this aspect are presented in section 6.2.

5. NUMERICAL SIMULATIONS

In this chapter the results obtained from the F.E. analyses are presented. The F.E. method allows evaluating a great amount of data (stresses, strains, displacements, etc.) which usually cannot be determined during the experimental tests. The scope of this kind of investigations is not only to obtain a reliable representation of the specimens behaviour in terms of load-displacement curve but also to extend the results database to further load cases without the need of experimental tests.
The F.E. commercial software Abaqus v.6.8 was adopted to model the column T-stub specimens. All the simulations were carried out in the large displacements field, taking into account mechanical and geometrical nonlinearities.

5.1 F.E. models of column T-stubs

In general the first useful operation to perform at the beginning of a F.E. modelling procedure is to identify all the possible simplification hypotheses. For example geometry or loads symmetries allow to make the problem simpler, reducing the complexity of the model (and consequently the analysis of the problem) implementing only one part of the specimen.
In this case, due to particular loading condition, only one plane of symmetry was identified for tests under combined actions. The plane of symmetry corresponded with the mid plane of the T-stub web, so only one half of the specimen was modelled as shown in Figure 5.1.

5.1.1 Model parts

The T-stub models were characterized by five different parts: a T-stub, a rigid support, a bolt, and two washers (Figure 5.2). Each part was defined taking into account the actual average dimensions assessed experimentally for each type of specimen.

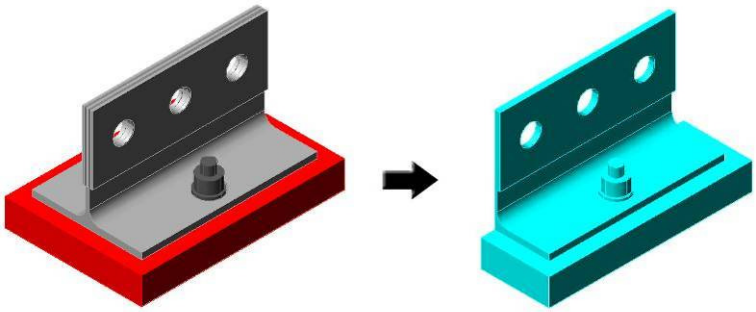

Figure 5.1 - Simplification of the F.E. models due to symmetry

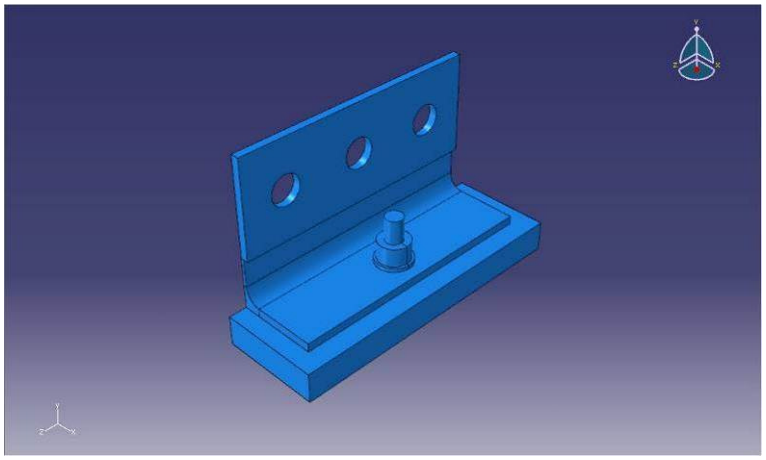

Figure 5.2 - Model parts assembly

A particular attention was paid to model the bolts because the failure of the specimens was related in all the cases to the bolts fracture. It is necessary to underline that the bolt was composed by four different solids interacting by contact surfaces. An exception was made for the nut which was coupled to the bolt shank so as to behave like a single solid element. This solution was selected to obtain the best compromise between simplicity of the modelling procedure and efficacy of the F.E. model. The bolt shank was modelled taking into account the section's reduction in correspondence of its threaded part. The reduction of the bolt diameter in the threaded part of the shank was made in order to obtain in this region an area of the shank section equal to the "effective" one (Figure 5.3). Thus was possible to consider the variation of stiffness and strength between the threaded and unthreaded parts of the shank. For a M20 bolt the unthreaded part of the shank has an area of 314 mm² while the threaded one has an

area of 245 mm². This led to a reduction of the bolt diameter in the threaded region from 20 mm to 17.662 mm.
As a consequence of this operation also the geometry of the nut was modified. The hole in the nut was reduced to the same diameter of the threaded part of the shank as to keep a perfect coupling between the two parts.

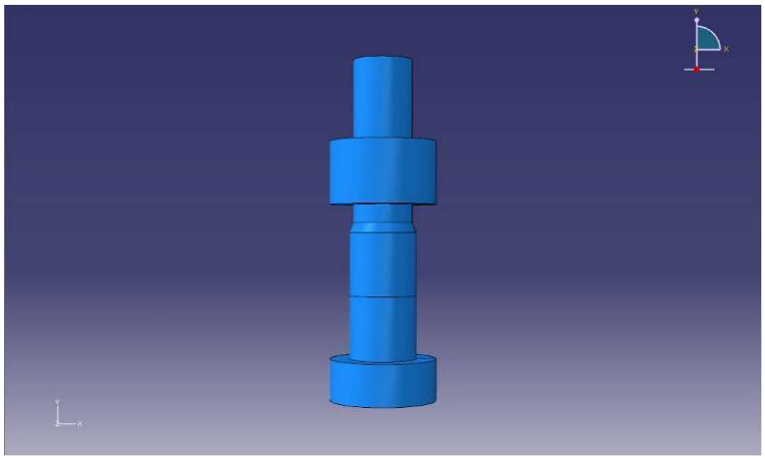

Figure 5.3 - Bolt model

In the model assembly, in order to reproduce the exact experimental conditions and avoid slips of the T-stub on the rigid support at "low" load levels, the bolt was positioned not concentrically to the holes. In detail the T-stub was "shifted" in the direction of the shear force to put in contact the bolt shank whit the holes in the T-stub flange and in the rigid support respectively. This allowed also to eliminate numerical problems due to rigid body motion of the T-stub ensuring the contact between the different contact surfaces from the beginning of the analysis.

5.1.2 Materials constitutive laws

A further basic aspect in the model definition is the accurate characterization of the constitutive stress-strain relationships for the different materials. In the model four different materials were defined: the “T-stub material”, the “bolt material”, the “washer material” and the “rigid support material”.

For the rigid support and for the washers materials a simplified elastic-plastic bilinear stress-strain relationship was used due to their limited influence on specimen behaviour and to the difficulty to acquire more detailed data (Figure 5.4 and Figure 5.5).

The characterization of T-stub and bolt materials assumes instead a fundamental role in the implementation of the F.E. model. An accurate description of these material properties was essential in order to obtain a correct response of the F.E. model in comparison with the experimental tests. For this reason the constitutive laws of these two materials were obtained from tensile tests on both bolts and steel specimens. These curves were described by a suitable number of point achieved from the “true strain - true stress” experimental curves associated to the bolts and the T-stub material (Figure 5.6 and Figure 5.7).

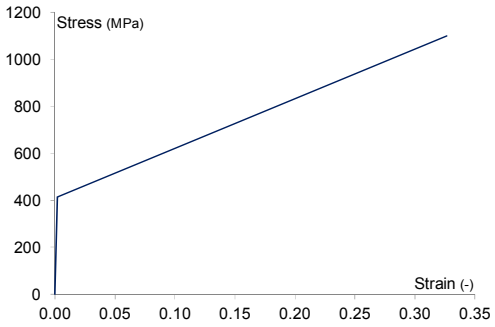

Figure 5.4 - Rigid support material

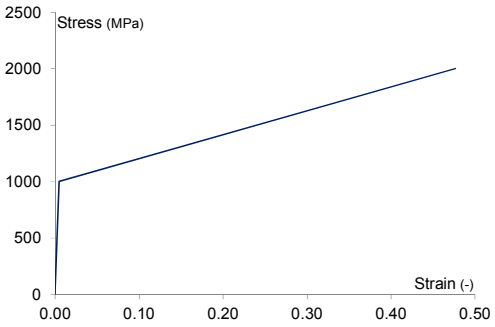

Figure 5.5 - Washers material

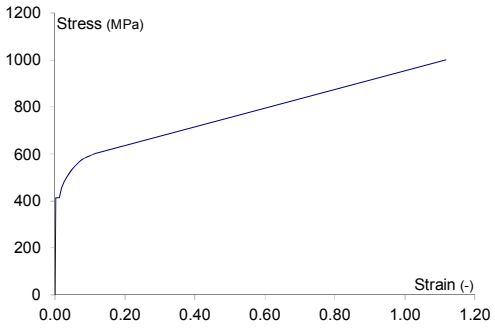

Figure 5.6 - T-stub material

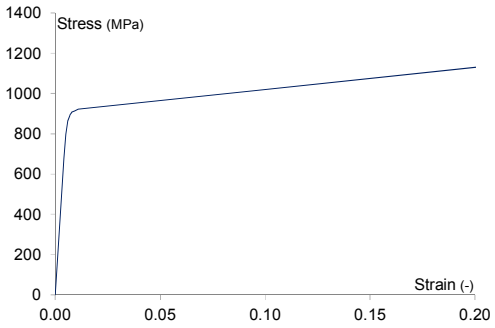

Figure 5.7 - Bolts material

5.1.3 Mesh definition

To create the mesh of the different parts two different data are necessary: the meshing technique and the finite element type. The first parameter depends on the geometrical complexity of the solids to be meshed while the second one depends mainly on the

type of analysis. In this study in the presented F.E. models a structured mesh was generally adopted, when this meshing method was not applicable due to geometrical irregularities it was substituted with a "swept mesh".
The finite element type selected for all parts (bolt, T-stub, washers, rigid support) was the C3D8R one, which is a three dimensional eight node element which permit to adopt a reduced integration formulation. The formulation of this element supports complex nonlinear analyses involving contact, plasticity, and large deformations. It adopts linear shape functions based on the nodal translational degrees of freedom to describe stress and strain fields. Furthermore the reduced integrated element doesn't suffer from “shear locking” behaviour. Shear locking frequently occurs in first order, fully integrated elements that are subjected to bending. The numerical formulation of the elements gives rise to shear strains that do not really exist (the so called "parasitic shear"). Therefore, these elements are too stiff in bending [58].
The size of the elements was selected so as to obtain especially in the bolt and across the T-stub flange thickness an adequate number of nodes to describe stress and strain distributions. These solutions in terms of meshing rule, element type and size were the result of an optimization process which involved a balance between the number of nodes (and hence the analysis processing time) and the solution accuracy (Figure 5.8).

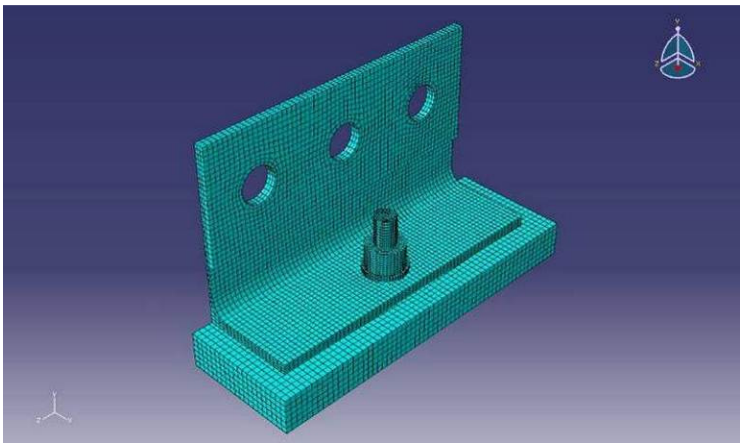

Figure 5.8 - T-stub model mesh

5.1.4 Definition of the interactions

The 3D F.E. models are composed as stated before by five different solid parts which interact each other. To allow the software to reproduce the contact phenomena the

characterization of six different contact zones called “interactions” was required (Figure 5.9). For each interaction two surfaces were respectively defined: the "master" and the "slave" ones.

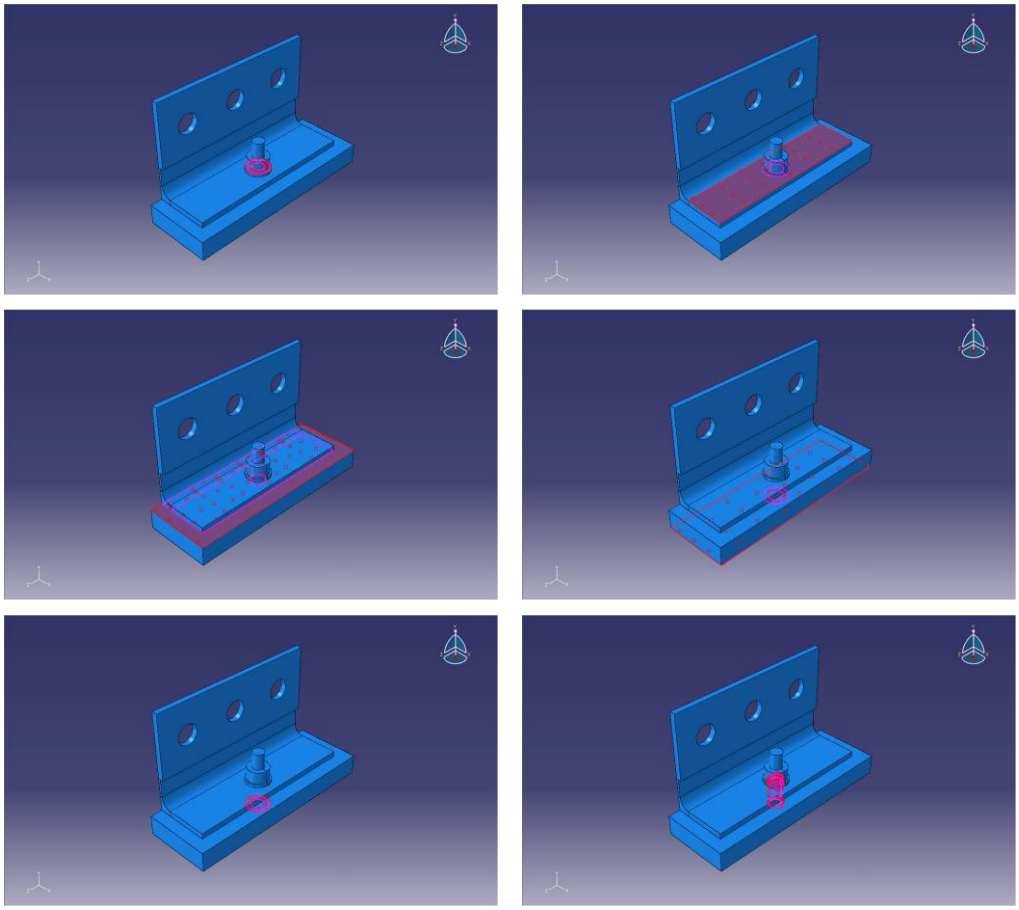

Figure 5.9 - T-stub interactions definition

The choice of the interactions formulation adopted in the final numerical models was made on the basis of the results of a wide number of preliminary numerical simulations. In these models the main difficulty in the definition of the different interactions was the calibration of all the parameters governing the contact formulation in order to reproduce in a suitable way the actual behaviour of the contact phenomena. At this aim a "trial and error" procedure was performed assuming as target reference the experimental results. Among the available formulations the "surface to surface" contact with finite sliding was selected. The "penalty" algorithm was adopted to describe both the normal and the tangential behaviour of the contact areas. For each of the six interactions the influence

of specific parameters like the friction coefficient, the penetration tolerance, etc. was checked. These parameters were assigned to the different interactions considering the physical surface properties. A higher value of penetration tolerance was assigned for example to the surfaces where a strong penetration due to the different hardness of the steel elements in contact (e.g. the T-stub flange and the washer) was experimentally observed. A similar approach was adopted for the friction coefficient, considering the roughness and the treatment of the different surfaces.

5.1.5 Definition of loads and boundary conditions

The last operation in the model completion was the definition of the loads and boundary conditions. As reported in paragraph 5.1 only a symmetry plane was used. On this plane is applied a “symmetry boundary condition” (Figure 5.10) to avoid displacements in the direction orthogonal to the symmetry plane to comply with the global equilibrium conditions of the model.

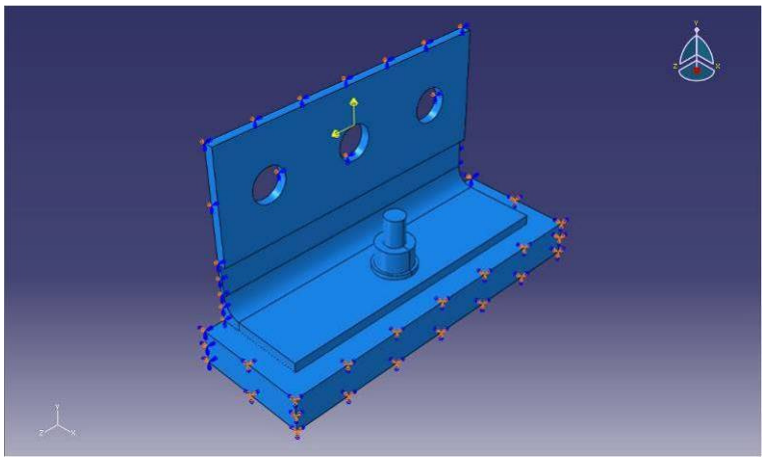

Figure 5.10 - Model loads and boundary conditions

Together with the symmetry boundary condition an “encastre" boundary condition was defined on the lateral surfaces of the rigid support.
The loading procedure was divided into three different steps. In the first step a pretension load of 125 kN was applied to the bolt (Figure 5.11), in the second step the external loads were increased up to collapse and in the third step the external loads were removed.

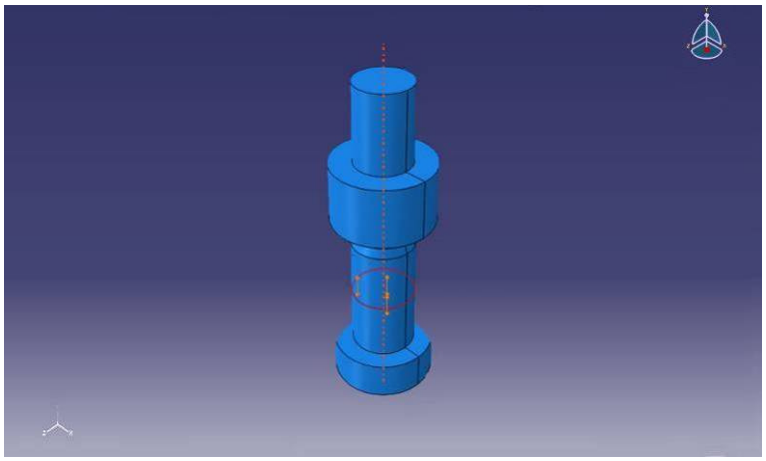

Figure 5.11 - Application of the bolt pretension load

The external loads represented by a shear and a tension force were applied at the T-stub web as shown in Figure 5.10. To apply the external loads avoiding local stress concentrations the application of an internal “tie multipoint constrain” was necessary (Figure 5.12). This constrain allowed also to eliminate the moment generated by shear force forcing the holes to move together like in the experimental procedure described in paragraph 4.2.2.

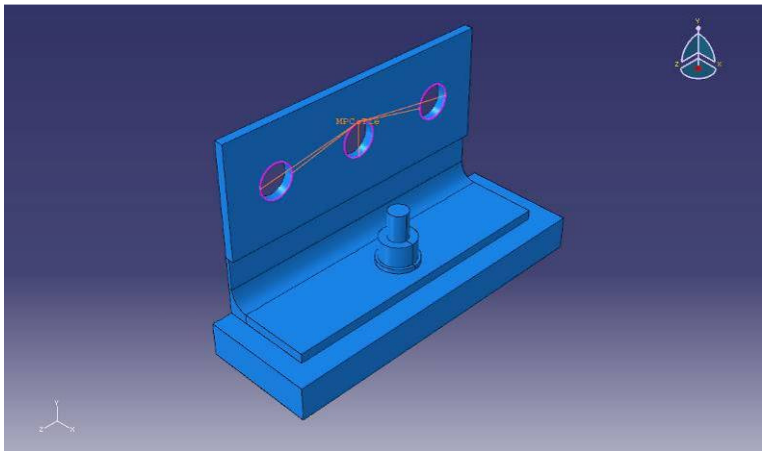

Figure 5.12 - Internal multipoint constrain

5.2 Numerical results

In this paragraph the experimental results are commented and compared with the ones obtained from the numerical simulations. A first comparison was done in terms of load-

displacement curves, while a second analysis was carried out comparing the residual deformations of bolts and steel plates (column flanges and end-plates).

5.2.1 Load-displacement curves

The numerical investigations simulated all the tests performed on the column T-stubs, starting from the pure tension loading condition up to the pure shear one. In the graphs reported in the following pages the red continuous curves refer to the experimental results while the blue dashed ones represent the numerical results.
In general a good agreement between the (average) experimental response and the numerical one was achieved for each angle of the test. A complete comparison between the numerical and experimental load-displacement results is reported in Figure 5.13 to Figure 5.19 for an inclination angle $\varphi = 45°$. In general, the initial stiffness of the specimen extrapolated from the simulations was slightly underestimated in the curves related to the transducers placed above the "bolt line" (TR03-04-05-06-09-10-13) while a little underestimation can be observed for the transducers under the bolt line (TR07-08-11-12-14). This was confirmed for all the different values of φ, as shown in Figure 5.20 to Figure 5.24 which refer to the load-displacement curves of TR13 and TR14 transducers. However, the difference from the average experimental behaviour can be considered negligible. This small deviation from the experimental results may be due to the non perfect representation of the load application procedure, of the pre-tensioning process of the bolts and the friction phenomena acting between the various parts of the model that could affect the response of the specimen. All these aspects were obviously reproduced in a simplified way in the F.E. models. In addition, the numerical models in general have no geometrical imperfections that may influence, even if in a limited way, the global response of the specimen.
The numerical evaluation of the "yielding" of the T-stub well approximated the experimental evidence. The "knee" in the load-displacement curves which characterize the transition between the elastic and the inelastic behaviour is in general coincident with the experimental data. It was possible to observe a limited overestimation of the post-elastic stiffness at the beginning of the hardening branch. However, the slope of the branch tended to rapidly decrease and approximate quite well the experimental data up to collapse.

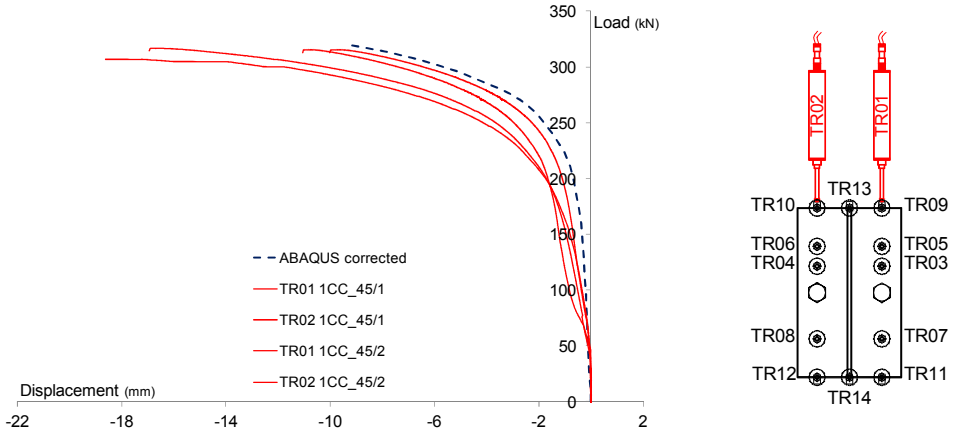

Figure 5.13 - TR01-02 numerical and experimental curves for φ = 45°

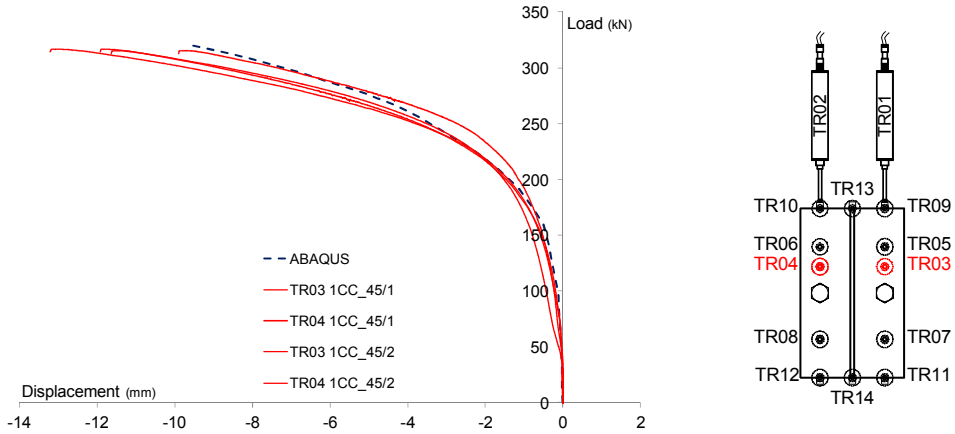

Figure 5.14 - TR03-04 numerical and experimental curves for φ = 45°

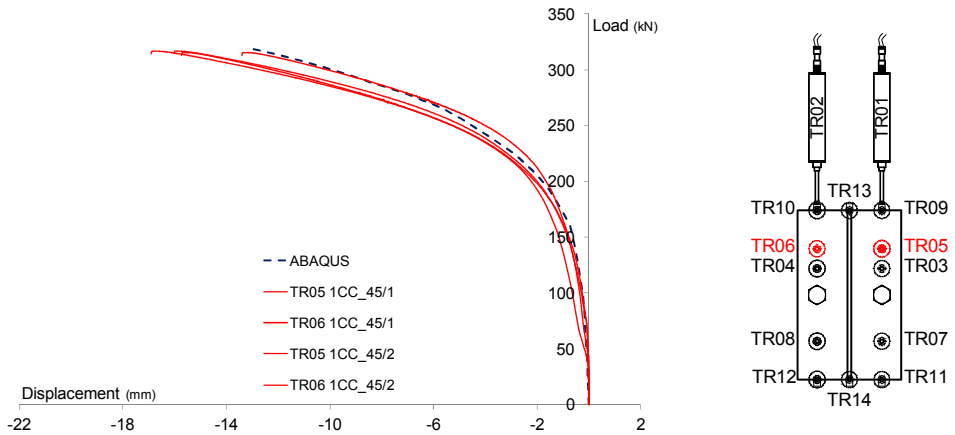

Figure 5.15 - TR05-06 numerical and experimental curves for φ = 45°

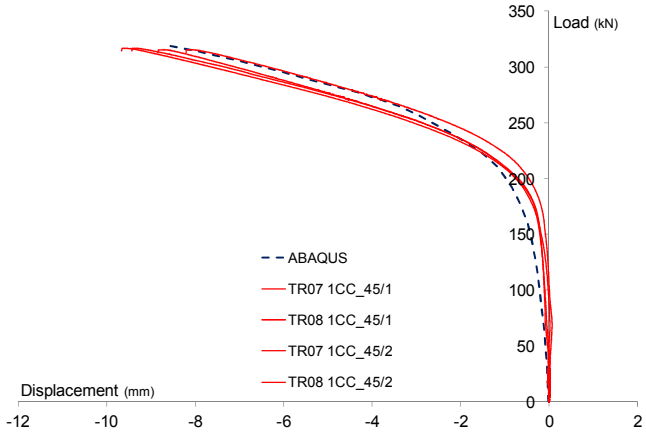

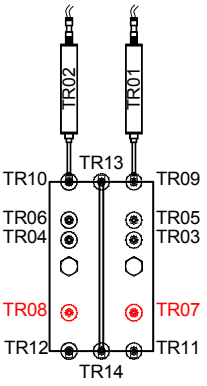

Figure 5.16 - TR07-08 numerical and experimental curves for φ = 45°

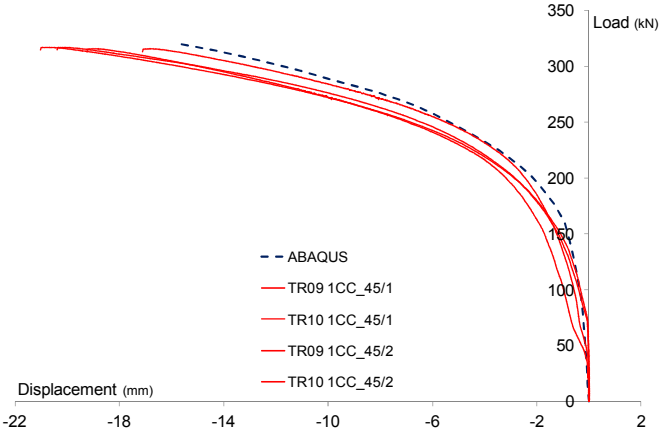

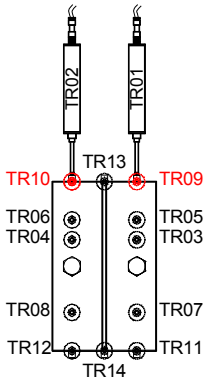

Figure 5.17 - TR09-10 numerical and experimental curves for φ = 45°

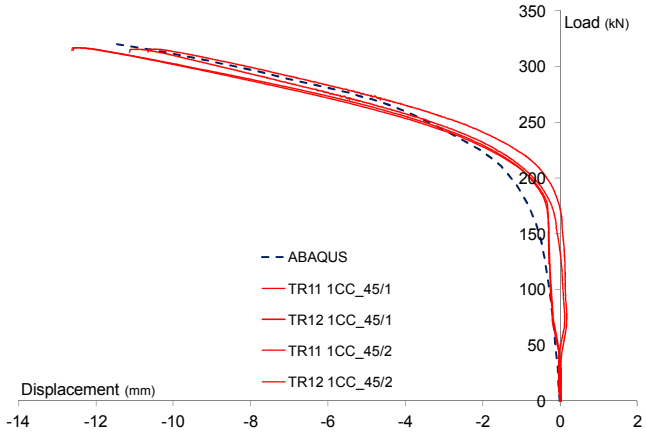

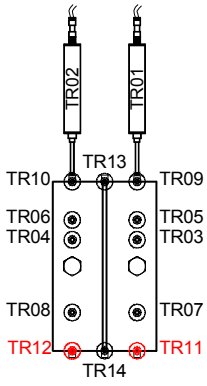

Figure 5.18 - TR11-12 numerical and experimental curves for φ = 45°

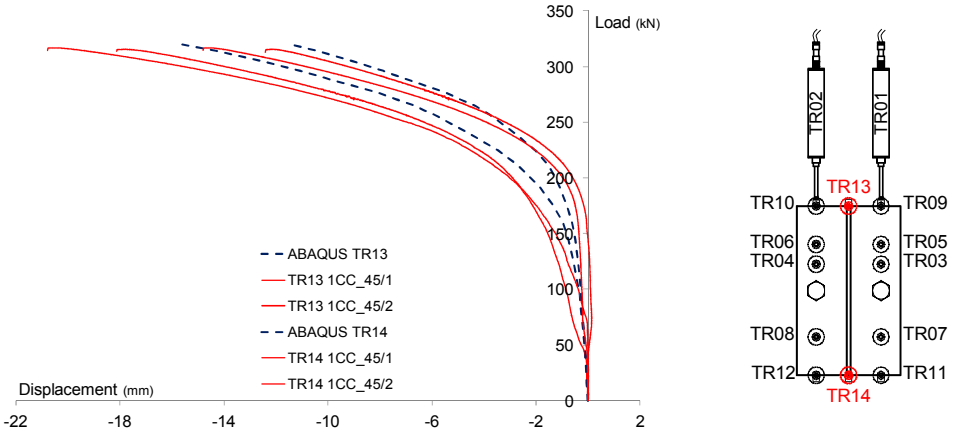

Figure 5.19 - TR13-14 numerical and experimental curves for φ = 45°

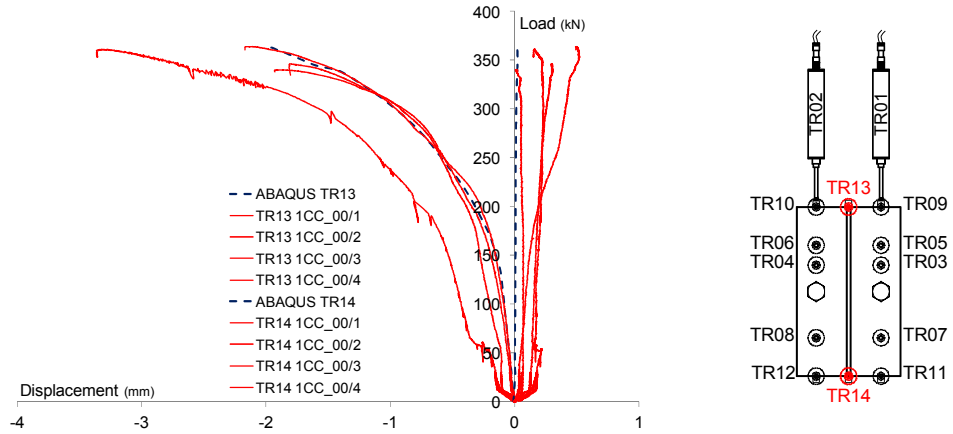

Figure 5.20 - TR13-14 numerical and experimental curves for φ = 0°

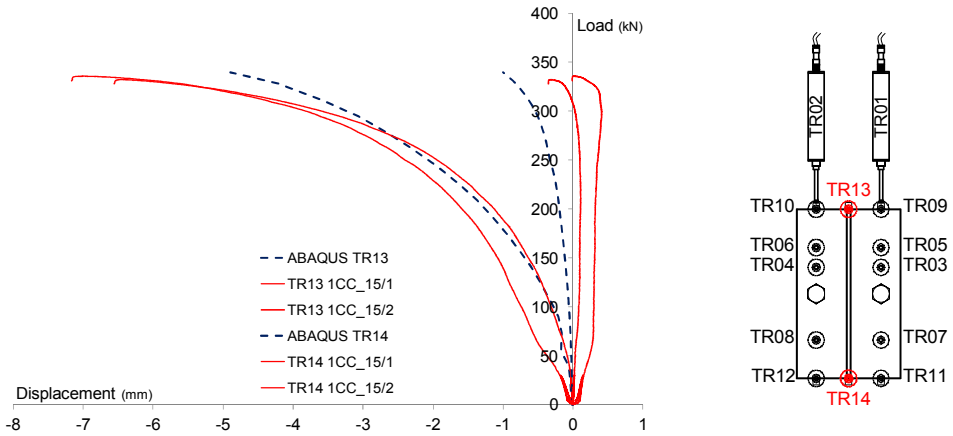

Figure 5.21 - TR13-14 numerical and experimental curves for φ = 15°

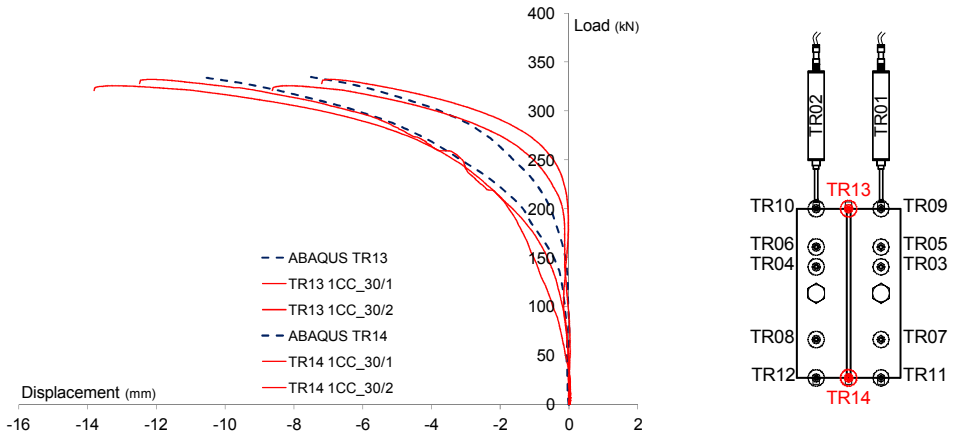

Figure 5.22 - TR13-14 numerical and experimental curves for φ = 30°

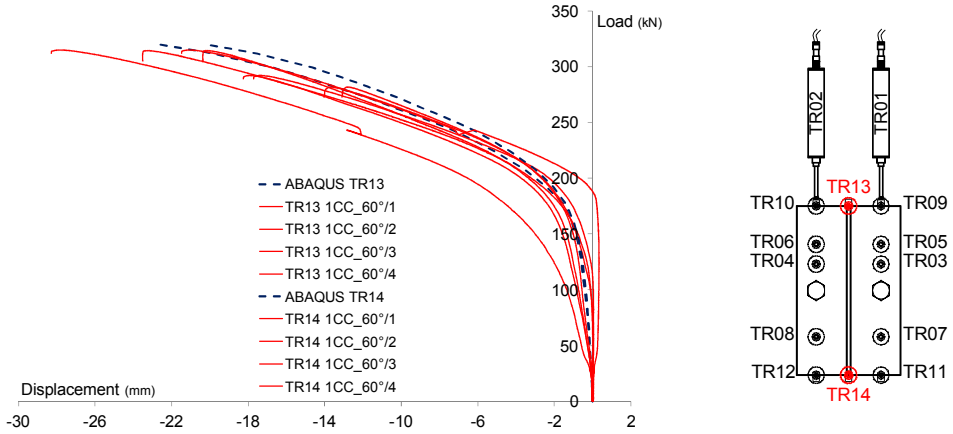

Figure 5.23 - TR13-14 numerical and experimental curves for φ = 60°

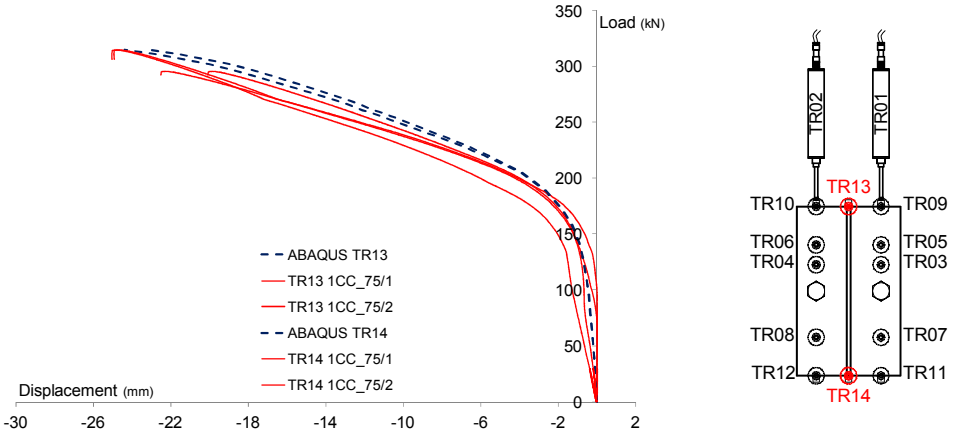

Figure 5.24 - TR13-14 numerical and experimental curves for φ = 75°

The only significant difference concerned the ultimate deformation capacity of the model that sometimes appeared numerically underestimated if compared with experimental results. Also in this case this behaviour was mainly related to the transducers placed above the bolt line. However, the difference was small enough to consider the numerical models sufficiently accurate.

Difficulties in reproducing the response of the vertical transducers TR01 and TR02 were encountered. They were mainly associated to the particular "acquisition conditions" as explained in paragraph 4.2.3.

Considering this aspect, a similar transformation to the one presented in Figure 4.27 for the experimental data, was applied to the numerical result, in order to mathematically simulate the presence of the screw in the numerical models.

From the real longitudinal and transverse displacements obtained from Abaqus, through a post-processing operation, it was possible to obtain the "corrected" curves associated to TR01 and TR02 transducers (Figure 5.25÷Figure 5.29). The numerical curves showed an initial stiffer behaviour and lower displacement at collapse than the ones experimentally observed.

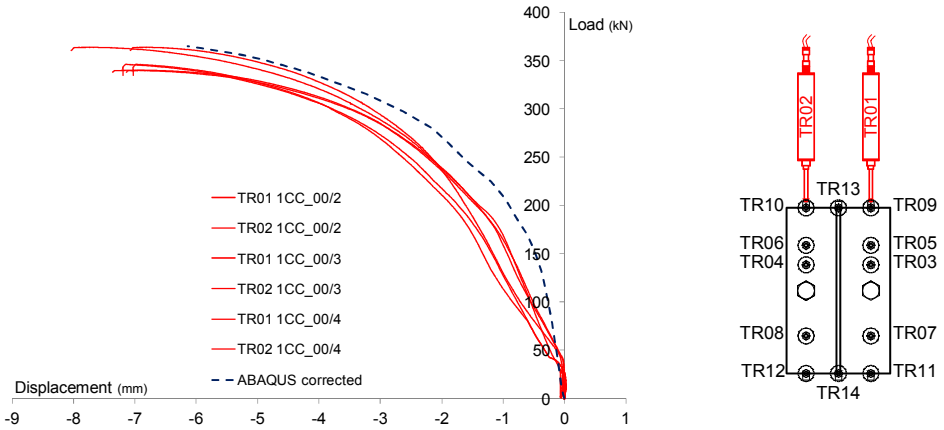

Figure 5.25 - TR01-02 numerical and experimental curves for φ = 0°

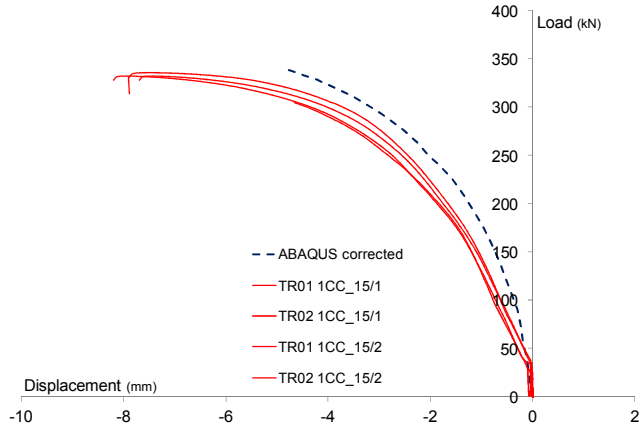

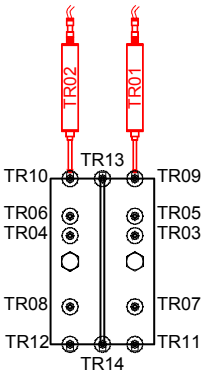

Figure 5.26 - TR01-02 numerical and experimental curves for φ = 15°

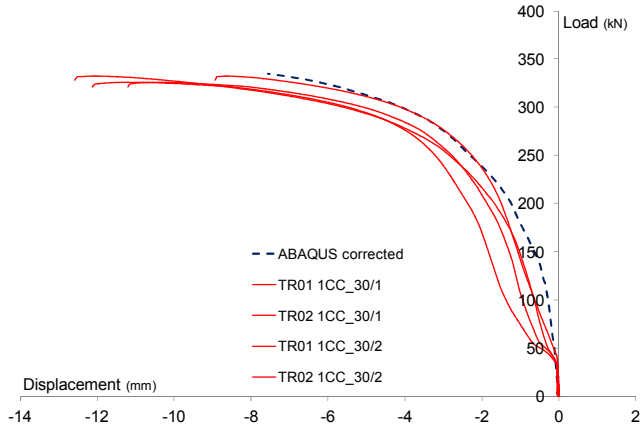

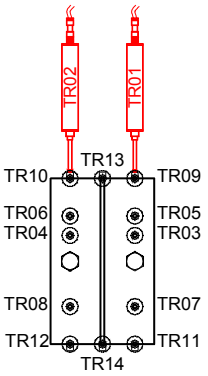

Figure 5.27 - TR01-02 numerical and experimental curves for φ = 30°

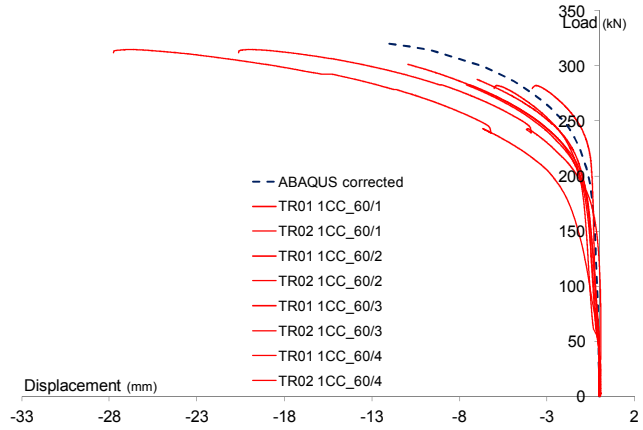

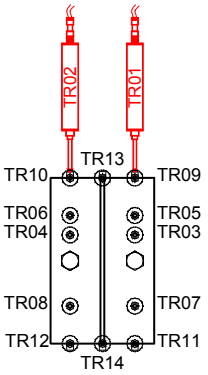

Figure 5.28 - TR01-02 numerical and experimental curves for φ = 60°

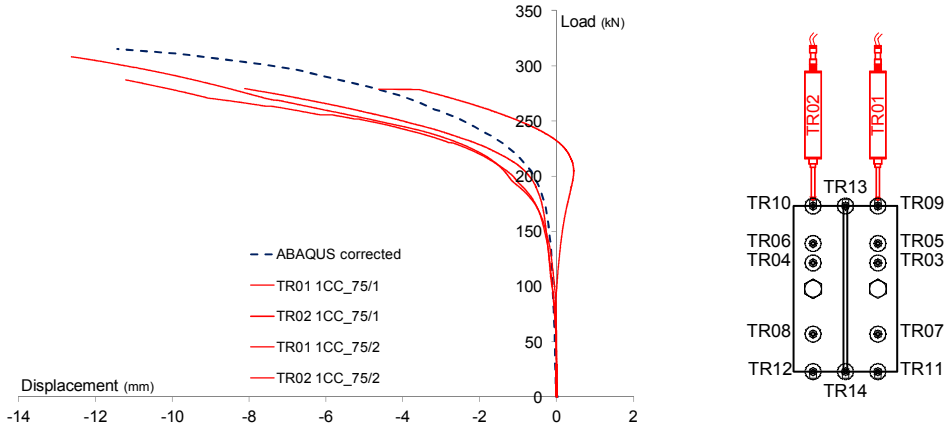

Figure 5.29 - TR01-02 numerical and experimental curves for φ = 75°

5.2.2 F-φ relationship and N-V domain

The good response of the F.E. models was also confirmed by the comparison between the numerical and experimental collapse loads. Both the F-φ relationship (Figure 5.30) and the N-V domain (Figure 5.31) show a very good agreement with the ones experimentally evaluated.

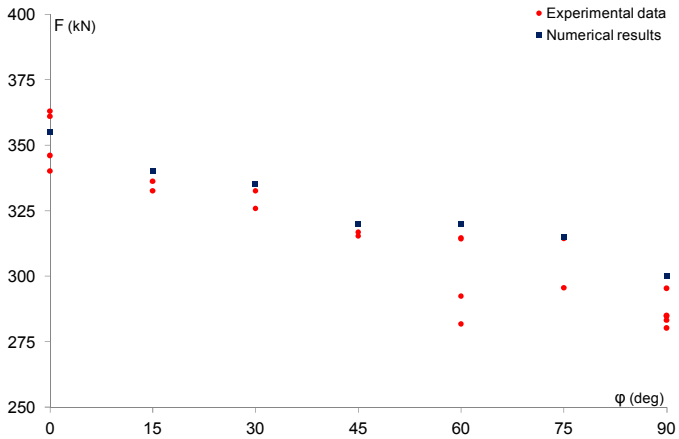

Figure 5.30 - Numerical F-φ relationship

The collapse loads obtained from the numerical simulations tends to be a little overestimated respect to the experimental data. However, the difference is negligible and in general is possible to consider the numerical results as an upper bound in the evaluation of the collapse loads.

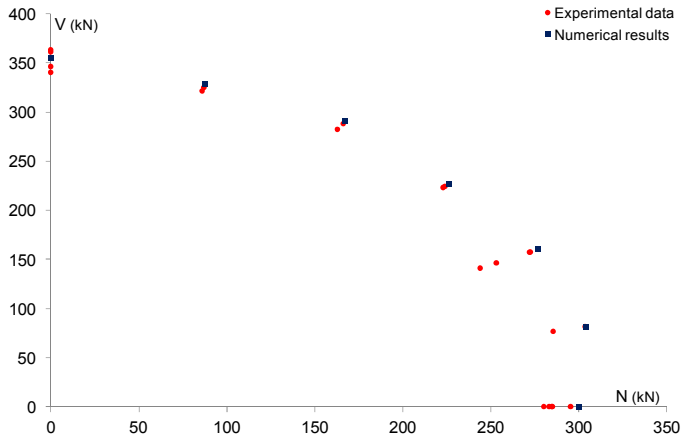

Figure 5.31 - Numerical N-V domain°

5.2.3 Residual deformations

As introduced in paragraph 5.1.5 the loading history of the numerical model was subdivided into three different load step. (Figure 5.32). The "preload" and the "collapse" steps were necessary to reproduce in a suitable way the loading process, considering also the tightening of the bolt. The "unload" step instead was carried out in order to remove the external load from the specimen so to evaluate the residual plastic deformations of the T-stub flange. The obtained data were compared with the experimental ones achieved from the laser scanning of the specimen performed after the experimental tests (Figure 5.33 ÷ Figure 5.39).

In analogy with the experimental data, for the numerical results a colour scale, representative of the magnitude of the residual deformation of the plate was adopted. The white colour indicates areas in which the deformations is very small or negligible, while for increasing deformations the colour turns to dark blue.

The comparison between the residual deformations obtained from the F.E. models and the experimental ones using laser showed remarkable similarities. The developments of the contour lines (level lines and slope lines) of the plates were in fact almost coincident.

The first aspect that can immediately be observed was, also for the numerical results, the strong asymmetry in the flange deformations for low values of the inclination angle of the external load φ. The asymmetry involved mainly the lower part of the flange,

while the upper one did not present significant differences in terms of flange mechanism shape.

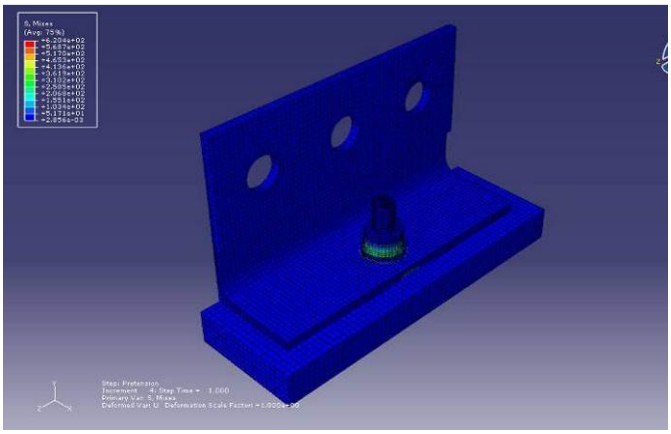

a) preload

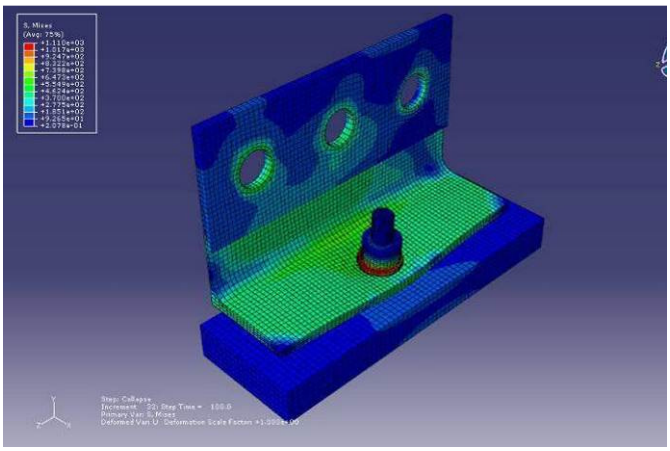

b) collapse

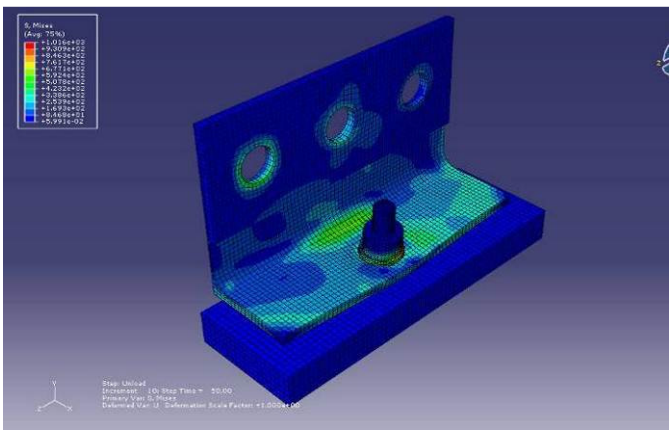

c) unload

Figure 5.32 - Preload, collapse and unload load steps

In the representations of Figure 5.33 ÷ Figure 5.39 the plates are upside-down respect to their original position during the tests. This means that the shear force direction is from the down side to the up side of the plate.

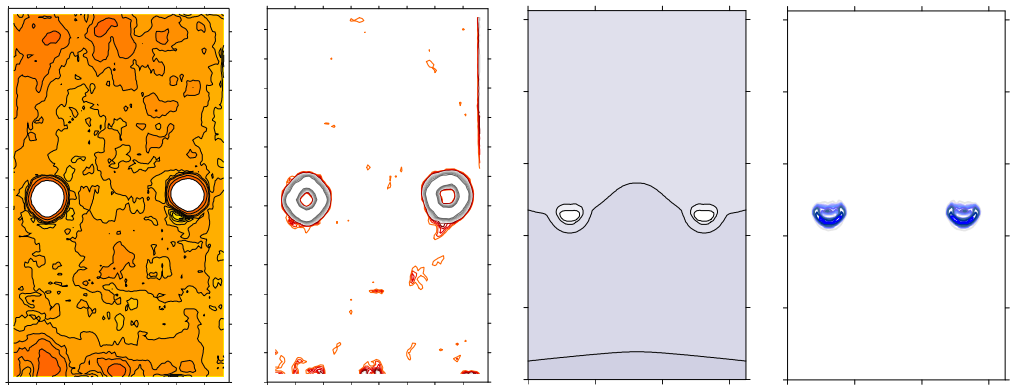

Figure 5.33 - Experimental and numerical flange deformations for φ = 0°

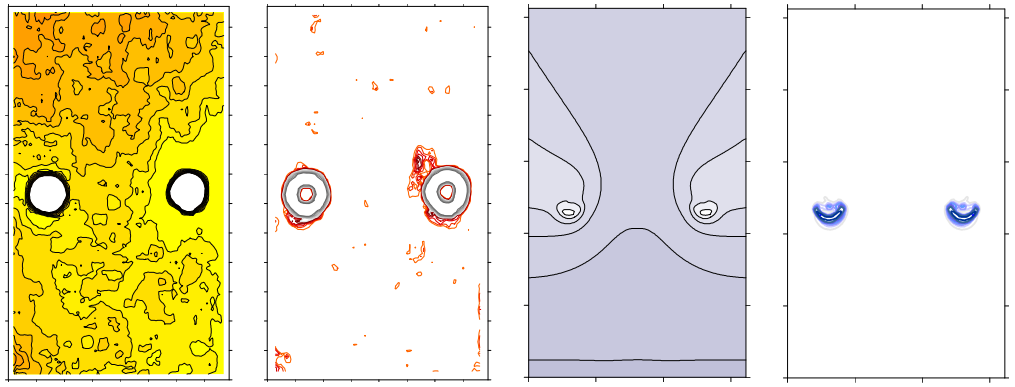

Figure 5.34 - Experimental and numerical flange deformations for φ = 15°

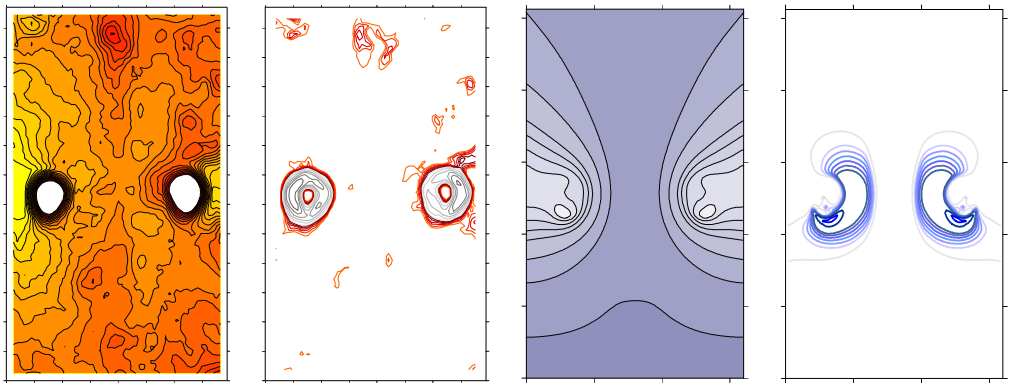

Figure 5.35 - Experimental and numerical flange deformations for φ = 30°

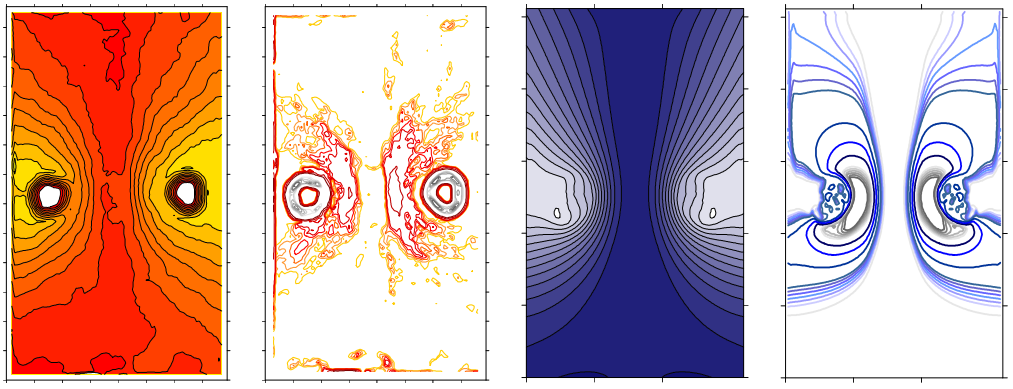

Figure 5.36 - Experimental and numerical flange deformations for φ = 45°

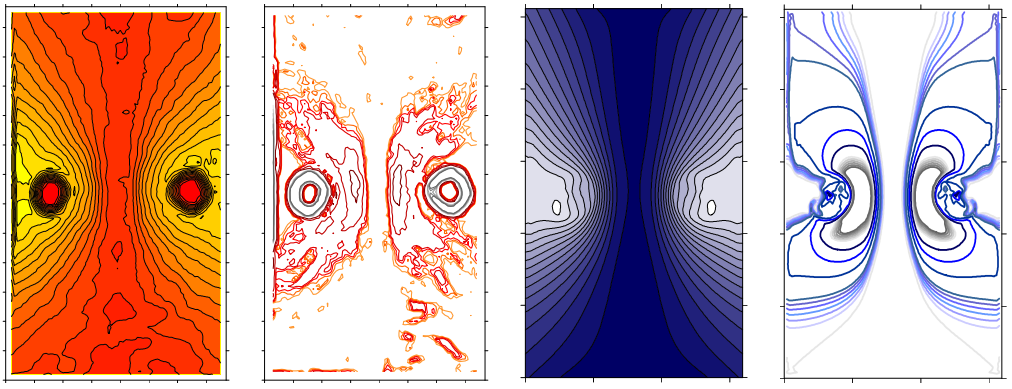

Figure 5.37 - Experimental and numerical flange deformations for φ = 60°

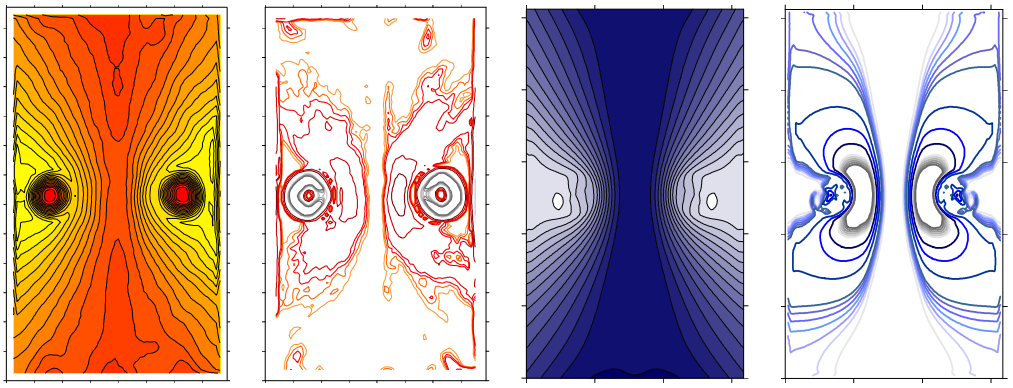

Figure 5.38 - Experimental and numerical flange deformations for φ = 75°

For φ = 30° the numerical results in terms of level lines showed the presence of a flange mechanism, but observing the slope lines it was clear that this mechanism involved only a limited area around the bolts. So, as evidenced experimentally a complete flange mechanism developed only for φ ≥ 45°, with the formation of two main yield lines, one at the bolt level and one at the web level.

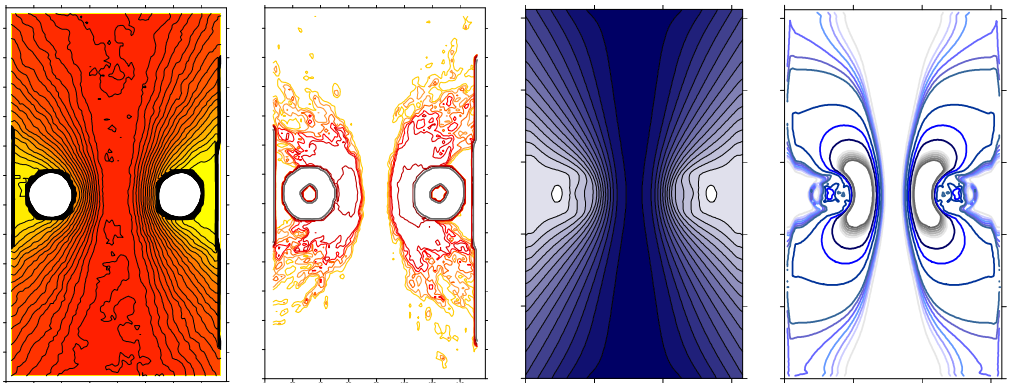

Figure 5.39 - Experimental and numerical flange deformations for φ = 90°

A further qualitative comparison can be done between the pictures took after the experimental tests and the deformed shape at collapse obtained from the models. Figure 5.40 to Figure 5.42 show a comparison of the specimens deformations for values of φ respectively of 15°, 45° and 75°.

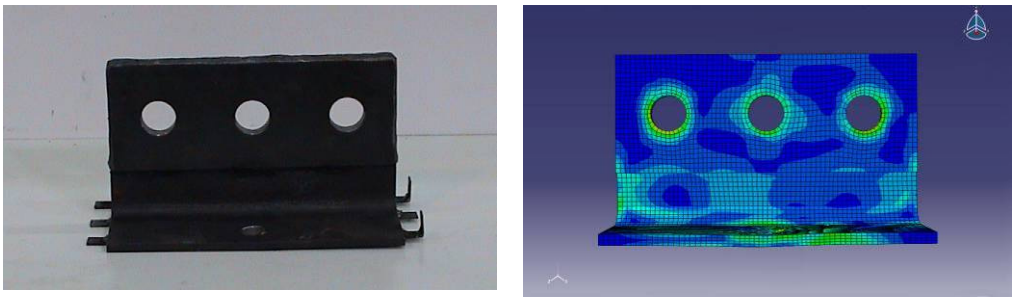

Figure 5.40 - Experimental and numerical specimen deformations for φ = 15°

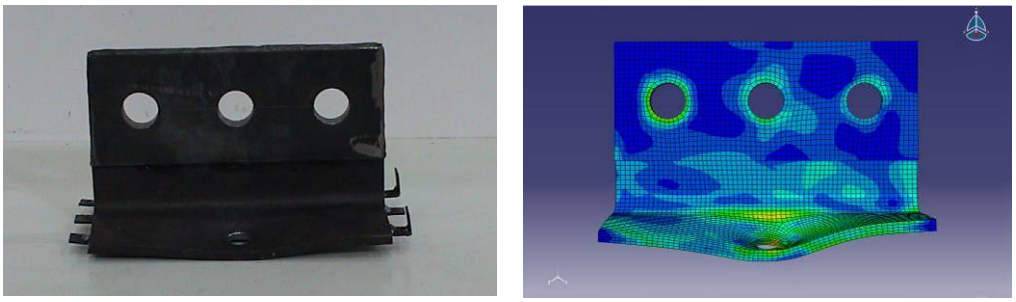

Figure 5.41 - Experimental and numerical specimen deformations for φ = 45°

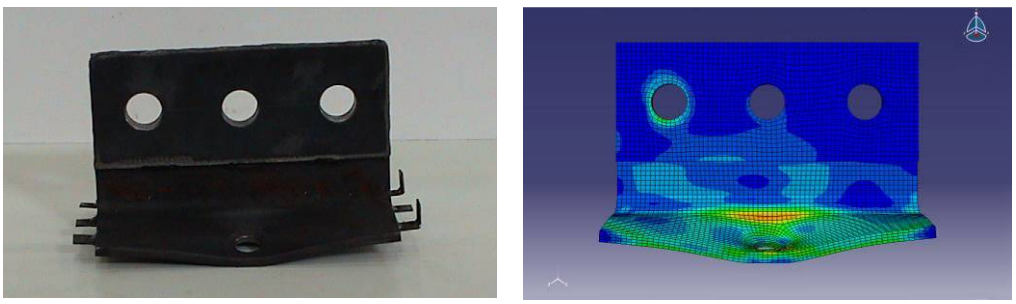

Figure 5.42 - Experimental and numerical specimen deformations for φ = 75°

The ultimate condition of the specimen was always associated to bolts failure. Their deformations in correspondence of the collapse load are compared in Figure 5.43 ÷ Figure 5.45.

Figure 5.43 - Experimental and numerical specimen deformations for φ = 15°

Figure 5.44 - Experimental and numerical specimen deformations for φ = 45°

Figure 5.45 - Experimental and numerical specimen deformations for φ = 75°

The flexural behaviour of the bolt is well represented by the numerical model. Both the magnitude of bending on the bolt and the phenomena of local necking of the shank were reproduced adequately. Difficulties in simulate the effect of pure shear on the bolt were encountered. The characterization of the model with the finite element method did

not allow to identify the failure surface as clearly as in the experimental tests where a dislocation of the bolt shank occurred in correspondence of the slip plane between the T-stub and the rigid support. This limit is due to purely numerical problems, to respect the congruence principle in the F.E. method no abrupt changes in the solid geometry are allowed.

6. ANALITICAL EVALUATION OF THE FLANGE MECHANISM

In this section an analytical evaluation of the flange failure mechanism of bolted connections is presented. The analysis is based on the kinematic theorem of the limit analysis, in order to get an estimation of the yield load associated to the development of flange mechanisms.

6.1 Connection under tension load

6.1.1 Zoetemeijer's model

As introduced in paragraph 3.2.1.3, this approach was originally adopted by Zoetemeijer [44] to evaluate the yield load of T-stub connections (Figure 6.1) subjected to tension. Zotemeijer's method was based on the development of plasticized areas in the T-stub flange, called yield lines. Along these yield lines plastic hinges were expected to grow in order to dissipate energy.

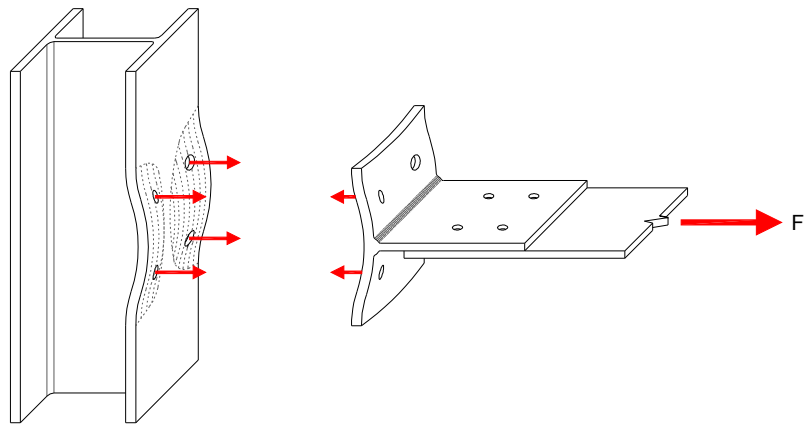

Figure 6.1 - T-stub connection

Two possible mechanisms were supposed to form: the first one, called “mechanism I” assumed that the bolt failure was the determining factor, while in the “mechanism II” the failure was related to the plasticization of the flange plate. In the next paragraph the attention focuses on the formulation of the mechanism II, which is the one that exhibit a ductile behaviour, activating a complete flange mechanism.

6.1.1.1 Hypothesis

In Zotemeijer’s mechanism II the development of prying forces due to the applied tensile force caused the formation of plastic hinges at the bolt line and near the T-stub web as shown in Figure 6.2. A simple plastic theory was adopted to describe the flange failure, under the hypothesis of negligible elastic deformations of the flange, negligible membrane effects in the T-stub flange and assuming that the bolt shank deformation did not dissipate energy.

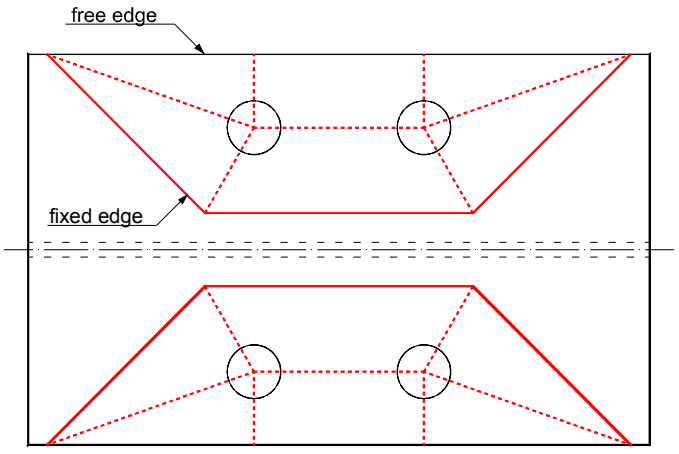

Figure 6.2 - Collapse mechanism II

6.1.1.2 Definition of the flange mechanism

The failure mechanism was described in function of the geometry of the plate. The variables of the problem were the plastic deflection of the plate δ_v and the two angles α and β (Figure 6.3). The problem was to appraise the values of α and β which gave the lowest value of the collapse load N. In other words it was necessary to indentify, between all the possible yield lines families the one which minimize the collapse load.

Zoetemeijer described the flange mechanism for a bolted T-stub with two bolt rows by ten different yield lines. For each of them the internal dissipation of energy ΔE_i was calculated. The sum of all the contributions ΔE_i is equated to the work done by the external tensile load ΔF (neglecting the elastic energy). Due to the symmetry of the problem for simplicity only one half of the mechanism was considered.

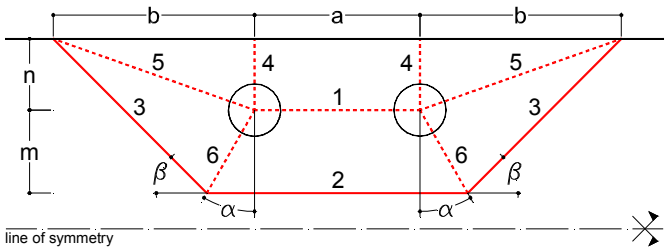

Figure 6.3 - Yield lines layout of mechanism B

6.1.1.3 Energy balance equations

As reported in the previous paragraph the problem was formulated in term of energy balance equations:

$$\Delta F = \Delta E = \sum_{i=1}^{n} \Delta E_i \tag{6.1}$$

where n is the number of yield lines necessary to describe the flange failure mechanism. The internal dissipation of energy of the i-th yield line was calculated as:

$$\Delta E_i = L_i \cdot \Phi_i \cdot m_{pl} \tag{6.2}$$

where:

- L_i is the length of the i-th yield line (if two yield lines have the same number L_i is calculated as the sum of the length of that yield lines: $L_i = L_i^{left} + L_i^{rigth}$);
- Φ_i is the plastic rotation in correspondence of the i-th yield line;
- m_{pl} is the plastic moment per unit length of the flange plate and it is given by:

$$m_{pl} = \frac{f_y \cdot t^2}{4} \tag{6.3}$$

In the following the equations of ΔE_i are summarized. For further information about their analytical evaluation see [44]:

1. *yield line 1:*

$$L_1 = a \tag{6.4}$$

$$\Phi_1 = \frac{\delta_v}{m} \tag{6.5}$$

$$\Delta E_1 = a \cdot \frac{\delta_v}{m} \cdot m_{pl} \tag{6.6}$$

2. *yield line 2:*

$$L_2 = a + 2 \cdot m \cdot \tan(\alpha) \tag{6.7}$$

$$\Phi_2 = \frac{\delta_v}{m} \tag{6.8}$$

$$\Delta E_2 = (a + 2 \cdot m \cdot \tan\alpha) \cdot \frac{\delta_v}{m} \cdot m_{pl} \tag{6.9}$$

3. *yield line 3:*

$$L_3 = 2 \cdot \frac{m + n}{\sin\beta} \tag{6.10}$$

$$\Phi_3 = \frac{\delta_v}{\frac{m}{\cos\alpha} \cdot \cos(\beta - \alpha)} \tag{6.11}$$

$$\Delta E_3 = 2 \cdot \frac{m + n}{\sin\beta} \cdot \frac{\cos\alpha}{\cos(\beta - \alpha)} \cdot \frac{\delta_v}{m} \cdot m_{pl} \tag{6.12}$$

4. *yield line 4:*

$$L_4 = 2 \cdot n \tag{6.13}$$

$$\Phi_4 = \frac{\delta_v}{b} \tag{6.14}$$

$$\Delta E_4 = 2 \cdot \frac{n}{b} \cdot \delta_v \cdot m_{pl} \tag{6.15}$$

5. yield line 5:

$$L_5 = 2 \cdot \sqrt{b^2 + n^2} = 2 \cdot l_5 \tag{6.16}$$

$$\Phi_5 = \frac{\delta_v}{l'_5} \cdot \frac{l'''_5}{l_5} - \frac{\delta_v - \delta_v \cdot \frac{l'''_5}{l_5}}{l''_5} \tag{6.17}$$

$$\Delta E_5 = \sqrt{b^2 + n^2} \cdot \left(\frac{l'''_5}{l_5 \cdot l'_5} - \frac{1}{l''_5} + \frac{l'''_5}{l_5 \cdot l''_5} \right) \cdot \delta_v \cdot m_{pl} \tag{6.18}$$

where l'_5, l''_5 and l'''_5 are the quantities represented in Figure 6.4. They can be simplified and expressed in terms of α, β, b, m, and n as follows:

$$\Phi_5 = \frac{1}{l_5} \left(\frac{c}{\frac{m}{\cos\alpha} \cdot \cos(\beta - \alpha)} + \frac{b}{n} + \frac{{l_5}^2}{b \cdot n} \right) \tag{6.19}$$

with:

$$c = \left(\frac{m}{\cos\alpha} \cdot \cos(\beta - \alpha) + \frac{n}{\cos(\beta)} \right) \cdot \cot(\beta) \tag{6.20}$$

Thus:

$$\Delta E_5 = 2 \cdot \left(\cot\beta + \frac{n}{m} \cdot \frac{\cos\alpha}{\sin\beta \cdot \cos(\beta - \alpha)} - \frac{n}{b} \right) \cdot \delta_v \cdot m_{pl} \tag{6.21}$$

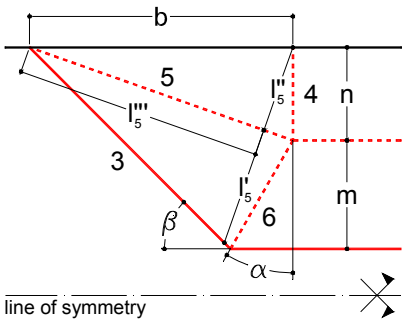

Figure 6.4 - Yield line 5 geometrical parameters

6. *yield line 6:*

$$L_6 = 2 \cdot \frac{m}{\cos\alpha} \tag{6.22}$$

$$\Phi_6 = \frac{\delta_v}{m} \cdot \frac{\sin\beta}{\cos(\beta - \alpha)} \tag{6.23}$$

$$\Delta E_6 = 2 \cdot \frac{m}{\cos\alpha} \cdot \frac{\delta_v}{m} \cdot \frac{\sin\beta}{\cos(\beta - \alpha)} \cdot m_{pl} \tag{6.24}$$

Finally the equation of the total internal energy dissipation ΔE is obtained summing the energy contribution of each yield line and carrying out a simplification:

$$\Delta E = \sum_{i=1}^{6} \Delta E_i = 2 \cdot \left(\frac{a}{m} + \frac{m + 2 \cdot n}{m} \cdot \frac{\cos\alpha}{\sin\beta \cdot \cos(\beta - \alpha)} + \tan\alpha + \cot\beta + \right. \\ \left. + \frac{\sin\beta}{\cos\alpha \cdot \cos(\beta - \alpha)} \right) \cdot \delta_v \cdot m_{pl} \tag{6.25}$$

while the work done by the external load is equal to:

$$\Delta F = N \cdot \delta_v \tag{6.26}$$

where N is the tensile load acting on half of the T-stub element. Thus, equating the internal and external energies gives:

$$N \cdot \delta_v = 2 \cdot \left(\frac{a}{m} + \frac{m + 2 \cdot n}{m} \cdot \frac{\cos\alpha}{\sin\beta \cdot \cos(\beta - \alpha)} + \tan\alpha + \cot\beta + \right.$$
$$\left. + \frac{\sin\beta}{\cos\alpha \cdot \cos(\beta - \alpha)} \right) \cdot \delta_v \cdot m_{pl} \tag{6.27}$$

6.1.1.4 Prediction of the collapse load

The minimum value of the collapse load N is evaluated by minimizing the left hand side of the previous equation. This means to fulfil the following conditions:

$$\frac{\partial \sum_{i=1}^{6} \Delta E_i}{\partial \alpha} = 0 \tag{6.28}$$

$$\frac{\partial \sum_{i=1}^{6} \Delta E_i}{\partial \beta} = 0 \tag{6.29}$$

Carrying out the differentiation and simplifying, the equation of the energy balance can be rewritten as:

$$N \cdot \delta_v = 2 \cdot \left(\frac{a}{m} + \frac{6 \cdot m + 8 \cdot n}{\sqrt{3 \cdot m^2 + 4 \cdot m \cdot n}} \right) \cdot \delta_v \cdot m_{pl} \tag{6.30}$$

so the collapse load N is equal to:

$$N = \frac{2}{m} \cdot \left(a + \frac{6 \cdot m + 8 \cdot n}{\sqrt{3 + \frac{4 \cdot n}{m}}} \right) \cdot m_{pl} \tag{6.31}$$

Zoetemeijer proposed for common m and n values an approximation of this equation based on experimental results. The approximated expression of the collapse load became:

$$N = \frac{2}{m} \cdot (a + 4 \cdot m + 1.25 \cdot n) \cdot m_{pl} \tag{6.32}$$

It should be noted that the value of N is calculated considering only one half of the flange mechanism, so to obtain the collapse load F of the bolted connection is necessary to multiply N by 2. Thus, multiplying by two and substituting Equation (6.3) into Equation (6.32) the yield load of the plate became:

$$F = \frac{f_y \cdot t^2}{m} \cdot (a + 4 \cdot m + 1.25 \cdot n) \tag{6.33}$$

6.1.2 Packer & Morris models

Alternative flange mechanisms for bolted connections were proposed by Packer & Morris giving different formulations for the evaluation of the yield load, as briefly presented in paragraph 3.2.1.4. Packer and Morris [45] proposed different yield line patterns associated to the failure modes I and II. Also in this case, focusing on collapse mechanism II, the main difference from Zotemeijer's approach was the introduction of curved boundary hinge patterns. The solution adopted by Packer and Morris was based on the mathematical formulation developed by Mansfield [59].

6.1.2.1 Hypothesis

Mansfield [59] analyzed different plates geometries and loading conditions in order to evaluate their collapse mechanisms and the related yield loads. Among these cases he considered collapse mechanism developed in the region between two consecutive edges of a plate with different boundary conditions (clamped and/or simply supported as shown in Figure 6.5).
In this formulation together with the curved boundary hinge a "radial hinge field" was also considered. Hence the internal work associated to the curved yield path is composed in this case by two terms, the first related to the curved boundary hinge and the second associated to the hinge field.

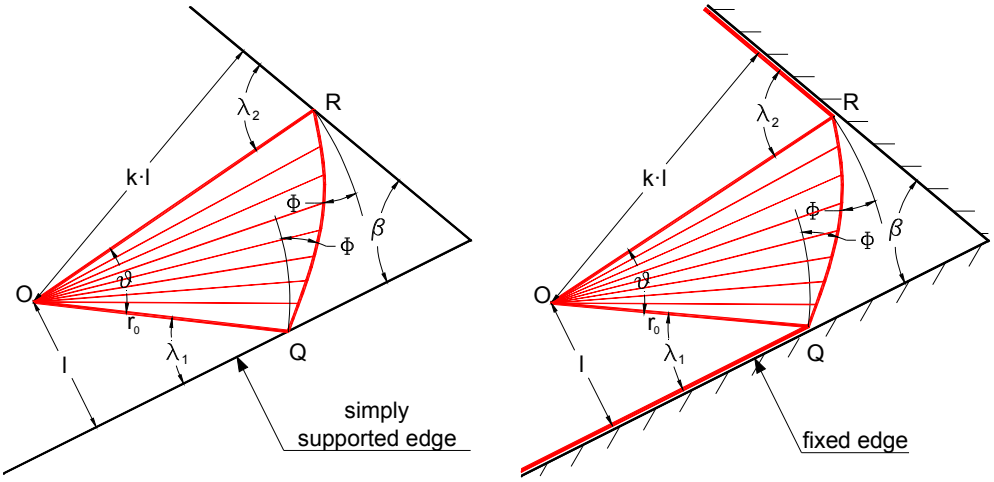

Figure 6.5 - Mansfield curved boundary hinges

To describe the curved boundary hinges two additional geometrical parameters r_0 and Φ were defined as functions of the angles λ_1 and λ_2:

$$r_0 = \frac{l}{\sin(\lambda_1)} \tag{6.34}$$

$$\tan(\Phi) = \frac{1}{(\lambda_1 + \lambda_2 - \beta)} \cdot \ln\left(\frac{k \cdot \sin(\lambda_1)}{\sin(\lambda_2)}\right) \tag{6.35}$$

where:

- r_0 is the lower bound of the radius of curvature of the curved boundary hinge;
- Φ is the angle between the spiral arc and the normal to the generic radius r as shown in Figure 6.5.

Considering the notation in Figure 6.6 Mansfield [59] computed the work done in a radial hinge field of arbitrary form.

The energy dissipated along the curved hinge is given by:

$$W_B = \delta_v \cdot m_{pl} \cdot \int_{\theta_1}^{\theta_2} \left(1 + \frac{1}{r^2} \cdot \left(\frac{dr}{d\theta}\right)^2\right) d\theta \tag{6.36}$$

while the energy dissipation in the radial hinge field is equal to:

$$W_F = \delta_v \cdot m_{pl} \cdot \int_{\theta_1}^{\theta_2} \left(1 + \frac{2}{r^2} \cdot \left(\frac{dr}{d\theta}\right)^2 - \frac{1}{r^2} \cdot \frac{d^2r}{d\theta^2}\right) d\theta \tag{6.37}$$

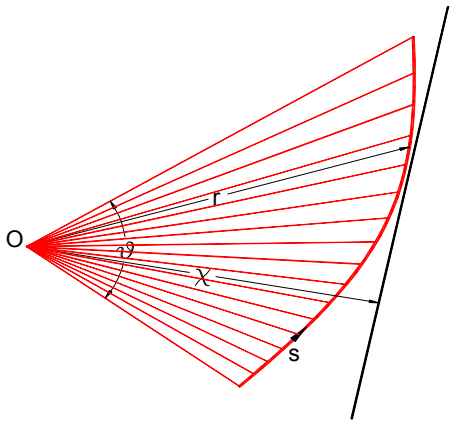

Figure 6.6 - Radial hinge field parameters

Summing these two contributions Mansfield obtained that the total energy dissipation was evaluated as:

$$W = W_B + W_F = 2 \cdot \delta_v \cdot m_{pl} \cdot \int_{\theta_1}^{\theta_2} \left(1 + \frac{3}{r^2} \cdot \left(\frac{dr}{d\theta}\right)^2 - \frac{1}{2 \cdot r} \cdot \frac{d^2r}{d\theta^2}\right) d\theta \tag{6.38}$$

The radius $r = r_0 \cdot e^{\theta \cdot \tan(\Phi)}$ and the angle θ are the polar coordinates of a generic point of the spiral arc, with $0 \le \theta \le \lambda_1 + \lambda_2 - \beta$. Hence the values of the radius r correspond to:

$$r = r_0 \qquad \text{for } \theta = 0 \tag{6.39}$$

$$r = r_0 \cdot \frac{k \cdot \sin(\lambda_1)}{\sin(\lambda_2)} = \frac{k \cdot m}{\sin(\lambda_2)} \qquad \text{for } \theta = \lambda_1 + \lambda_2 - \beta \tag{6.40}$$

Substituting the equation of the radius r in Equation (6.38) Mansfield obtained that the total energy dissipation in the curved hinge was:

$$W = 2 \cdot \delta_v \cdot m_{pl} \cdot \int_{\theta_1}^{\theta_2} \left(1 + \tan^2(\Phi)\right) d\theta = 2 \cdot \delta_v \cdot m_{pl} \cdot (\theta_2 - \theta_1) \cdot \sec^2(\Phi) \quad (6.41)$$

and remembering the physical meaning of the angle θ it could be rewritten as:

$$W = 2 \cdot \delta_v \cdot m_{pl} \cdot (\lambda_1 + \lambda_2 - \beta) \cdot \sec^2(\Phi) \quad (6.42)$$

In addition to the hypothesis of curved boundary hinge patterns Packer & Morris adopted the same basic assumptions of Zoetmeijer, reported in paragraph 6.1.2.1.

6.1.2.2 Definition of the flange mechanisms

In Figure 6.7 are reported the different flange mechanisms proposed by Packer and Morris [45].

6.1.2.3 Energy balance equations

In this paragraph the equations of the yield load associated to the mechanisms proposed by Packer and Morris [45] showed in Figure 6.7 are summarized. The procedure adopted to evaluate F is equivalent to the one described for Zotemeijer's model.

Starting from Mansfield's general formulation it was possible, operating some simplifications, to obtain the equations of the yield load proposed by Packer and Morris [45]. Mansfield [59] demonstrated that for a curved hinge between two intersecting clamped (or fixed) edges the minimization of the dissipated energy gives $\lambda_1 = \lambda_2 = \frac{\pi}{2}$.

This physically means that the curved hinge line leaves the clamped edges tangentially. Thus Equation (6.42) can be rewritten as:

$$W = 2 \cdot \delta_v \cdot m_{pl} \cdot (\pi - \beta) \cdot \sec^2(\Phi) \quad (6.43)$$

In addition considering the case of a rectangular plate $\left(\beta = \frac{\pi}{2}\right)$ it is possible to further simplify the equation in the form:

$$W = 2 \cdot \delta_v \cdot m_{pl} \cdot \frac{\pi}{2} \cdot \sec^2(\Phi) = \delta_v \cdot m_{pl} \cdot \pi \cdot \sec^2(\Phi) \tag{6.44}$$

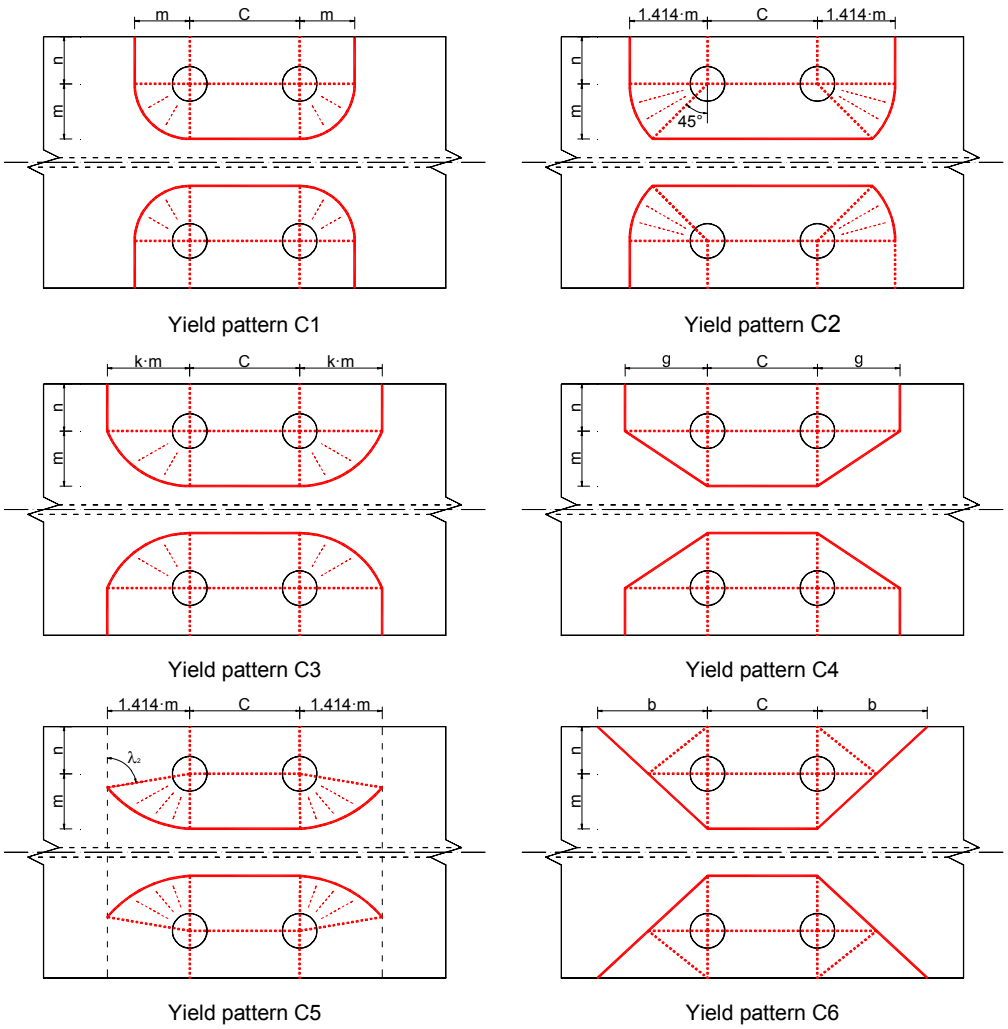

Figure 6.7 - Packer & Morris flange mechanisms

In the following, for brevity, only the final equations for the different collapse mechanisms are reported.

In the yield pattern C1 the value k = 1 identifies circular hinge fields with a radius r = m, an angular extension of $\frac{\pi}{2}$ and centre points coincident with the bolt axis. The yield load for this mechanism is:

$$F = \left(\pi + \frac{2 \cdot n + C - D'}{m}\right) \cdot f_y \cdot t^2 \tag{6.45}$$

where

- n and m are geometrical parameters of the plate which identify the position of the bolts;
- D' is the bolt holes diameter;
- f_y is the yield stress of the steel plate;
- t is the thickness of the plate.

Yield pattern C2 is described by circular hinge fields with a radius $r = \sqrt{2} \cdot m$ and are extended through an angle of $\frac{\pi}{4}$. Also in this case the centre points are coincident with the bolt axis. The load associated to the formation of this mechanism is:

$$F = \left(\frac{2.57 \cdot m + 0.85 \cdot C + 1.41 \cdot n - 0.71 \cdot D'}{m}\right) \cdot f_y \cdot t^2 \tag{6.46}$$

Yield pattern C3a is similar to mechanism C1, the only difference is the value of the parameter k. In the C3a yield pattern $k = \frac{C}{m}$, where C is the bolt pitch. The resultant yield load is

$$F = \left(\frac{C - 0.5 \cdot D'}{m} + \frac{2 \cdot n - 0.5 \cdot D'}{C} + \pi \cdot \sec^2\left(\tan^{-1}\left(\frac{2 \cdot \ln\left(\frac{C}{m}\right)}{\pi}\right)\right)\right) \cdot f_y \cdot t^2 \tag{6.47}$$

If in the yield pattern C3a the influence of bolt holes is neglected (D' = 0), yield pattern C3b is produced, with an associate load of:

$$F = \left(\frac{C}{m} + \frac{2 \cdot n}{C} + \pi \cdot \sec^2\left(\tan^{-1}\left(\frac{2 \cdot \ln\left(\frac{C}{m}\right)}{\pi} \right) \right) \right) \cdot f_y \cdot t^2 \tag{6.48}$$

Yield pattern C4 is described by straight yield lines only, similarly to the Zoetemeijer's one, even if the geometry of the mechanism is different. It gives a yield load of:

$$F = \left(\frac{2 \cdot n + 2 \cdot m - D'}{g} + \frac{C - D' + 2 \cdot g}{m} \right) \cdot f_y \cdot t^2 \tag{6.49}$$

where:

$$g = \sqrt{m \cdot (n + m - 0.5 \cdot D')} \tag{6.50}$$

The parameter g is obtained minimizing the values of F, imposing the condition:

$$\frac{dF}{dg} = 0 \tag{6.51}$$

In yield pattern C5 the curved hinges are described by spiral arcs. The equation of the yield load is:

$$F = \left(\frac{a - 0.5 \cdot D' + \sqrt{2} \cdot (n - 0.5 \cdot D') + 2.57 \cdot m}{m} \right) \cdot f_y \cdot {t_{fc}}^2 \tag{6.52}$$

Finally, for yield pattern C6, characterized by straight yield lines only but with a more complex configuration than yield pattern C4, the load at yielding is given by:

$$F = \left(\frac{C - 0.5 \cdot D' + 2 \cdot b}{m} + \frac{(m + n) \cdot (2 \cdot m + 2 \cdot n - D')}{m \cdot b} + \frac{b}{m + n} \right) \cdot f_y \cdot {t_{fc}}^2 \tag{6.53}$$

where:

$$b = \sqrt{\left(m^2 + n^2\right) \cdot \frac{2 \cdot m + 2 \cdot n - D'}{3 \cdot m + 2 \cdot n}} \tag{6.54}$$

As for yield pattern C4 the value of b is obtained imposing the condition:

$$\frac{dF}{db} = 0 \tag{6.55}$$

6.1.3 Prediction of the yield load

The available formulations for predicting the yield load of bolted T elements were applied to the T-stub specimens tested during the experimental activity to evaluate the effectiveness of the different analytical models.

First of all was necessary to evaluate the experimental load associated to the specimen yielding. At this aim was assumed as yield loads the force relative to the point in the load-displacement plane identified by the intersection between the line approximating the elastic branch and the hardening one of the experimental diagram (Figure 6.8).

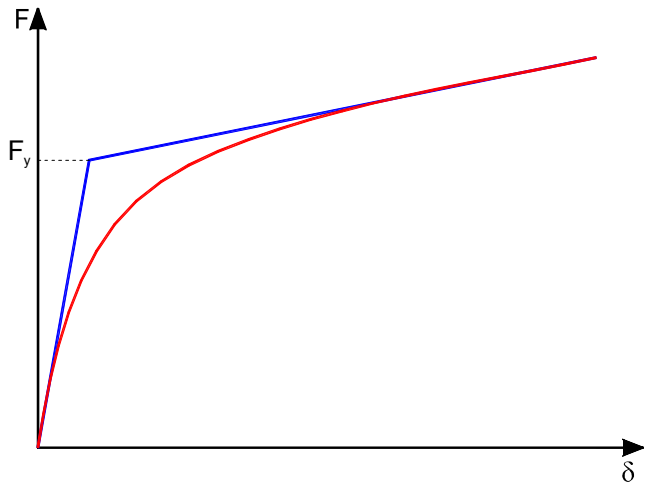

Figure 6.8 - Evaluation of experimental yield load

For the T-stub under pure tension an average yield load of 175.97 kN was evaluated. Considering the actual dimensions and material properties, applying the different mechanisms formulations gives:

Analytical model		Yield Load (kN)	Δ (%)
Zoetmeijer		151.159	-14.10
Packer & Morris	Yield Pattern C1	125.999	-28.40
	Yield Pattern C2	99.508	-43.45
	Yield Pattern C3a	---	---
	Yield Pattern C3b	---	---
	Yield Pattern C4	129.355	-26.49%
	Yield Pattern C5	90.140	-48.78%
	Yield Pattern C6	217.995	+23.88%

Table 6.1 - Analytical yield loads evaluation

It is possible to notice that the behaviour of the T-stub is better approximated by Zoetmeijer's model.

No yield loads for mechanisms C3a and C3b are available for the T-stub. To apply the theoretical models to the T-stubs it was necessary to assume the bolt pitch C = 0, this led to obtain yield loads which tend to infinity because they are inverse functions of C.

In general a strong underestimation of the yield loads was achieved. The worst solutions were associated to Packer and Morris' models in which the geometry of the mechanism was defined "a priori" without any considerations about the minimization of the energy dissipated by the development of the yield lines.

Moreover, the introduction of curved yield lines, despite a closer similarity to the experimental evidence (Figure 4.38) did not provide an improvement in the estimation of the load associated to the formation of the flange mechanism.

Focusing on T-stub response the results obtained through the Zoetmeijer's model suggested to extend this formulation also to the case of combined actions (shear and axial forces).

6.2 T-stub under combined actions

In this section, starting from the Zoetemeijer’s analytical model, the extension to the case of column T-stub under combined tension and axial force is proposed.

In this modified formulation the effect of the shear force is represented in a simplified way by the introduction of an asymmetry of the flange mechanism.

6.2.1 Hypothesis

The base hypotheses are the same of the Zoetemeijer's formulation. Additional helpful information were obtained from the experimental results presented in paragraph 4.3. The experimental evidence suggested to introduce a limit: the proposed model can be considered applicable for values of inclination angle of the external load φ equal or greater than 45°. It can be seen that for inclination angles lower than 45° no appreciable flange mechanism developed. In this first stage the effect of shear was simply modelled as asymmetry of the flange mechanism.

6.2.2 Definition of the flange mechanism

In case of combined actions it was necessary to introduce three new variables in order to describe the problem. The first two variables related to the flange mechanism are the angles θ and ω evaluated as represented in Figure 6.9.

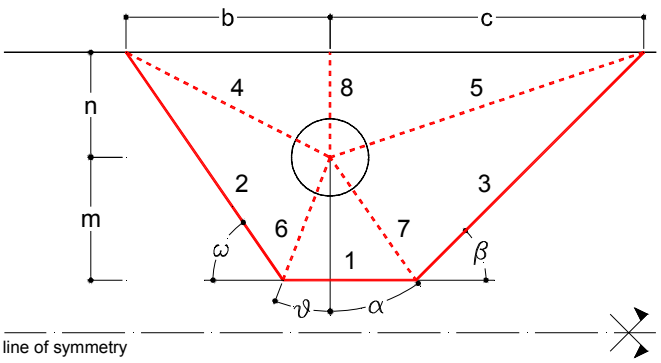

Figure 6.9 - T-stub Yield lines in presence of shear and axial force

To fully describe the flange mechanism of a T-stub element eight different yield lines are required. Also in this case for simplicity the symmetry of the problem respect to the web plane of the T-stub is considered.

6.2.3 Energy balance equations

The contributions of each yield line to the internal energy dissipation can be written as follows:

1. yield line 1:

$$L_1 = m \cdot \tan(\theta) + m \cdot \tan(\alpha) \tag{6.56}$$

$$\Phi_1 = \frac{\delta_v}{m} \tag{6.57}$$

$$\Delta E_1 = m \cdot (\tan(\theta) + \tan(\alpha)) \cdot \frac{\delta_v}{m} \cdot m_{pl} \tag{6.58}$$

2. yield line 2:

$$L_2 = \frac{n+m}{\sin(\omega)} \tag{6.59}$$

$$\Phi_2 = \frac{\delta_v}{\frac{m}{\cos(\theta)} \cdot \cos(\omega - \theta)} \tag{6.60}$$

$$\Delta E_2 = \frac{n+m}{\sin(\omega)} \cdot \frac{\delta_v}{\frac{m}{\cos(\theta)} \cdot \cos(\omega - \theta)} \cdot m_{pl} \tag{6.61}$$

3. yield line 3:

$$L_3 = \frac{n+m}{\sin(\beta)} \tag{6.62}$$

$$\Phi_3 = \frac{\delta_v}{\frac{m}{\cos(\alpha)} \cdot \cos(\beta - \alpha)} \tag{6.63}$$

$$\Delta E_3 = \frac{n+m}{\sin(\beta)} \cdot \frac{\delta_v}{\frac{m}{\cos(\alpha)} \cdot \cos(\beta - \alpha)} \cdot m_{pl} \tag{6.64}$$

4. yield line 4:

$$L_4 = \sqrt{b^2 + n^2} = l_4 \tag{6.65}$$

$$\Phi_4 = \frac{\delta_v}{l'_4} \cdot \frac{l'''_4}{l_4} - \frac{\delta_v - \delta_v \cdot \frac{l'''_4}{l_4}}{l''_4} \tag{6.66}$$

$$\Delta E_4 = \sqrt{b^2 + n^2} \cdot \left(\frac{l'''_4}{l_4 \cdot l'_4} - \frac{1}{l''_4} + \frac{l'''_4}{l_4 \cdot l''_4} \right) \cdot \delta_v \cdot m_{pl} \tag{6.67}$$

hence simplifying the equation of Φ_4 and E_4:

$$\Delta E_4 = \left(\cot(\omega) + \frac{n \cdot \cos(\theta)}{m \cdot \sin(\omega) \cdot \cos(\omega - \theta)} - \frac{n}{b} \right) \cdot \delta_v \cdot m_{pl} \tag{6.68}$$

5. yield line 5:

$$L_5 = \sqrt{c^2 + n^2} = l_5 \tag{6.69}$$

$$\Phi_5 = \frac{\delta_v}{l'_5} \cdot \frac{l'''_5}{l_5} - \frac{\delta_v - \delta_v \cdot \frac{l'''_5}{l_5}}{l''_5} \tag{6.70}$$

$$\Delta E_5 = \sqrt{b^2 + n^2} \cdot \left(\frac{l'''_5}{l_5 \cdot l'_5} - \frac{1}{l''_5} + \frac{l'''_5}{l_5 \cdot l''_5} \right) \cdot \delta_v \cdot m_{pl} \tag{6.71}$$

applying the same simplification adopted for the yield line 4:

$$\Delta E_5 = \left(\cot(\beta) + \frac{n \cdot \cos(\alpha)}{m \cdot \sin(\beta) \cdot \cos(\beta - \alpha)} - \frac{n}{c} \right) \cdot \delta_v \cdot m_{pl} \tag{6.72}$$

6. yield line 6:

$$L_6 = \frac{m}{\cos(\theta)} \tag{6.73}$$

$$\Phi_6 = \frac{\delta_v}{m} \cdot \frac{\operatorname{sen}(\omega)}{\cos(\omega - \theta)} \tag{6.74}$$

$$\Delta E_6 = \frac{m}{\cos(\theta)} \cdot \frac{\delta_v}{m} \cdot \frac{\operatorname{sen}(\omega)}{\cos(\omega - \theta)} \cdot m_{pl} \tag{6.75}$$

7. yield line 7:

$$L_7 = \frac{m}{\cos(\alpha)} \tag{6.76}$$

$$\Phi_7 = \frac{\delta_v}{m} \cdot \frac{\operatorname{sen}(\beta)}{\cos(\beta - \alpha)} \tag{6.77}$$

$$\Delta E_7 = \frac{m}{\cos(\alpha)} \cdot \frac{\delta_v}{m} \cdot \frac{\operatorname{sen}(\beta)}{\cos(\beta - \alpha)} \cdot m_{pl} \tag{6.78}$$

8. yield line 8:

$$L_8 = n \tag{6.79}$$

$$\Phi_8 = \frac{\delta_v}{b} + \frac{\delta_v}{c} \tag{6.80}$$

$$\Delta E_8 = n \cdot \left(\frac{\delta_v}{b} + \frac{\delta_v}{c} \right) \cdot m_{pl} \tag{6.81}$$

Therefore the equation of the total internal energy dissipation ΔE is obtained summing the energy contribution of each yield line and simplifying:

$$\begin{aligned} \Delta E = \sum_{i=1}^{8} \Delta E_i = \Bigg(& \tan(\alpha) + \cot(\beta) + \frac{m + 2 \cdot n}{m} \cdot \frac{\cos^2(\alpha) + m \cdot \sin^2(\beta)}{\sin(\beta) \cdot \cos(\alpha) \cdot \cos(\beta - \alpha)} + \tan(\theta) + \\ & + \cot(\omega) + + \frac{m + 2 \cdot n}{m} \cdot \frac{\cos^2(\theta) + m \cdot \sin^2(\omega)}{m \cdot \sin(\omega) \cdot \cos(\theta) \cdot \cos(\omega - \theta)} \Bigg) \cdot \delta_v \cdot m_{pl} \end{aligned} \tag{6.82}$$

The asymmetric mechanism is supposed to fully include the effect of shear force, so the work done by the external load is also in this case associated to the axial component of the applied force:

$$\Delta F = N \cdot \delta_v \tag{6.83}$$

The associated shear component can be easily evaluate as

$$V = \frac{N}{\tan(\varphi)} \tag{6.84}$$

where φ is the inclination angle of the resultant of external loads $F = \sqrt{N^2 + V^2}$ and represents the third variable necessary to describe the problem. A value of the inclination angle φ = 0° correspond to a pure shear condition while φ = 90° is related to a bolted connection subjected only to tension load. Equating the internal and external energies gives:

$$\begin{aligned} N \cdot \delta_v = \Bigg(& \tan(\alpha) + \cot(\beta) + \frac{m + 2 \cdot n}{m} \cdot \frac{\cos^2(\alpha) + m \cdot \sin^2(\beta)}{\sin(\beta) \cdot \cos(\alpha) \cdot \cos(\beta - \alpha)} + \tan(\theta) + \\ & + \cot(\omega) + \frac{m + 2 \cdot n}{m} \cdot \frac{\cos^2(\theta) + m \cdot \sin^2(\omega)}{m \cdot \sin(\omega) \cdot \cos(\theta) \cdot \cos(\omega - \theta)} \Bigg) \cdot \delta_v \cdot m_{pl} \end{aligned} \tag{6.85}$$

6.2.4 Calibration of the model

The minimization of the dissipated energy means also in this case to minimize the right hand side of the equation which corresponds to the expression of the internal work. In this case from the theoretically point of view it should be necessary to impose these four conditions:

$$\frac{\partial \sum_{i=1}^{8} \Delta E_i}{\partial \alpha} = 0 \tag{6.86}$$

$$\frac{\partial \sum_{i=1}^{8} \Delta E_i}{\partial \beta} = 0 \tag{6.87}$$

$$\frac{\partial \sum_{i=1}^{8} \Delta E_i}{\partial \theta} = 0 \tag{6.88}$$

$$\frac{\partial \sum_{i=1}^{8} \Delta E_i}{\partial \omega} = 0 \tag{6.89}$$

To simplify this operation empirical relationships calibrated on the available experimental data between α and θ and between β and ω were introduced. Thus the number of independent variables necessary to describe the flange mechanism decreased from four (α, β, θ, ω) to only two (α, β, θ = θ(α), ω = ω(β)).

This operation was done assuming as reference criteria the comparison between Zoetmeijer's solution and the flange mechanism evaluated experimentally for the T-stub under pure tension load. Once identified a criteria for approximating the experimental results by the analytical solution, the procedure was extended also to the T-stubs subjected to different loading conditions. This operation is summarized for different values of the inclination angle φ in Figure 6.10.

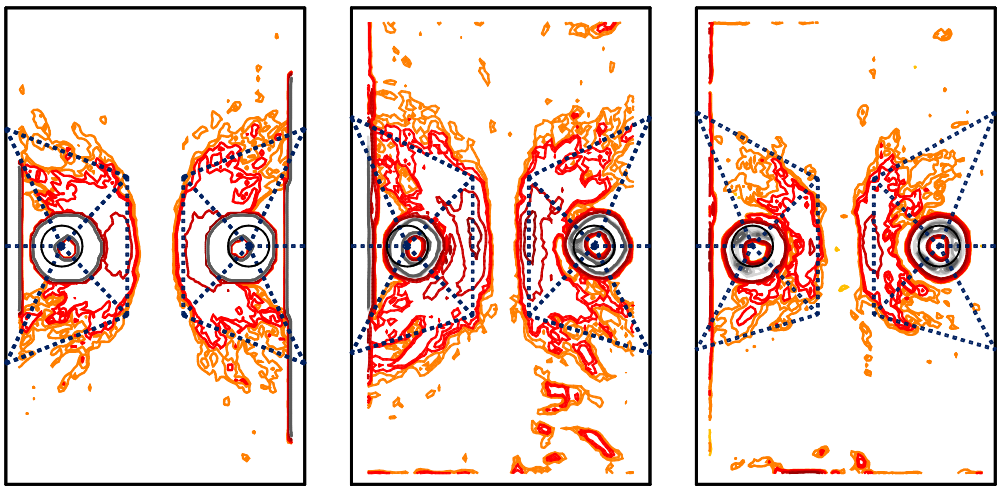

Figure 6.10 - Approximation of the flange mechanism

From Figure 6.10 it was possible to estimate the values of α, β, θ, ω and then the ratios α/θ and β/ω. Starting from these data two interpolation functions were built, forcing the

formulation to give α = θ and β = ω for φ = 90°, so to obtain the Zoetmeijer's solution for the case of pure tension.

As first attempt linear equations were adopted to approximate the two functions θ = θ(α) and ω = ω(β). In Figure 6.11 and Figure 6.12 the two approximation functions are plotted and compared with the experimental results.

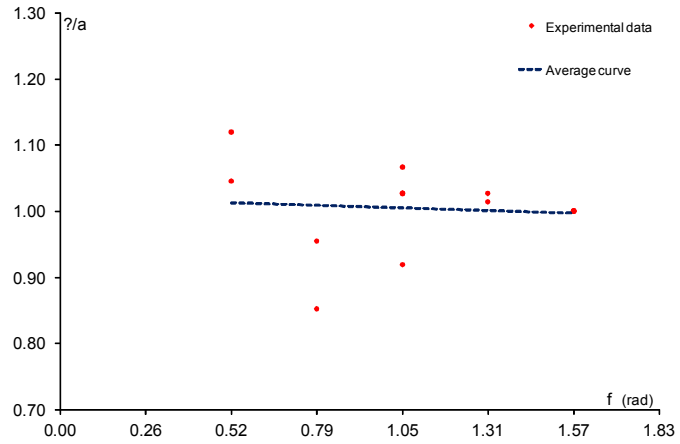

Figure 6.11 - Interpolation function α/θ

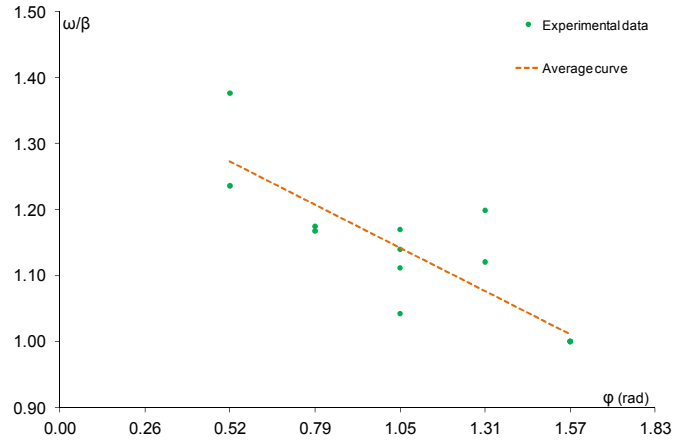

Figure 6.12 - Interpolation function ω/β

A second attempt was done adopting two quadratic polynomial functions to approximate the experimental results but no significant improvements were obtained.

Considering all the aspects of the proposed procedure an objection can be made: the formulation of the theoretical prediction of the yield load is based on the observation of the flange mechanisms experimentally obtained. These mechanisms are associated to the collapse of the specimen and not to the yielding condition. In Figure 6.14 is presented the case of specimen under pure tension, which is the one that exhibits the wider differences in terms of flange transverse displacements between the yielding and the collapse.

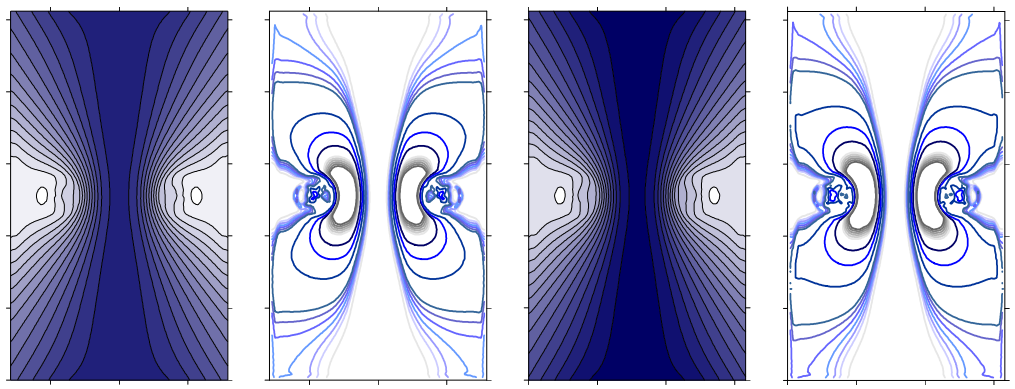

Figure 6.13 - Yielding vs. collapse flange residual deformations for specimen 1CB (φ = 90°)

However, from numerical models was possible to observe, comparing the level lines maps and the slope isolines maps, that the differences in the deformed configuration of the T-stub flanges at yielding and at collapse (in the latter case after the unloading of the specimen) were negligible.

This comparison allowed to justify the considerations based on the slope isolines maps acquired after the collapse and the unloading of the T-stub and adopted to calibrate the theoretical model for the prediction of the yield load.

6.2.5 Prediction of the collapse load

Considering the empirical approximation which correlate α with θ and β with ω, to calculate the minimum of the internal dissipation of energy it was sufficient to carry out only the differentiations with respect to α and β. The solution of this equation system gives the values of the geometrical parameters α and β. Substituting the values of α and β into the approximated equations of θ(α) and ω(β) the values of the other two

angles necessary to describe the flange mechanism can easily calculated. Substituting the values of α, θ, β and ω and simplifying δ_v in the energy balance equation is possible to have an appraisal of the axial component N of the yield load of the T-stub flange. The yield load and its shear component V can be evaluated as:

$$F = \frac{N_y}{\text{sen}(\varphi)} \tag{6.90}$$

$$V = \frac{N_y}{\tan(\varphi)} \tag{6.91}$$

A comparison of the results with the experimental data shows that in general a good agreement between the analytical prediction of the yield loads and the experimental results was obtained (Figure 6.14). A further comparison was carried out in terms of yield load components (N and V) as shown in Figure 6.15.

From Figure 6.15 it was clear that despite a good approximation of the global value of F there are some problems related to the correct evaluations of its components N and V. In particular the value of N seemed not to be so sensitive to the variation of the inclination angle φ. This suggested that the simplified approach that took into account the effect of shear on the development of the shape of flange mechanism was not sufficient to have a good appraisal of the yield load.

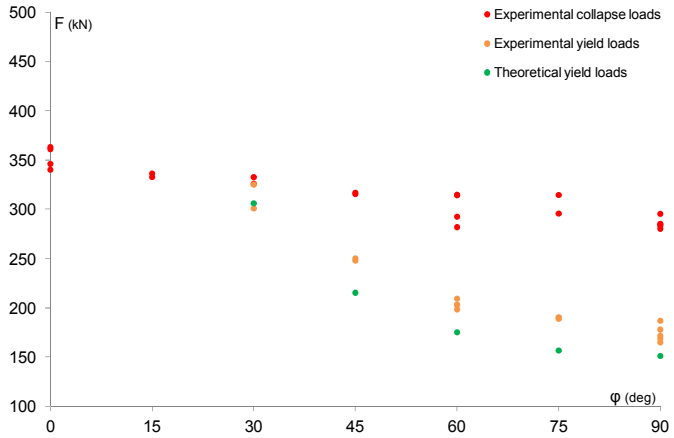

Figure 6.14 - Analytical and experimental yield loads

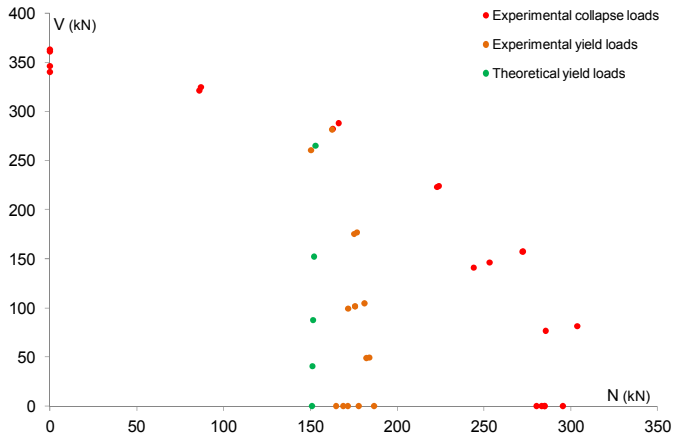

Figure 6.15 - Analytical and experimental yield load components

6.2.6 Reduction of the plastic moment

The following step in the theoretical description of the T-stub flange yielding process was the adoption, together with the asymmetric yield lines configuration, of a reduced plastic moment along specific yield lines. The objective was to couple directly the effect of the shear force with the energy dissipation capacity of the plastic mechanism.

The improvement of the previously described approach considered uniform distributed loads applied on the outer yield lines which describe the mechanism (Figure 6.16).

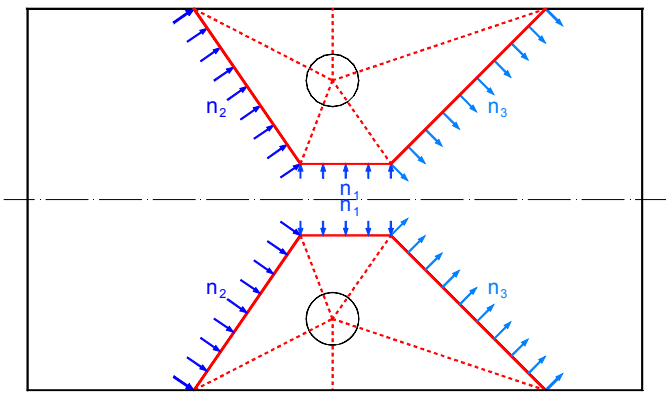

Figure 6.16 - Outer yield lines normal loads due to shear force

The generic uniform load n_i acts perpendicularly to the yield line on which is applied. Thus the plastic moment of the yield line on which the load n_i is applied is:

$$m_{pl,red} = m_{pl} \cdot \left(1 - \left(\frac{n_i}{n_{Rd}} \right)^2 \right) \tag{6.92}$$

where n_{Rd} is the design axial resistant per unit length of the T-stub flange, evaluated as:

$$n_{Rd} = f_y \cdot t \tag{6.93}$$

The different load distributions n_i are calibrated in order to obtain an overall resultant parallel to the T-stub web with a magnitude equal to V. The magnitude of the resultant is obtained through an iterative process in which the "first tentative value" is assumed to be coincident with shear force $V^{(1)}$ obtained from the flange mechanism with no reduction of plastic moments.

From the first tentative value of shear $V^{(1)}$ is possible to calculate the values of the uniform load distributions $n_i^{(1)}$, then evaluate the reduced plastic moment $m_{pl,red}$ for the outer yield lines and through the energy balance equations calculate a new yield load and hence a new shear component $V^{(2)}$ necessary to recalculate the load distributions $n_i^{(2)}$. Carrying out few iterations it is possible to obtain the "corrected" value of the yield load. The iterative process is stopped when the gap between the values of the collapse load obtained in two consecutive iterations is sufficiently small.

In Table 6.2 the theoretical results obtained from the model are summarized and compared with the experimental ones.

φ (°)	$N_{theoretical}$ (kN)	$V_{theoretical}$ (kN)	$F_{theoretical}$ (kN)	$F_{experimental}$ (kN)	Δ (%)
45.000	147.155	147.155	208.109	239.089	-16.40%
60.000	150.083	86.651	173.301	197.028	-14.77%
75.000	151.006	40.462	156.333	184.295	-17.53%
90.000	151.158	0.000	151.158	175.969	-13.11 %

Table 6.2 - Theoretical results for the T-stub under combined actions

Is clear that the proposed model combining the asymmetry and the reduction of m_{pl} due to the shear force is able to give a good approximation of the experimental results.

Figure 6.17 and Figure 6.18 show the graphic representation of the results respectively in terms of F-φ relationship and N-V domain. Despite small differences from the

previous model (which neglects the reduction of m_{pl}) this formulation is able to better approximate the actual response of the T-stub.

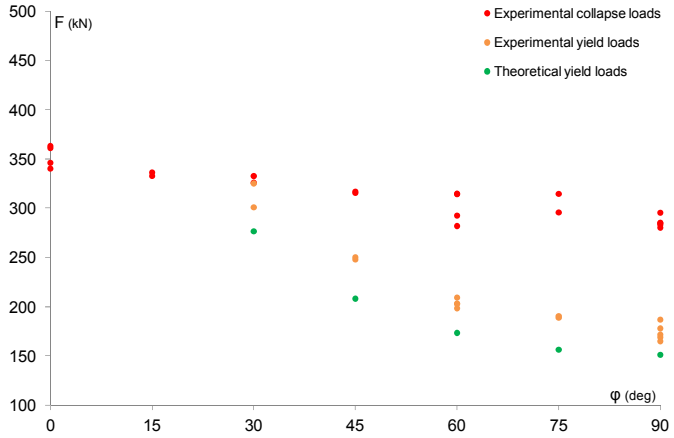

Figure 6.17 - Analytical vs. experimental yield loads

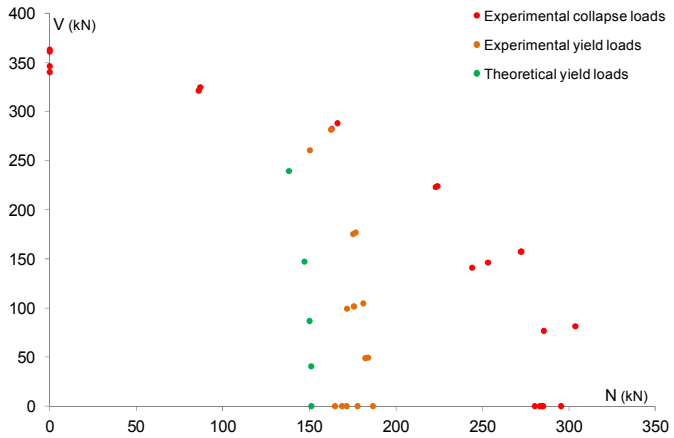

Figure 6.18 - Analytical vs. experimental yield load components

A more detailed comparison is made in Figure 6.19 where the theoretical yield loads are compared with the respective experimental bilinear approximations of the load-displacement curves.

In Figure 6.20 are compared the flange mechanism configurations obtained from the theoretical model with the yield lines experimentally evaluated. Also in this case a very good agreement was achieved.

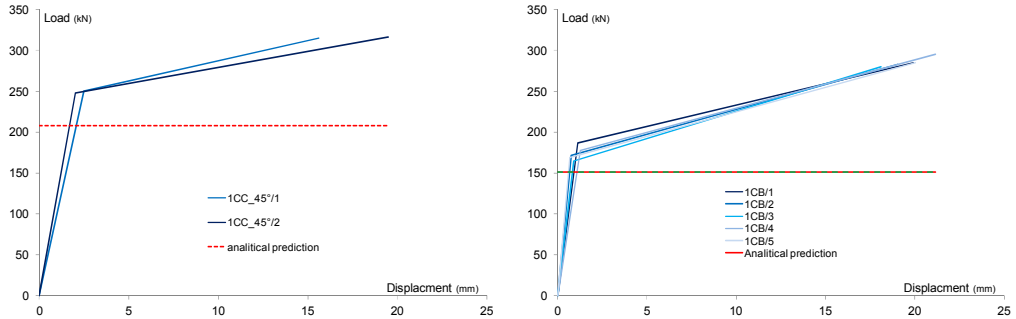

Figure 6.19 - Bilinear load-displacement curves vs. analytical results for φ=45° and φ=90°

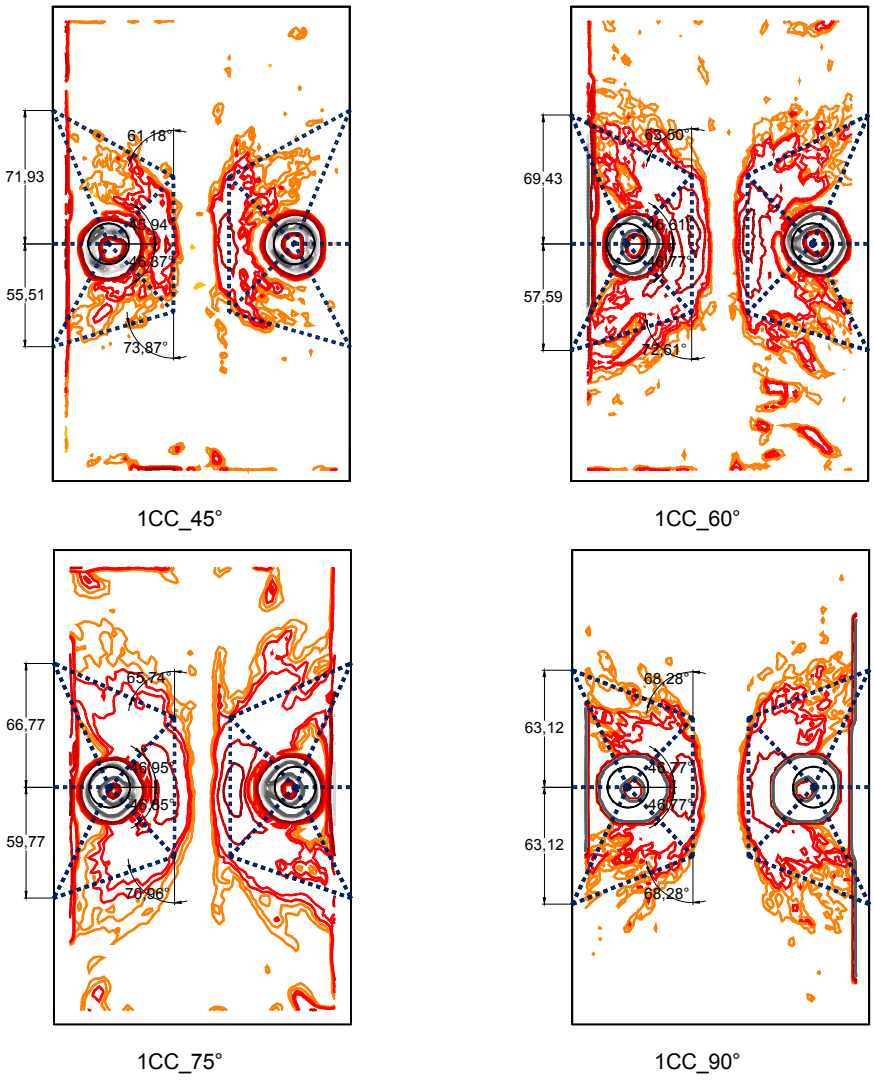

Figure 6.20 - Comparison of analytical and experimental flange mechanisms

6.3 T-stub stiffness

Considering the philosophy of the component method to fully characterize each basic component it is necessary to know not only the yield load but also the elastic stiffness. These two parameters allow defining a simplified elastic-plastic load-displacement relationship that describe the behaviour of the component.
Considering the case of T-stub under different combinations of N and V, the objective is now to identify a relationship between the elastic stiffness k and the inclination angle φ.
At this aim considering the load-displacement curves of Figure 6.19 is quite simply to evaluate the stiffness for the different values of φ. The results are reported in Figure 6.21 and in Table 6.3.

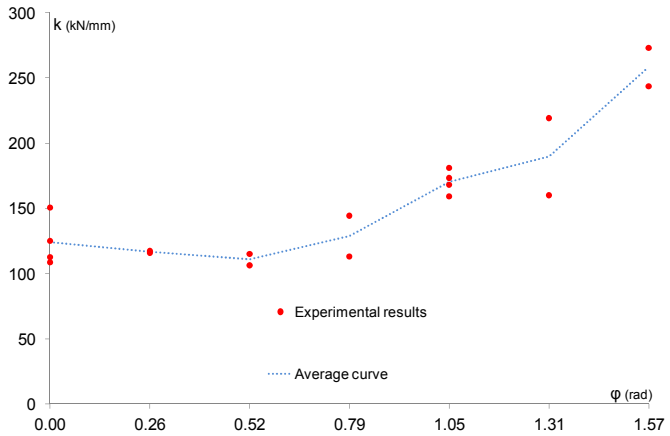

Figure 6.21 - Experimental stiffness in function of φ

As for the collapse load the evaluation of the elastic stiffness was carried out in the range 45° ≤ φ ≤ 90°. In Figure 6.21 however, are reported also the values of stiffness for φ < 45°, in order to give a complete representation of the problem.
Observing the average curve in Figure 6.21 is possible to see that for 0° ≤ φ ≤ 45°. no significant changes in the value of the average elastic stiffness are present. Between 45° and 90° the increment of stiffness seems to be almost linear.
This behaviour suggests defining a k-φ "discontinuous" function, constant between 0° and 45° and with a direct proportionality to φ between 45° and 90° as shown in Figure 6.22.

Specimen	$K_{experimental}$ (kN/mm)	$k_{exp,average}$ (kN/mm)
1CC_00°/1	108.623	124.217
1CC_00°/2	112.639	
1CC_00°/3	150.598	
1CC_00°/4	125.007	
1CC_15°/1	117.395	116.657
1CC_15°/2	115.919	
1CC_30°/1	115.107	110.721
1CC_30°/2	106.334	
1CC_45°/1	144.349	128.727
1CC_45°/2	113.105	
1CC_60°/1	180.959	170.397
1CC_60°/2	159.190	
1CC_60°/3	173.329	
1CC_60°/4	168.109	
1CC_75°/1	219.153	189.613
1CC_75°/2	160.072	
1CB/1	(not preloaded)	258.240
1CB/2	272.954	
1CB/3	243.525	
1CB/4	(not preloaded)	
1CB/4	(not preloaded)	

Table 6.3 - Elastic stiffness for different values of φ

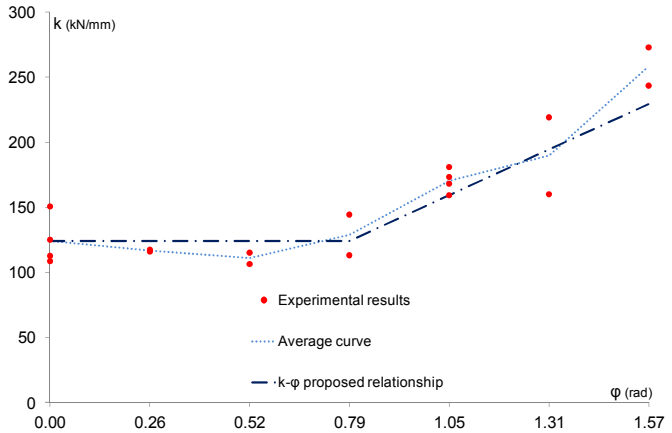

Figure 6.22 - k-φ relationship

Considering the case of pure tension, adopting a simple elastic theory the stiffness of the bolt can be evaluated as:

$$k_b = \frac{E_b \cdot A_s}{L_b} \tag{6.94}$$

while the stiffness associated to the plate deformation can be written as:

$$k_p = \frac{E \cdot L_{eff} \cdot t^3}{6 \cdot m^3} \tag{6.95}$$

Hence the stiffness of the T-stub subjected to a pure tension loading condition is given, coupling in series, the two stiffness:

$$k_{90°} = \frac{1}{\frac{1}{k_b} + \frac{1}{k_p}} \tag{6.96}$$

The EN1993-1-8 [41] gives, respectively for a bolt row (two bolts) and the column flange T-stub the following stiffness formulations:

$$k_{10} = 1.6 \cdot \frac{A_s}{L_b} \tag{6.97}$$

$$k_4 = 0.9 \cdot \frac{L_{eff} \cdot t^3}{m^3} \tag{6.98}$$

which are very similar to the ones evaluated trough the elastic theory, when multiplied for their respective elastic moduli E_b and E. The corrective coefficients in k_4 and k_{10} formulas come from the experimental calibration of the theoretical equations.
Of course an equivalent approach can be applied to the opposite case (φ = 0°). In this case, for brevity, only the EN1993-1-8 [41] formulation is reported. For pure shear loading condition the active components are the bolts in shear, identified by the stiffness k_{11} and the bolts in bearing associated to the stiffness k_{12}. For preloaded bolts

both the stiffness tends to infinity, while for non-preloaded ones the standard suggests the following values:

$$k_{11} = \frac{16 \cdot n_b \cdot f_{ub}}{E \cdot d_{M16}} \tag{6.99}$$

$$k_{12} = \frac{24 \cdot k_b \cdot k_t \cdot d \cdot f_u}{E} \tag{6.100}$$

Of course also in this case the two values of stiffness have to be coupled in series.

The comparison between the experimental values of stiffness and the values recommended by the EN1993-1-8 [41] (combined for their respective loading case with the Equation (6.96)) is shown in Figure 6.23.

Summarizing, the proposed value of stiffness can be evaluated in function of the loading condition (or inclination of the resultant of the external loads) as follows:

$$k = \begin{cases} k_{shear} & \text{for } \varphi \le \dfrac{\pi}{4} \\ \left(k_{tension} - k_{shear}\right) \cdot \left(\dfrac{4 \cdot \varphi}{\pi} - 1\right) + k_{shear} & \text{for } \varphi > \dfrac{\pi}{4} \end{cases} \tag{6.101}$$

where φ is in radians.

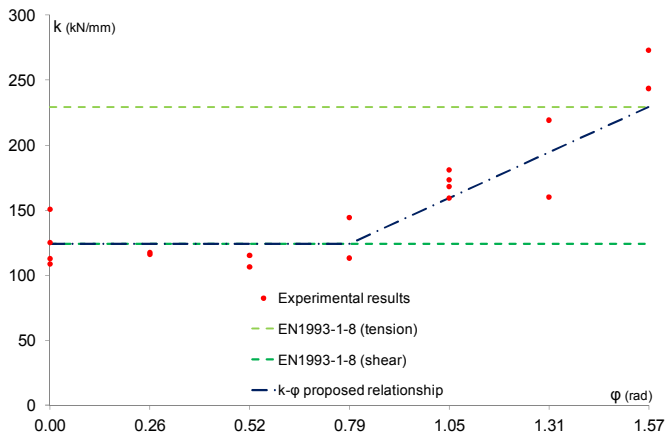

Figure 6.23 - Experimental values vs. EN1993-1-8 formulation

7. PARAMETRICAL ANALYSES

In this section the numerical and analytical models developed to describe the flange failure mechanism are applied to different specimen geometries. The numerical results are compared with the analytical ones to appraise the effectiveness of the proposed formulation for the evaluation of the yield load.

The attention focuses on three main parameters:

- flange thickness (t);
- plate edge - bolt distance (n);
- bolt diameter (d).

In detail, starting from the "reference case" represented by 1CC and 1CB specimens and characterized by t = 8.5 mm, n = 25 mm and d = 20 mm, the following cases were selected:

1. t = 6.5 mm;
2. t = 10.5 mm;
3. n = 25 mm
4. n = 35 mm
5. d = 16 mm;
6. d = 24 mm;

The different values of each parameter were selected in order to have constant increments of the investigated variable. In detail between one case and another for the flange thickness increments of 2 mm were fixed, for the bolts position a constant variation of 5 mm was set, while for the bolt diameter increments of 4 mm were considered.

For each T-stub configuration numerical simulations were carried out under different load combinations, ranging from $\varphi = 0°$ to $\varphi = 90°$. The aim of these parametrical analyses is to evaluate the sensitivity of the column T-stub to the variation of the main geometrical parameters on which depends its strength. On the other hand there was

the need to understand the effectiveness (or the limits) of the developed analytical model considering a few changes respect to the geometry of the reference specimen on which its calibration was based.

As preliminary operation the theoretical failure modes of the new specimen configurations were checked adopting the formulation proposed by the EN1993-1-8 [41], considering the actual dimensions and material properties of the steel components. In Table 7.1 the results of the failure mode evaluation are presented.

For all the specimen configurations the activation of a complete flange mechanism under pure tension loading condition was expected.

Case	$F_{TR,d,1}$ (kN)	$F_{TR,d,2}$ (kN)	$F_{TR,d,3}$ (kN)	Failure mode
"reference"	151.159	230.128	410.435	I
t = 6.5 mm	88.394 (-41.52%)	213.230 (-7.34%)	410.435 (+0.00%)	I
t = 10.5 mm	230.661 (+52.59%)	251.533 (9.30%)	410.435 (+0.00%)	I
n = 25 mm	142.510 (-5.72%)	201.709 (-12.35%)	410.435 (+0.00%)	I
n = 35 mm	162.691 (+7.63%)	258.548 (+12.35%)	410.435 (+0.00%)	I
d = 16 mm	151.159 (+0.00%)	162.088 (-29.57%)	263.014 (-35.92%)	I
d = 24 mm	151.159 (+0.00%)	313.633 (+36.29%)	591.362 (+44.08%)	I

Table 7.1 - Failure modes for different T-stub geometries (actual material properties)

As to obtain a complete overview of the problem the collapse loads associated to the different failure modes were evaluated considering also the nominal material properties instead of the actual ones (Table 7.2). The comparison between Table 7.1 and Table 7.2 highlights the remarkable influence of the material properties. It is apparent that the "over strength" of the materials plays a significant role in the development of a specific failure mechanism rather than another. This may lead is some cases to an incorrect failure mode prediction, depending from the over strength ratio between the T-stub flange material and the bolts one.

Case	$F_{TR,d,1}$ (kN)	$F_{TR,d,2}$ (kN)	$F_{TR,d,3}$ (kN)	Failure mode
"reference"	130.076	197.851	352.800	I
t = 6.5 mm	76.065 (-41.52%)	183.310 (-7.35%)	352.800 (+0.00%)	I
t = 10.5 mm	198.489 (52.59%)	216.270 (9.31%)	352.800 (+0.00%)	I
n = 25 mm	122.633 (-5.72%)	173.426 (-12.35%)	352.800 (+0.00%)	I
n = 35 mm	139.999 (7.63%)	222.277 (-17.56%)	352.800 0.00%	I
d = 16 mm	130.076 (+7.63%)	139.365 (+12.35%)	226.080 (+0.00%)	I
d = 24 mm	130.076 (+0.00%)	269.630 (+36.29%)	508.320 (+44.08%)	I

Table 7.2 - Failure modes for different T-stub geometries (nominal material properties)

If the over strength of the steel plate is greater than the bolts one the failure mode tends to move towards mode III (weak bolts - strong plate), otherwise if the over strength of the plate is smaller than the bolts one the failure mode tends to mode I (strong bolts - weak plate).

7.1 Numerical simulations

In order to analyze the behaviour of T-stub elements with different geometries numerical simulations were carried out adopting the F.E. models developed on the basis of the experimental available results. Maintaining all the properties of the models described in chapter 5, only the geometrical parameters of interest were changed as above mentioned. In the following sections an overview of the main results obtained is presented. The attention focused mainly on the global response of the T-stub elements. For the different cases (in terms of geometry and loading conditions) only the "actuator" load-displacement curves are reported. These curves are rebuilt through the combination of the displacements measured by transducers TR01-02 and TR13-14 as explained in paragraph 4.2.3.

7.1.1 Flange thickness

The variation of the flange thickness leads to a direct modification of the resistance properties of the specimens. The capability to develop a full flange mechanism is strictly related to the capacity of the flange to reach the plastic moment m_{pl}. The value of the plastic moment depends from the square of the flange thickness t, thus small variations of t could result in significant increments or decrements of m_{pl}. This strongly influences the failure mode of the specimen. From Table 7.1 it is possible to observe that despite a variation of ± 2.0 mm in the flange thickness for all the three cases the collapse is associated to the so called mode I. This means that for all the considered cases the T-stub flange is able to develop the plastic moment both at the bolts and at the web lines. Additionally, the variation of the flange thickness can induce significant increments or decrements of its bearing resistance.

In Figure 7.1, Figure 7.2 and Figure 7.3 the load-displacement curves for the different loading conditions ($\varphi = 0 \div 90°$) are reported respectively for t = 6.5 mm, t = 8.5 mm and t = 10.5 mm.

From a first comparison of the load-displacement curves it is possible to observe that to an increase of the inclination angle φ is associated a reduction of the collapse load.

This effect is stronger for t = 6.5 mm, while becomes very limited for t = 10.5 mm. Furthermore, for a certain value of φ the collapse load associate to t = 6.5 mm is always lower than the one evaluated for higher values of t. In addition the reduction of t produces a decreasing of the elastic branch of the load-displacement curves, especially for $\varphi \geq 45°$. This means that the development of a complete flange mechanism is achieved in thinner plates for smaller values of φ than for thicker ones. Of course this is due to the significant differences in the value of the plastic moment m_{pl}.

Considering the tree values of thickness selected for the parametrical analysis the plastic moments associated to the different plates are respectively:

- $4357 \ \frac{N \cdot mm}{mm}$ for t = 6.5 mm
- $7452 \ \frac{N \cdot mm}{mm}$ for t = 8.5 mm
- $11371 \ \frac{N \cdot mm}{mm}$ for t = 10.5 mm

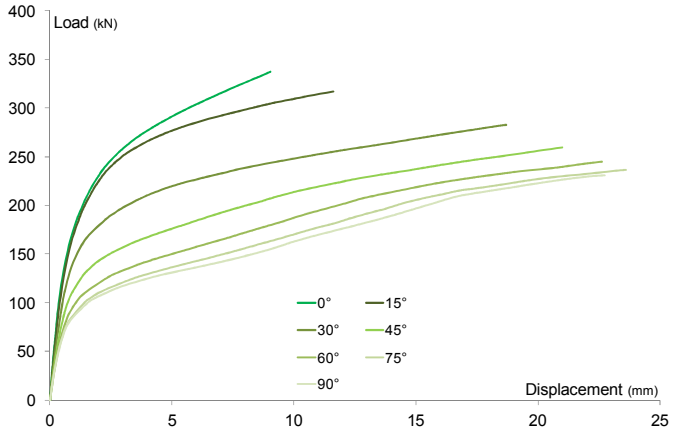

Figure 7.1 - Load-displacement curves for t = 6.5 mm

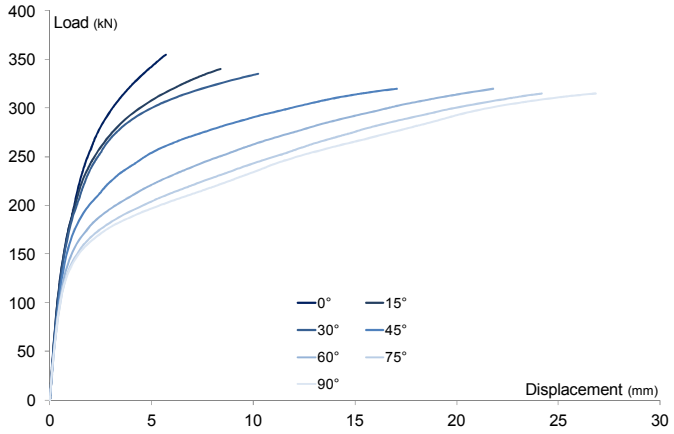

Figure 7.2 - Load-displacement curves for t = 8.5 mm

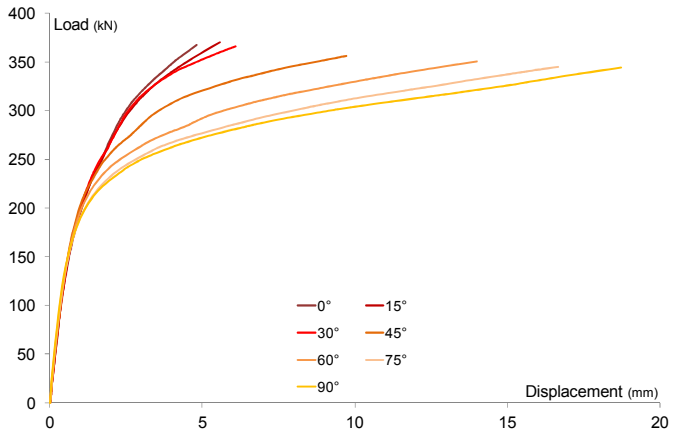

Figure 7.3 - Load-displacement curves for t = 10.5 mm

From Table 7.3 and Figure 7.4 is possible to appraise the strong influence on the bending resistance of a steel plate of very limited variations in its thickness. For example deviations from nominal plate thickness due to hot rolling fabrication process (usually ± 0.5 ÷ 1.0 mm) can induce variations of m_{pl} between 10% and 25%. It is important to underline that the percentage variations of m_{pl} in function of t are totally independent from the value of f_y.

t (mm)	f_y = 355 MPa (nominal)		f_y = 415.54 MPa (actual)	
	m_{pl} (N·mm/mm)	Δ (%)	m_{pl} (N·mm/mm)	Δ (%)
6.5	3750	-41.52%	4357	-41.52%
7.0	4349	-32.18%	5054	-32.18%
7.5	4992	-22.15%	5801	-22.15%
8.0	5680	-11.42%	6601	-11.42%
8.5	6412	---	7452	---
9.0	7189	+12.11%	8354	+12.11%
9.5	8010	+24.91%	9308	+24.91%
10.0	8875	+38.41%	10314	+38.41%
10.5	9785	+52.60%	11371	+52.60%

Table 7.3 - Variation of the plastic moment m_{pl} in function of the plate thickness t

Significant differences in the values of the displacement at collapse are detected in the range 0° ≤ φ ≤ 30°. In particular for φ = 0° this phenomena is directly associated to the different bearing resistances offered by the plates. In fact the case t = 6.5 mm shows greater displacements respect to the other cases, due to a greater deformation associated to higher bearing stresses induced by the bolts on the plate. For combined loading condition of N and V bearing phenomena become less important and the displacement at collapse is influenced mainly by the flexural and membrane deformations of the steel plate. In fact smaller thickness gives more deformable plates as evidenced also from the different elastic stiffness exhibited by the specimens with t = 6.5 mm.

For the pure shear condition the differences in the bearing resistance of the plates affect also the collapse loads. In fact, as expected, the lowest values is obtained for t = 6.5 mm while the highest one for t = 10.5 mm (Figure 7.5 and Figure 7.6).

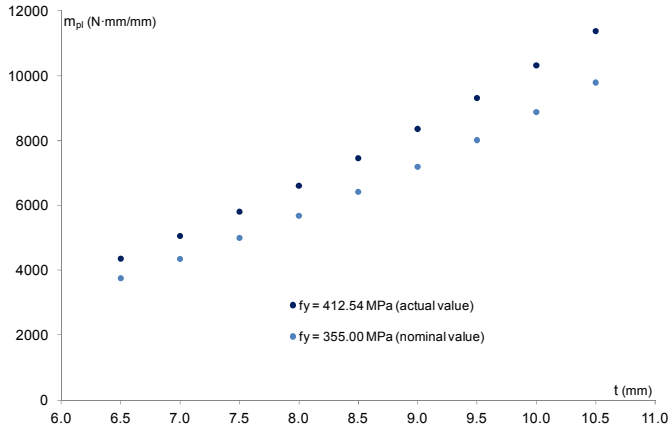

Figure 7.4 - Variation of m_{pl} in function of the plate thickness t

In Figure 7.5 the relationships between the collapse loads and the inclination angle φ are compared for the selected values of t. In general all the specimens exhibit an approximately linear behaviour, with greater reductions of the collapse load with the increasing of φ for lower values of t, as already evidenced from the load-displacement curves. The three series of data tend to diverge for higher value of φ, resulting in greater differences between the collapse loads associated to the different geometries.

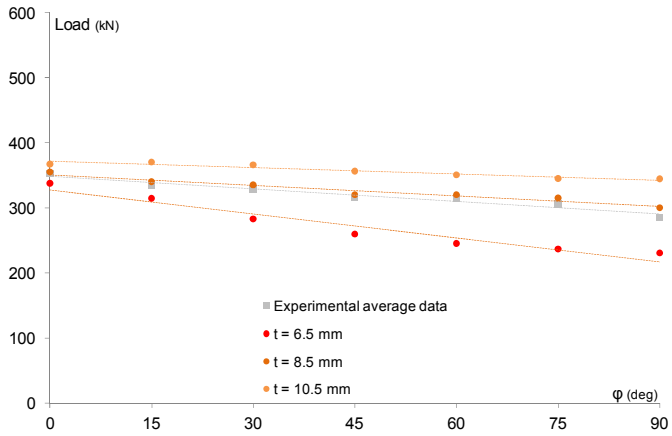

Figure 7.5 - F-φ relationships for different values of t

In Figure 7.6 is presented the comparison of the T-stubs N-V domain respectively for t = 6.5 mm, t = 8.5 mm and t = 10.5 mm. A progressive "expansion" of the limit domain is related to the increment of t. This effect becomes more evident with the increasing of the axial component of the load.

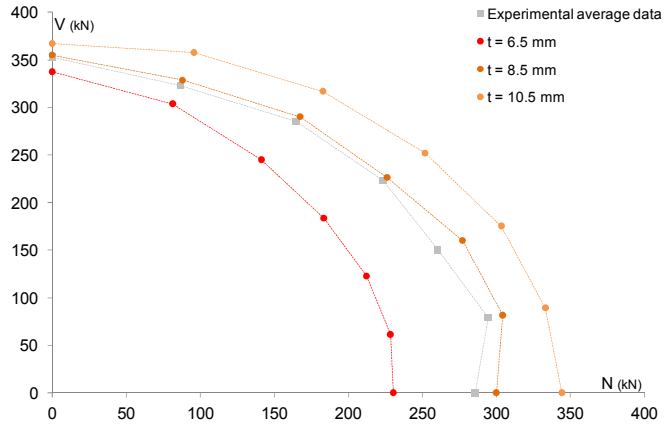

Figure 7.6 - N-V domains different values of t

To better understand how the T-stubs behave in the different cases in Figure 7.7 to Figure 7.10 are shown the residual deformations and the slope isolines maps that allow identifying the flange mechanisms. The comparison is limited to the extreme cases of t= 6.5 mm and t = 10.5 mm. Observing the slope isolines maps for φ = 0° the area involved by local bearing deformations is clearly identified. With the increasing of φ the behaviour described in section 4.3 for the "reference case" is confirmed: the shear force induces an asymmetry in the flange deformation.

Additionally it is possible to observe comparing the colour scale that the specimens with t = 6.5 mm are subjected to grater displacements, highlighted by darker tones of blue. Respect to the reference case with t = 8.5 mm, in which a clear flange mechanism develops only starting from φ = 45° (Figure 5.36) for t = 6.5 mm a significant portion of the flange is involved by the formation of yield lines for φ ≥ 30° (Figure 7.8). On the opposite side for t = 10.5 mm a considerable flange mechanism is visible only for φ > 60° (Figure 7.9). The greater plate thickness allows the developing of more "confined" plastic mechanism, in which the extension of the yield lines is lower than in the other cases. In addition also the asymmetry due to the presence of the shear force is less evident respect to the other considered cases.

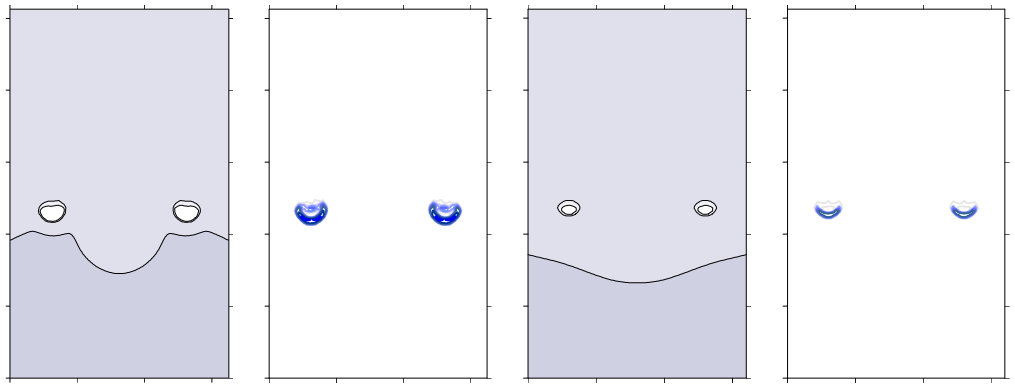

t = 6.5 mm t = 10.5 mm

Figure 7.7 - Residual deformations and slope isolines of T-stubs with different values of t (φ = 0°)

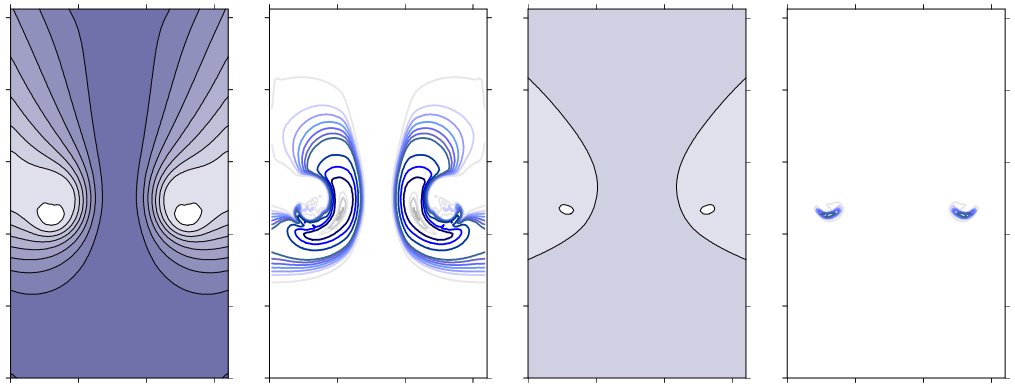

t = 6.5 mm t = 10.5 mm

Figure 7.8 - Residual deformations and slope isolines of T-stubs with different values of t (φ = 30°)

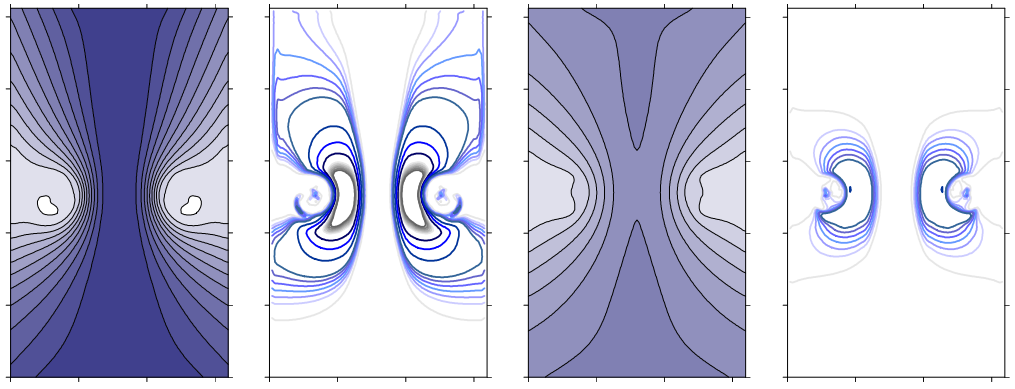

t = 6.5 mm t = 10.5 mm

Figure 7.9 - Residual deformations and slope isolines of T-stubs with different values of t (φ = 60°)

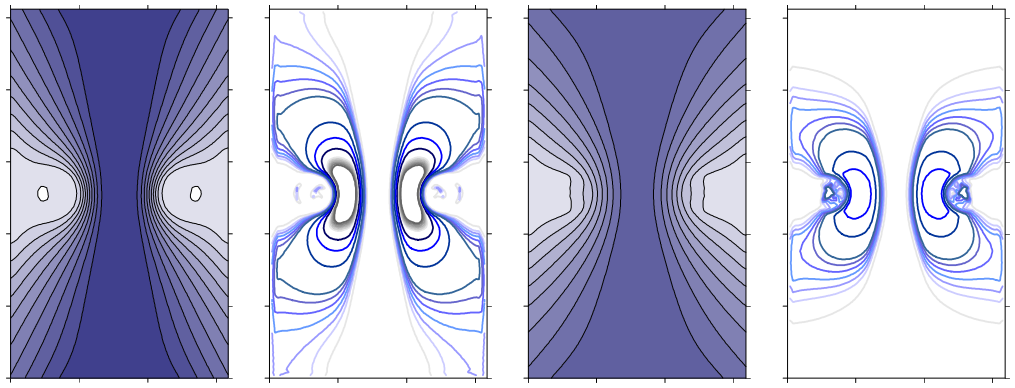

Figure 7.10 - Residual deformations and slope isolines of T-stubs with different values of t (φ = 90°)

7.1.2 Bolts position

The bolts position, identified by the parameters n and m (Figure 3.12), have also a direct influence on the capability of the specimen to develop the plastic moment m_{pl} along the yield lines. In fact, considering for example Figure 3.12, the bolts' position affects the distribution of the forces acting on the steel plate and hence the moment distribution. In general a greater value of n means a higher lever arm of the prying forces Q respect to the bolt position and consequently an higher bending moment acting on the T-stub flange at the bolt line and a lower bending moment at the web line.

For the specific case of failure mode I (Figure 7.11) the plastic moment is reached both at the bolt line and at the web line independently from the bolt position. The variation of n results only in a variation in the position of the plastic hinge where M'_{pl} develops, as evidenced in Figure 7.11.

Furthermore the variation of the geometrical parameters n and m affects directly the shape of the flange mechanism (whichever models is considered, like Zoetmaijer, Packer and Morris and also in the proposed model for the N-V interaction). This leads to a change of the length of every single yield line that defines the flange mechanism, resulting in a small variation of the mechanism shape.

As for the flange thickness the preliminary check (Table 7.1) confirms that for all the three cases the failure mode I is expected. This is due to the limited variations in the values of n (and consequently of m).

The lowest value of n is fixed assuming as reference the limit suggested by the EN1993-1-8 about the minimum distance of the bolt holes from the plate edge.

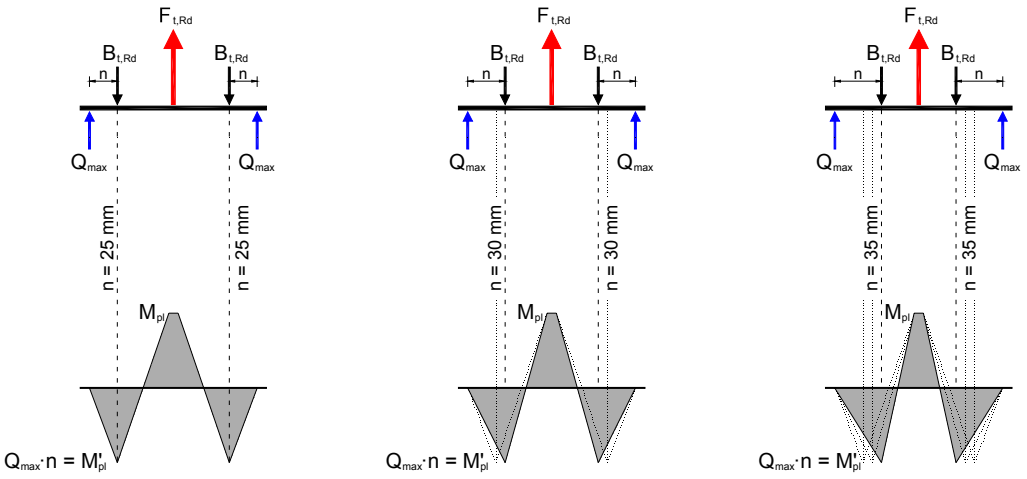

Figure 7.11 - Moment distribution on T-stub flange in function of the bolt position n

In Figure 7.12, Figure 7.13 and Figure 7.14 are shown the load-displacement curves respectively for n = 25 mm, n = 30 mm and n = 35 mm.

Also in this case it is immediately apparent a different behaviour at collapse, with a greater reduction of the collapse load with the increasing of φ for n = 25 mm rather than n = 35 mm. Remarkable differences of the displacement at collapse are identifiable for n = 35 mm especially in the range 60° ≤ φ ≤ 90°. For the other cases, the displacements at collapse are in general very similar with limited differences.

The T-stub with n = 35 mm represents the more deformable specimen, independently from the loading condition to which the specimen is subjected.

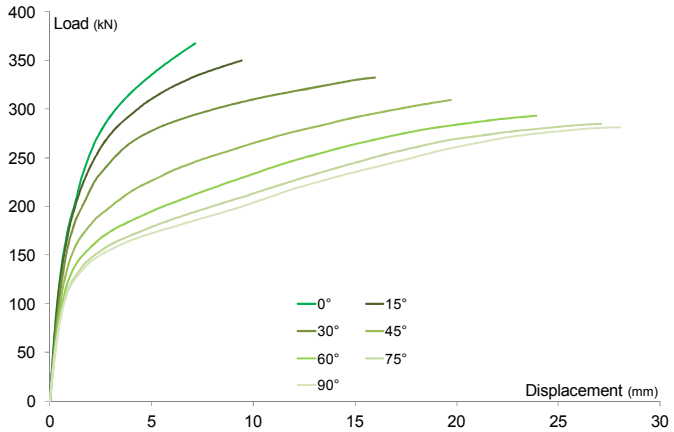

Figure 7.12 - Load-displacement curves for n = 25 mm

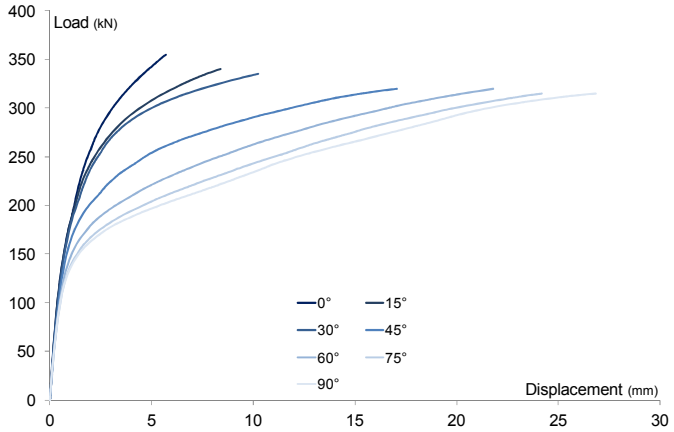

Figure 7.13 - Load-displacement curves for n = 30 mm

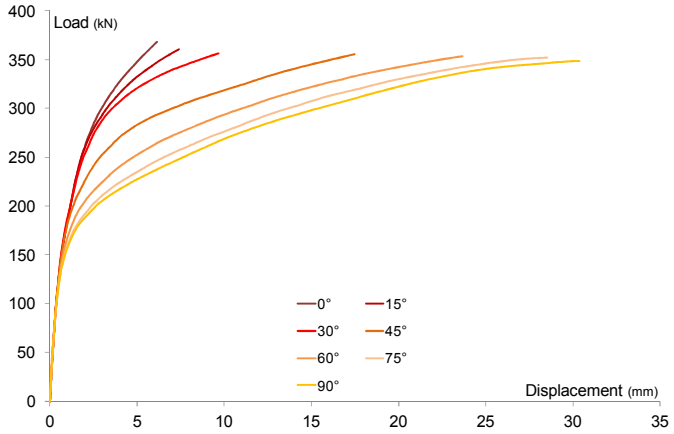

Figure 7.14 - Load-displacement curves for n = 35 mm

No significant variations in the specimens' elastic and post-elastic stiffness can be seen comparing the numerical simulations carried out for the same value of the inclination angle φ.

For the pure shear condition the behaviour of the three specimens is very similar, with negligible differences between the load-displacement curves.

In Figure 7.15 the variation of the collapse load with φ is compared for the three cases. The differences in terms of collapse loads are limited if compared with the results obtained from the previous cases referred to a variation of t (Figure 7.5). Also in this case the data show a linear decreasing trend with the increasing of φ. Very limited variations in the values of the collapse loads are identified for n = 35 mm ranging from

φ = 0° to φ = 90°. Similarly to Figure 7.5 greater differences in terms of collapse loads are visible for high values of φ.

Figure 7.16 offers a representation of the axial component of the applied load in function of the shear one. It can be seen that the curves start approximately from a common point for a pure shear condition, and hence they tend to diverge with the increasing of the axial component of the load.

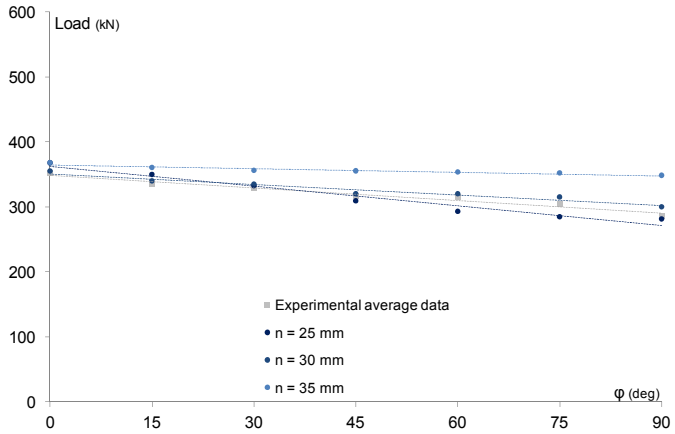

Figure 7.15 - F- φ relationships for different values of n

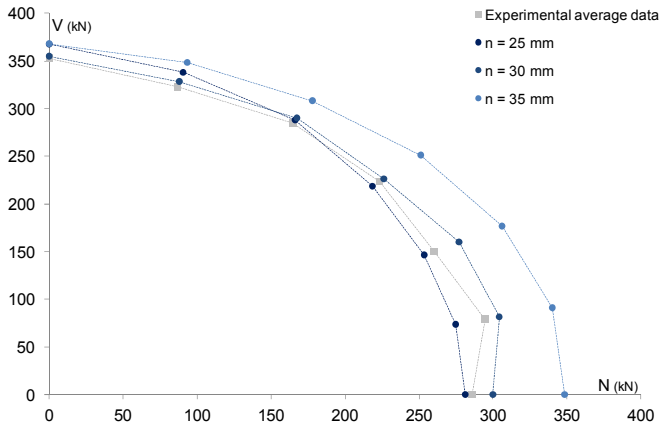

Figure 7.16 - N-V domains for different values of n

The analysis of the residual deformations (Figure 7.17 ÷ Figure 7.20) highlights limited differences between the cases n = 25 mm and n = 35 mm. The distribution of the residual deformations is very similar, with only a magnitude difference.

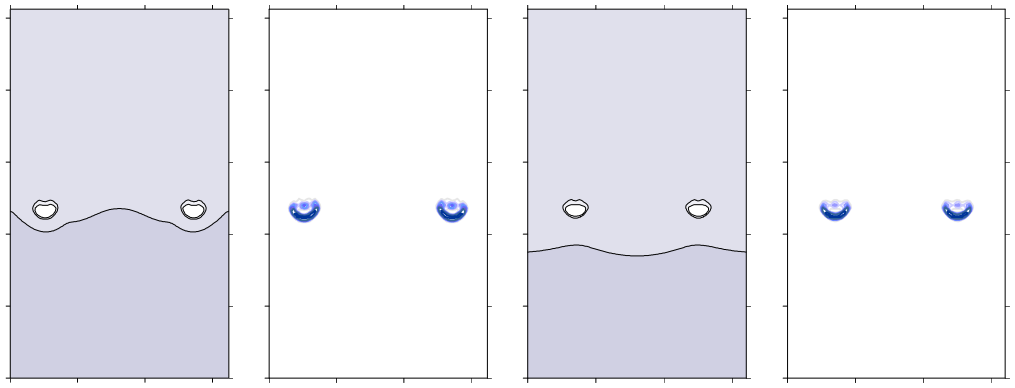

Figure 7.17 - Residual deformations and slope isolines of T-stubs with different values of n (φ = 0°)

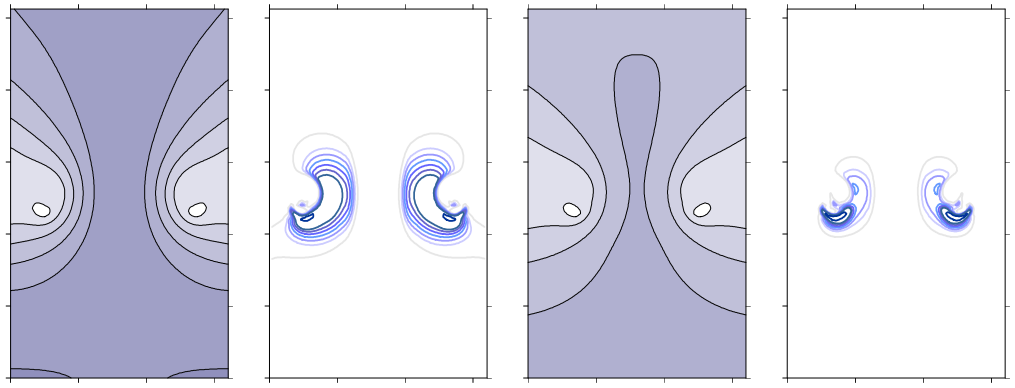

Figure 7.18 - Residual deformations and slope isolines of T-stubs with different values of n (φ = 30°)

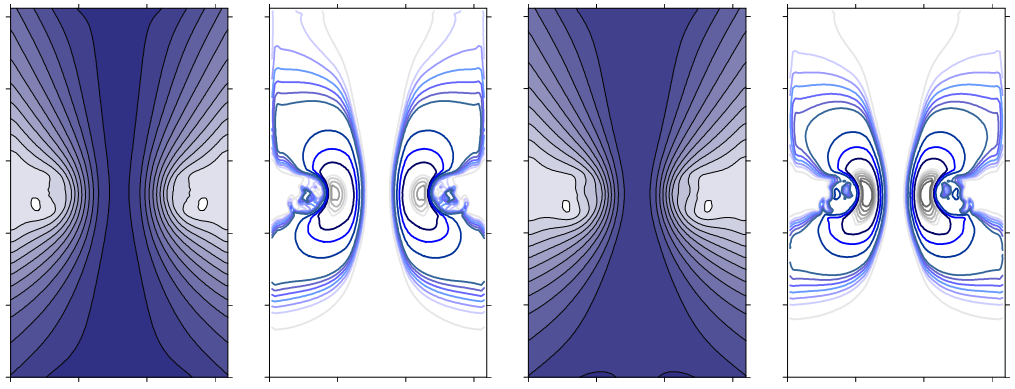

Figure 7.19 - Residual deformations and slope isolines of T-stubs with different values of n (φ = 60°)

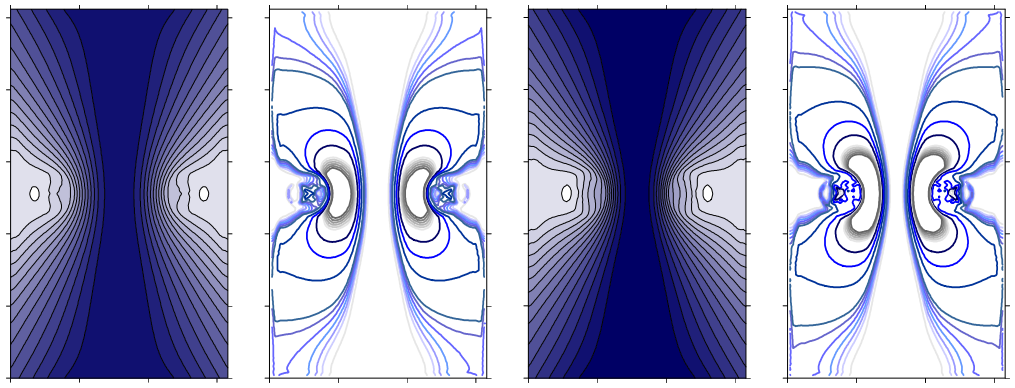

Figure 7.20 - Residual deformations and slope isolines of T-stubs with different values of n (φ = 90°)

The case n = 35 mm, as evidenced also by the load-displacement curves, shows greater displacements of the T-stub flange respect to the others. The shapes of both level lines and slope isolines remain practically unchanged with the variation of the bolt position. The development of a complete flange mechanism takes place for all the three cases for φ > 30° (Figure 7.19)

7.1.3 Bolt diameter

The last investigated case concerns the influence on the T-stub behaviour of the bolt diameter d. As for the flange thickness and the bolts position, different bolt strengths can results in significant variation of the failure mode, ranging from mode I (strong bolts - weak plate) to mode III (weak bolts - strong plate). Similarly to the previous cases the selected values of bolt diameter (M16, M20 and M24 bolts) are close enough to not change the failure mode. For all the three cases in fact failure mode I is expected under pure tension loading condition (Table 7.1).

Different amounts of the bearing deformations are also expected due to the variation of the contact areas between the holes and the bolts.

The load-displacement curves of Figure 7.21, Figure 7.22 and Figure 7.23 show also in these analyses a decreasing trend, more evident for d = 24 mm. For d = 16 mm it seems to be very limited.

The variation of the bolt size gives strong differences in the collapse loads between the three cases.

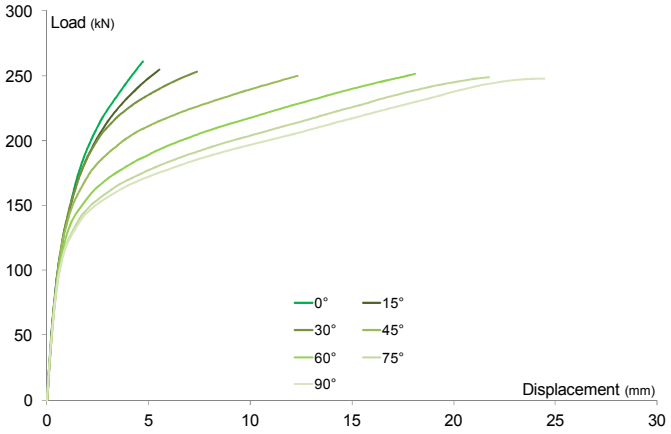

Figure 7.21 - Load-displacement curves for M16 bolts

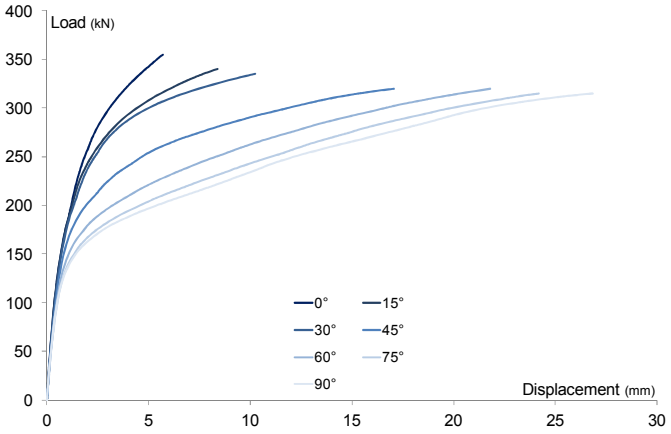

Figure 7.22 - Load-displacement curves for M20 bolts

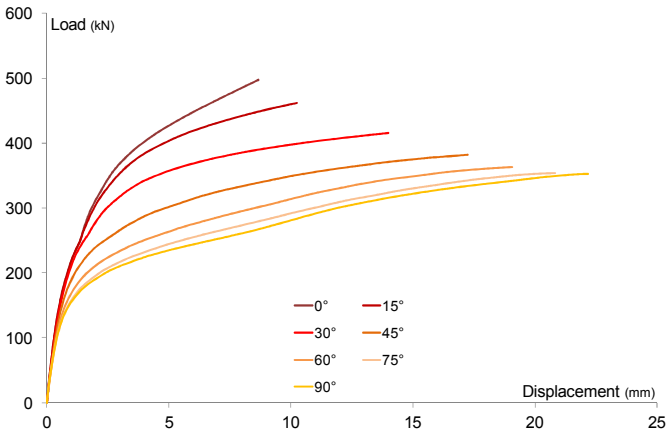

Figure 7.23 - Load-displacement curves for M24 bolts

These differences tends to decrease with the increasing of φ, but remain remarkable also for the pure tension loading condition. Also the deformation capacity at collapse is very sensitive to the variations of bolts size.

For low values of the inclination angle φ the case associated to M24 bolts presents greater displacements at collapse respect to the other cases, while for φ > 45° the specimen with M20 bolts presents the highest displacements at collapse.

The bolt diameter affects also the stiffness of the elastic branch of the specimens' load-displacement curves. To a greater diameter corresponds an higher elastic stiffness. On the contrary the post yield stiffness seems not to be influenced by the different bolts sizes.

Figure 7.24 shows as for the other investigated parameters a decreasing trend of the collapse loads with the increasing of the inclination angle. For d = 16 mm and d = 20 mm the behaviour is approximately linear as for the cases previously presented. For d = 24 mm instead the fitting curve presents a non linear behaviour.

Dissimilarly from the analysis carried out for t and n, in this case the grater differences in terms of collapse loads corresponds to pure shear condition rather than the pure tension one.

Also the N-V domains in Figure 7.25 present a different general behaviour respect to the ones reported in Figure 7.6 and Figure 7.16. The domains for different values of d present almost an uniform expansion between one case and another. As already evidenced from Figure 7.24 also the N-V domain for d = 24 mm presents an unusual behaviour, showing a divergence respect to the other values of d when the shear component of the applied load is greater than the axial one.

The evaluation of the residual deformations (Figure 7.26 ÷ Figure 7.29) as expected shows remarkable differences. In Figure 7.26 the isolines maps show the different areas involved by bearing phenomena. In Figure 7.27 for d = 16 mm only local bearing of the plate occurs while for d = 24 mm a beginning of the development of a flange mechanism is present, despite it does not represent a full flange mechanism. Only in Figure 7.28 is present a completely developed mechanism for both bolt diameters. For the pure tension case (Figure 7.29) the residual deformations and the flange mechanisms for M16 and M24 bolts respectively are very similar, with limited differences in terms of displacements and mechanism shapes. This is probably due to the fact that in both cases failure mode I is expected.

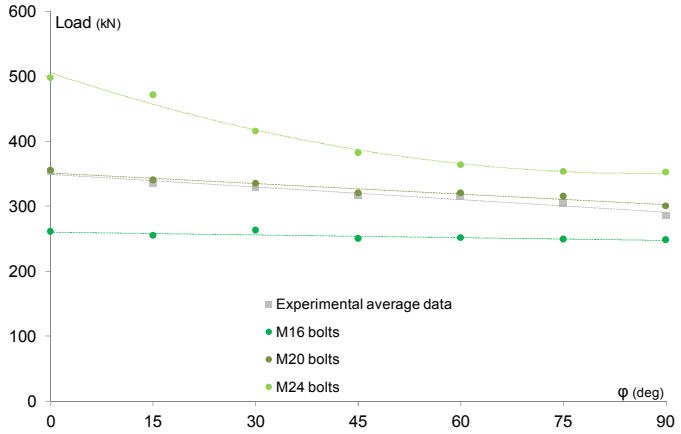

Figure 7.24 - F- φ relationships for different values of d

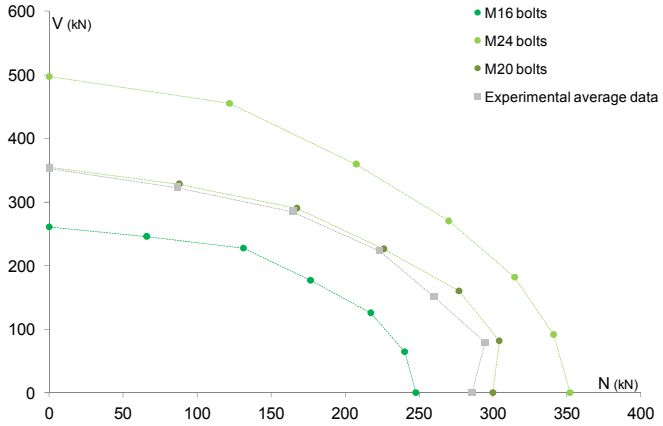

Figure 7.25 - N-V domains for different values of d

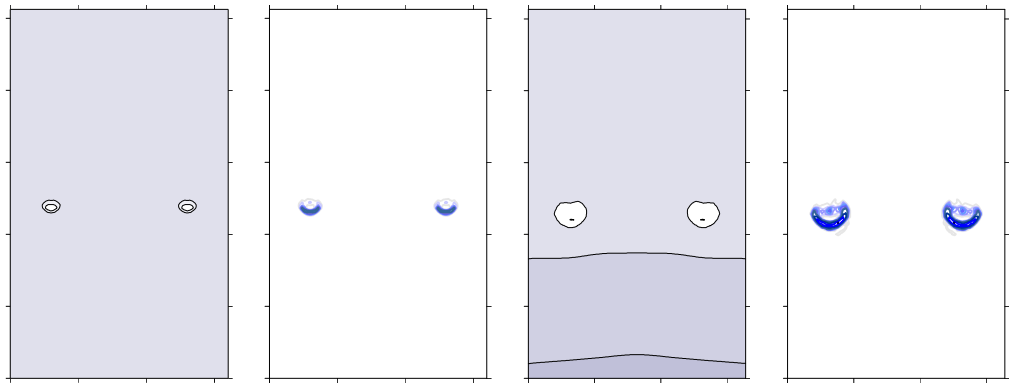

Figure 7.26 - Residual deformations and slope isolines of T-stubs with different values of d (φ = 0°)

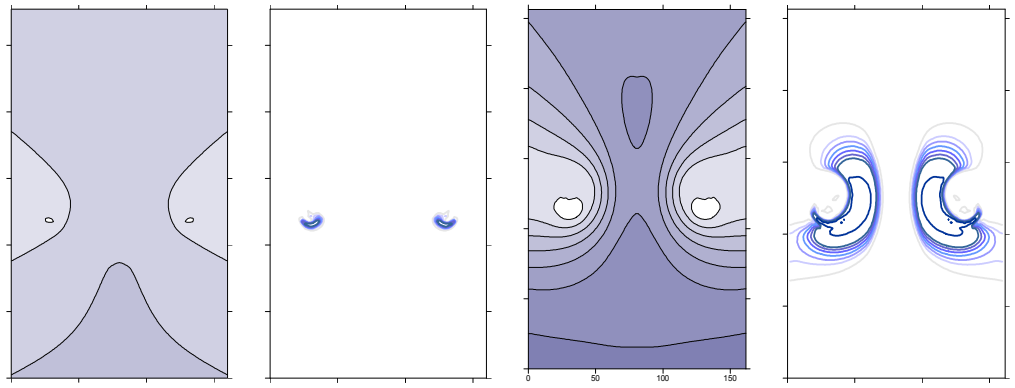

M16 bolts M24 bolts

Figure 7.27 - Residual deformations and slope isolines of T-stubs with different values of d (φ = 30°)

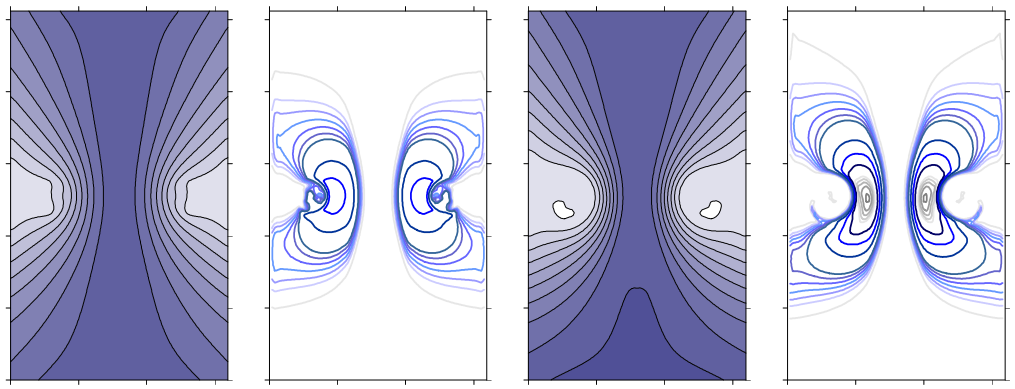

M16 bolts M24 bolts

Figure 7.28 - Residual deformations and slope isolines of T-stubs with different values of d (φ = 60°)

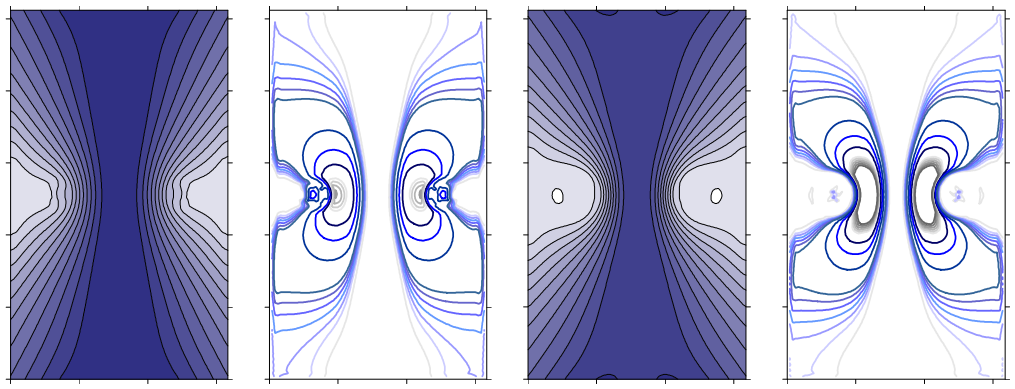

M16 bolts M24 bolts

Figure 7.29 - Residual deformations and slope isolines of T-stubs with different values of d (φ = 90°)

7.2 Analytical results

In this section the theoretical model developed for the prediction of the yield load of T-stubs under combined actions of axial and shear force is applied to the cases numerically investigated in the previous paragraphs. It should be mentioned that a key aspect on which is based the model calibration is the correlation functions between the angles which define the yield lines patterns. The relationships between α and θ (Figure 6.11) or β and ω (Figure 6.12) in fact were calibrated on the experimental evidence, which are not available for the investigated cases in the parametrical analyses. This may cause a small error in the evaluation of the specimens strength. However it is expected to be sufficiently small to be considered negligible.

As first operation the numerical load-displacement curves are approximated by a bilinear relationship, similarly to what is carried out for the experimental data, in order to estimate the yield load. In Table 7.4 are summarized the yield loads for the different cases. Once obtained the numerical yield loads they are compared with the results obtained from the analytical model (Table 7.5). The attention focused on the cases associated to $45° \leq \varphi \leq 90°$ which show the development of a flange mechanism. An exception is represented by the cases t = 10.5 mm and d = 16 mm in which a significant flange mechanism develops only for $\varphi > 60°$. From the results in Table 7.5 it is possible to observe that the analytical evaluation of the T-stub yield load is independent from the bolt diameter d. In fact the model formulation presented in the previous chapter doesn't take in account the geometry of the bolts, which represents only a restrain accordingly to the hypotheses relative to the bolts behaviour concerning the yielding phase.

φ	reference	t		n		d	
(deg)	case	6.5 mm	10.5 mm	25 mm	35 mm	16 mm	24 mm
0	273.489	245.892	262.364	271.567	264.244	348.668	179.191
15	277.644	249.128	284.059	270.702	287.018	368.794	183.899
30	283.390	209.575	300.721	273.804	298.201	344.890	198.887
45	245.260	145.527	299.673	207.971	269.130	276.048	192.838
60	201.953	120.067	279.441	171.817	233.824	228.164	175.004
75	183.118	106.964	268.444	154.514	209.631	207.311	163.886
90	173.233	102.670	261.524	146.064	192.961	158.9278	163.291

Table 7.4 - Numerical yield loads

φ	reference	t		n		d	
(deg)	case	6.5 mm	10.5 mm	25 mm	35 mm	16 mm	24 mm
45	208.11 (-15.15%)	123.426 (-15.19%)	no flange mechanism	193.49 (-6.96%)	225.56 (-16.19%)	no flange mechanism	208.11 (-24.61%)
60	173.30 (-14.19%)	101.812 (-15.20%)	no flange mechanism	160.55 (-6.56%)	188.84 (-19.24%)	173.30 (-0.97%)	173.30 (-24.05%)
75	156.33 (-14.63%)	91.508 (-14.45%)	238.266 (-11.24%)	144.65 (-6.39%)	170.66 (-18.59%)	156.33 (-4.61%)	156.33 (-24.59%)
90	151.16 (-12.74%)	88.393 (-13.91%)	230.659 (-11.80%)	139.81 (-4.28%)	192.961 (-14.45%)	151.16 (-4.89%)	151.16 (-23.60%)

Table 7.5 - Analytical vs. numerical yield loads

In Table 7.5 are reported the deviations of the yield load analytically evaluated respect to the numerical ones. For the reference case the underestimation of the analytical yield load is analogous to the one evaluated respect to the experimental data (Table 6.2). For the different analyzed cases the underestimation seems to remain rather limited.

Considering the variation of the T-stub flange thickness the underestimation ranges between about 11% and 15%. Lower discrepancies are obtained for higher values of t.

In Figure 7.30 and Figure 7.31 a graphical comparison between the numerical and analytical results is presented respectively in terms of F-φ and N-V relationships. In the graphs the dots represent the numerical yield loads while the triangles connected by a dashed line indicate the analytical yield load. In the N-V domains the dashed lines without any symbols show the collapse loads for the different load combinations.

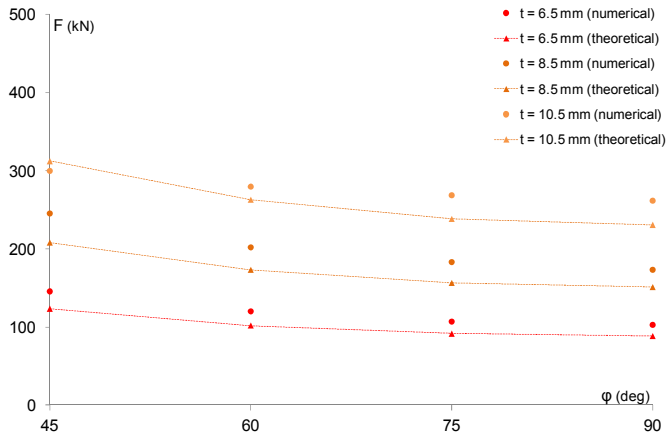

Figure 7.30 - Analytical vs. numerical F-φ curves for different t

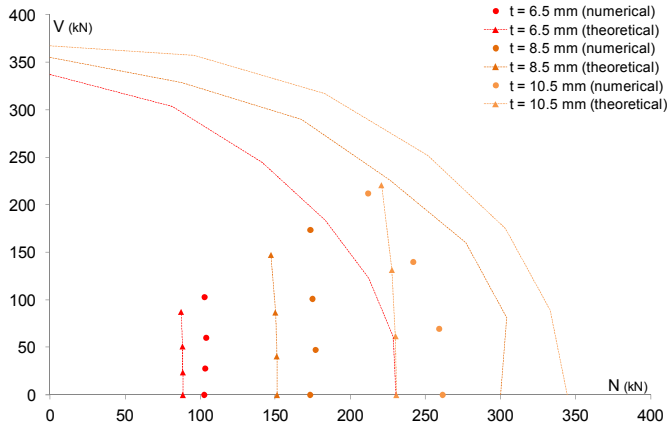

Figure 7.31 - Analytical vs. numerical N-V domains for different t

In general the variation of t in both the numerical and the analytical models gives very similar effects. In Figure 7.30 the behaviour of the three couples of curves for different t values are in good agreement. No significant differences between the numerical and theoretical values are detected. Hence the variation in the T-stub behaviour numerically analyzed seems to be confirmed also by the theoretical model.

The results in Figure 7.31 also show a close similarity, despite for t = 10.5 mm the analytical model is applicable only for $\varphi > 60°$ (a complete flange mechanism develops only for $\varphi = 75°$ and $\varphi = 90°$). However, in Figure 7.31 are reported the analytical yield load also for $45° < \varphi < 60°$.

Figure 7.32 and Figure 7.33 refer to the yield loads obtained for different values of n.

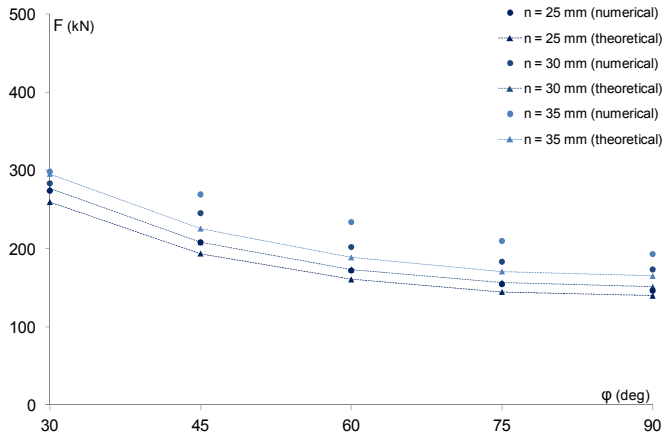

Figure 7.32 - Analytical vs. numerical F-φ curves for different n

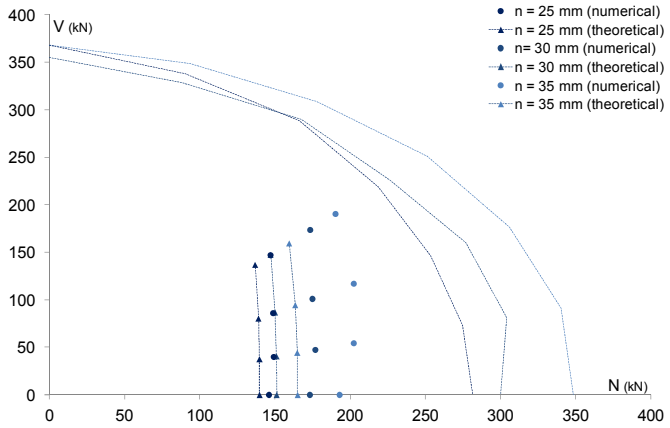

Figure 7.33 - Analytical vs. numerical N-V domains for different n

For n = 25 mm very limited differences are observed between numerical and analytical data (between 4% and 6%). The gap tends to increase for higher values of n, up to approximately 20%. The behaviour both in terms of F-φ and N-V curves is equivalent also in this case.

Finally, in Figure 7.34 and Figure 7.35 are reported the results for different bold diameters d. For this specific case the analytical model is not able to differentiate the yield loads values for different d. That is the reason why in Figure 7.34 and Figure 7.35 only one series of theoretical data is visible.

However, the average behaviour of the numerical models is sufficiently well approximated.

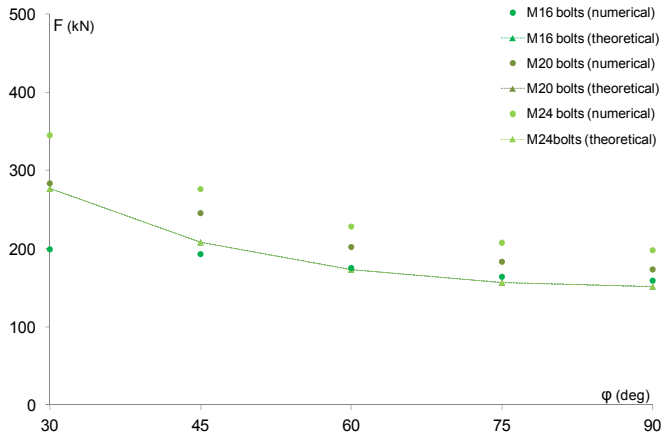

Figure 7.34 - Analytical vs. numerical F-φ curves for different d

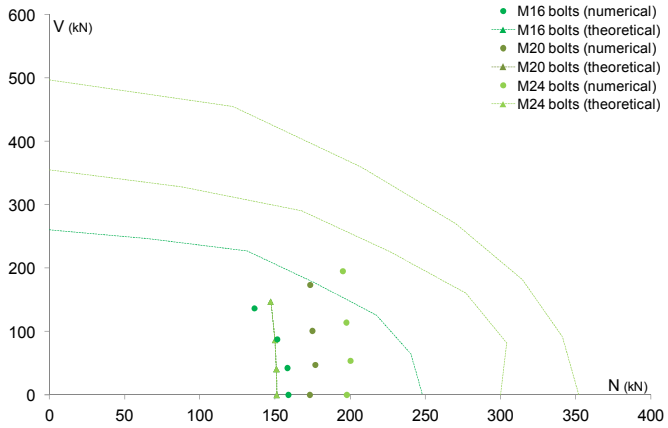

Figure 7.35 - Analytical vs. numerical N-V domains for different d

8. CONCLUSIONS AND OUTLOOKS

The present work focused on structural design problems in case of accidental actions. Accidental actions can induce localized damages which may spread within the structure activating chain reactions which may cause its partial o total collapse. If a structure is "robust" accidental actions result in damages not disproportioned to the event which have generated them. Therefore, the design of robust structures aims to "confine" the extent of the damage within limits considered acceptable, avoiding its spreading to the rest of the structure. This aspect highlights the need to define reliable and economically sustainable rules for the design of robust structures.

Studies and researches on progressive collapse led to the adoption by several design codes of guidelines for robust design. These general principles are characterized by a common philosophy and similar approaches. Summarizing, to limit the failure probability and the risk associated to the progressive collapse is possible to:

- act on actions by events control techniques;
- act on damage spreading, designing robust structures characterized by low sensibility to progressive collapse;
- act on structural response, designing redundant and ductile structures.

Considering this last topic joints and especially the beam-to-column ones assume a key role in ensuring an adequate robustness level. In fact the connections have to possess specific requirements of strength and ductility to guarantee the activation of alternative load paths in the damaged structure. Considering the case of loss of a column the redistribution of the internal forces occurs with the development of catenary actions in the floor systems and large displacements. These events considerably affect the joints response. From an initial bending exposure they are progressively subjected to increasing axial and shear forces while the bending moment tends to decrease. Therefore, in the new equilibrium condition the joints are subjected mainly to combined axial and shear forces.

The scope of this work was the investigation of the response of steel joints under different combination of axial force (N), shear force (V) and bending moment (M). The starting point of this study was a research carried out at the University of Trento in the framework of an European project on robustness. The research project considered as a reference case the loss of a column in a three-storey office building. The activation of catenary actions in the floor system to allow for alternative load path was the selected robustness design strategy.

The analysis of joints response was carried out adopting the philosophy of the component method implemented in the EN 1993-1-8 [41]. It is a general procedure for the evaluation of the joints behaviour in terms of moment-rotation relationship (M-Φ). However the component method doesn't give any information about the behaviour of joints (and their components) under combined actions.

Several researches aim at extending the component method also to the case of joint subjected to combined actions which actually is not covered by the EN 1993-1-8 [41]. The present work is among them. The attention focused on the tension region of the connection which represent the main source of ductility. The basic joint components in the tension region can be well approximated by equivalent T-stubs elements. The response of T-stubs under different loading conditions was investigated.

8.1 Conclusions

The starting point of the present work was an experimental campaign carried out at University of Trento in the framework of the European research project "Robust Structures by Joint Ductility". In detail the column T-stub response was deeply analyzed under different combination of axial (N) and shear force (V) to evaluate the influence of the shear force on the response of this joint component. At this aim specific experimental tests were performed considering different inclination angle φ of the applied load. To an inclination angle φ = 0° corresponded the condition of pure shear, while φ = 90° was associated to a pure tension load.

The experimental outcomes highlighted the strong influence of the shear force on the T-stub response. The shear force considerably affected not only the resistance of the specimens but also the deformation capacity. This resulted in significant changes also in the failure mechanism of the T-stub.

The results allowed to clearly indentify a N-V interaction domain for the T-stub. The variation of the collapse load as function of the inclination angle φ of the resultant applied load was almost linear, showing its maximum value for pure the shear condition (φ = 0°) and its minimum in case of pure tension (φ = 90°).

A further investigation concerned the residual deformations of the T-stubs flanges. The deformed shapes of the specimens were acquired with a laser system. This allowed to appraise on one hand the magnitude and the distribution of the plastic residual deformations (through the level lines maps) and on the other hand the development of flange mechanisms (through the slope isolines maps). For the pure shear condition no flange mechanism was detected. The (brittle) collapse of the specimen was associated to the bolts fracture in shear with consequent bearing phenomena in correspondence of the holes in the T-stub flange. Starting from an inclination angle φ = 45° (N = V) a clear flange mechanism developed. The maximum flange deformation was achieved for φ = 75°.

3D finite elements models were developed in Abaqus v.6.8 to better understand the complex behaviour of the T-stub under combined loading conditions. An accurate calibration of the F.E. models was performed considering the available experimental tests data. A good agreement between the numerical and the experimental results was achieved not only in terms of load-displacement curves, but also in terms of T-stub flange residual deformations. Additionally, the comparison of the numerical slope isolines maps, which identify the flange mechanism, showed a very good agreement with the experimental ones which were measured by the laser acquisition system.

The results obtained from the F.E. models suggested to extend the numerical simulations to different specimen configurations. The influence of geometrical parameters like the flange thickness, the bolts position and the bolts diameter was investigated. The load-displacement curves as the residual deformations and the flange mechanism obtained from the slope isolines maps were compared for the different geometries and loading conditions. This allowed to obtain a clearer overview of the T-stub response.

In all the analyses were confirmed that to an increment of the inclination angle φ was associated a reduction of the collapse load.

Variations of the flange thickness (t) considerably affected both the strength and the deformability of the T-stubs. In case of pure shear condition to thinner plates were associated greater bearing phenomena. With the increasing of the inclination angle φ (and hence of the axial component of the load) the T-stubs with thicker plates appeared

less deformable. Also the development of the flange mechanisms was influenced. In fact for t = 10.5 mm a complete plastic mechanism was visible only for φ ≥ 75° while for t = 6.5 mm and t = 8.5 mm it developed for φ ≥ 45°.

If the bolt position (n) was changed remarkable differences in the displacement at collapse especially for φ > 45° were observed. The more deformable specimens were the ones with greater values of n (35 mm). The collapse loads was not influenced as much as for the other cases in which the flange thickness or the bolts diameter were changed. However, greater reductions of the collapse load were observed for n = 25 mm and n = 30 mm while for n = 35 mm they were very limited.

An increment of the bolts diameter (d) resulted in a stronger reduction of the collapse load with the increasing of φ. However, in this case dissimilarly from the analysis carried out for t and n, the wider differences in terms of collapse loads corresponded to pure shear condition rather than the pure tension one. As expected the flange deformations were influenced by the variations of the bolts size. For φ = 0° was possible to observe differences in the areas involved by bearing phenomena. With the increasing of φ flange mechanisms started to develop. The formation of a complete flange mechanism occurred firstly for φ = 45° in the specimen whit grater bolt diameters (M20 and M24) and only for φ = 60° in the specimen with M16 bolts.

A further aspect of the work focused on the analytical analysis of the T-stub response in case of combined actions. The aim was to obtain a simplified elastic-perfectly plastic load-displacement relationship for the T-stub under a generic combination of N and V. Therefore, to fully describe the T-stub behaviour was necessary to assess the yield load and the elastic stiffness.

The evaluation of T-stubs yield load, resulting in the development of a flange mechanisms, can be obtained by using the principles of the limit analysis and in particular the kinematic theorem. Adopting a flange mechanism described by a family of plastic lines (yield lines), it is possible to estimate the collapse load considering the balance between the internal work associated with the development of the yield lines and the work done by the external force. An effective definition of the failure mechanisms of bolted T-stubs in pure tension was carried out by Zoetemeijer: this study still represents a reference formulations which was also adopted in EN1993-1-8 [41]. Zoetemeijer proposed a flange mechanism described by a family of straight yield lines. An extension of Zoetmeijer formulation to the case of combined action of axial (N) and shear force (V) was developed in this study. The analyses were limited to the cases in which during the tests the activation of flange mechanisms was achieved (φ ≥

45°). The flange mechanisms experimentally observed suggested the possibility to introduce the effect of the shear force in a simplified way: imposing the asymmetry of the flange mechanism and reducing the plastic moment developed along specific yield lines on the basis of the value of the shear component of the external load. The asymmetry of the yield lines configuration was imposed through experimentally calibrated functions which correlate the geometrical parameters required to describe the flange mechanism. This allowed indentifying a simplified model able to predict with sufficient accuracy the T-stub yield load, with an underestimation respect to the experimental results ranging from a minimum 13.11% for $\varphi = 90°$ up to 17.53% for $\varphi = 75°$.

The proposed analytical model was also applied to the different specimen configurations adopted in the F.E. parametrical analyses. Also in these cases good results were obtained. The gap between the numerical and theoretical yield loads ranges from -15.20% to +4.17% when the flange thickness was varied, from -19.24% to -4.28% when different bolts positions were considered and from -24.61% to +7.92% for different bolt diameters.

Finally the last aspect of the study concerned the evaluation of the stiffness of the T-stub as function of the loading condition. The experimental outcomes showed that the elastic stiffness in the range $0° \leq \varphi < 45°$ can be assumed whit a good approximation coincident with the one suggested by the EN 1993-1-8 [41] for the pure shear condition. Also for $\varphi = 90°$ the formulation proposed by the Eurocode gives a good estimation of the elastic stiffness of the T-stub. For intermediate cases ($45° \leq \varphi < 90°$) a linear variation of the stiffness is proposed.

8.2 Outlooks

The presented work can be considered as a first step for the analysis of T-stub elements under combined actions. The limited amount of available experimental data at the current time does not permit more extensive evaluations. Hence, further tests on different configurations of T-stubs may help to analyze more extensively and confirm the outcomes of this study.

Further developments of the presented work may concern two main topics:

1. the analytical evaluation of T-stub collapse conditions;
2. the extension of the theoretical models to:
    - stiffened T-stubs;

- complete joint.

The first topic concern the development of analytical models for the T-stub under combined axial and shear force able to predict the load and the displacement at collapse. This will allow, together with the theoretical models proposed in this thesis, to have a direct estimation in function of the loading conditions of:

- the component ductility (evaluated as ratio between the displacement at collapse and at yielding);
- the available reserve of strength (defined as the ratio between the collapse and the yield load).

These two aspects may assume a key role for the development of detailing rules for the robust design of beam-to-column connections.

The second topic involves the development of analytical formulations for the response of stiffened T-stubs (at yielding and at collapse) under different combinations of N and V. This may help to complete the characterization of the T-stub behaviour in case of combined actions. In this case, so as for the unstiffened T-stubs, the simplified load-displacement relationship can be introduced in the formulation of the component method to the evaluate the mechanical properties of the whole connection subjected to combined actions.

As alternative to the component method the limit analysis may be adopted to describe the response of the complete connection. Trough the limit analysis principles, it may be possible to analyze separately the column flange and the end-plate by the definition of two distinct yield lines patterns. The two yield line patterns may be defined in order to take into account in a simplified way the simultaneous effect of axial, shear force and bending moment on the connection. One of the main difficulties in developing such type of theoretical model will concern the extension of the procedure to multiple bolt rows which interact with each other.

BIBLIOGRAPHY

[1] Office of the Deputy Prime Minister (ODPM), The Building Regulations 2000, “Part A, Schedule 1:A3, Disproportionate Collapse”, London, UK (2004).

[2] American Society of Civil Engineers (ASCE), “Minimum Design Loads for Buildings and Other Structures (ASCE 7-05/ANSI A.58)”, New York (2005).

[3] European Committee for Standardization (CEN), EN 1991-1-7, "Actions on structures - General actions – Accidental actions”, Brussels (2006).

[4] Office of the Deputy Prime Minister (ODPM), The Building Regulations, "Fifth Amendment", London, UK (1970).

[5] Office of the Deputy Prime Minister (ODPM), The Building Regulations, "Approved Document A", London, UK (1976).

[6] American National Standards Institute, “Building Code Requirements for Minimum Design Loads in Buildings and Other Structures (ANSI A58.1-1972),” American National Standards Institute, New York (1972).

[7] American National Standards Institute, , “Minimum Design Loads in Buildings and Other Structures (ANSI A58.1-1982),” American National Standards Institute, New York (1982).

[8] American Society of Civil Engineers (ASCE), “Minimum Design Loads for Buildings and Other Structures (ASCE 7-02/ANSI A.58, New York (2002).

[9] Department of Defence (DoD), “Interim Antiterrorism/Force Protection Construction Standards, Guidance on Structural Requirements", USA (2001).

[10] Department of Defence (DoD), UFC 4-023-03, “Unified Facilities Criteria, Design of Buildings to Resist Progressive Collapse”, Washington D.C. (2010).

[11] U.S General Service Administration (GSA), "Progressive collapse analysis and design guidelines for new federal office buildings and major modernization projects", Washington D.C. (2003).

[12] Interagency Security Committee (ISC), "ISC Security Design Criteria for New Federal Office Buildings and Major Modernization Projects”, Washington D.C. (2004).

[13] National Research Council of Canada, "National Building Code of Canada 1975", Ottawa, Canada (1975).

[14] National Research Council of Canada, "National Building Code of Canada 1977", Ottawa, Canada (1978).

[15] National Research Council of Canada, "National Building Code of Canada 1980", Ottawa, Canada (1980).

[16] National Research Council of Canada, "National Building Code of Canada 1995", Ottawa, Canada (1995).

[17] Ministero delle Infrastrutture e dei Trasporti, "D.M. 14/01/2008 - Norme Tecniche per le Costruzioni", Rome, Italy (2008)

[18] European Committee for Standardization (CEN), EN 1990, "Basis of structural design”, Brussels (2002).

[19] H. Gulvanessian, J. A. Calgaro, M. Holický, “Designers' guide to EN 1990 Eurocode: Basis of structural design”, Thomas Telford Publishing, London (2002).

[20] W. M. Wilson, H. F. Moore, “Tests to determine the rigidity of riveted joints in steel structures - Bulletin no. 104”, Engineering Experiment Station, University of Illinois, Urbana (1917).

[21] S. W. Jones, P. A. Kirby, D. A. Nethercot, “Effect of semi-rigid connections on steel column strength”, J. construt. Steel Res. 1 (1980).

[22] D. A. Nethercot, “Utilisation of Experimentally Obtained Connection Data in Assessing the Performance of Steel Frames. Connection Flexibility and Steel Frames”, American Society of Civil Engineering, New-York, USA (1985).

[23] A. V. Goverdhan, “A collection of experimental moment-rotation curves and evaluation of prediction equations for semi-rigid connections”, Ph. D. Thesis, Vanderbilt University, Nashville, TN (1984).

[24] N. Kishi, W. F. Chen, “Steel Connection Data Bank Program”, Structural Engineering Report No. CE-STR-86-18, School of Civil engineering, Purdue University, West Lafayette, IN, USA (1986a).

[25] N. Kishi, W. F. Chen, “Database of Steel Beam-to-Column Connections, Vol. 1 and 2”, Structural Engineering Report No. CE-STR-86-26, School of Civil engineering, Purdue University, West Lafayette, IN, USA (1986b).

[26] J. C. Rathbun, “Elastic Properties of Riveted Connections”, Transactions of the ASCE, 101:524-596. (1936).

[27] G. R. Monforton, T. S. Wu, “Matrix Analysis of Semi-Rigidly Connected Steel Frames”, Journal of Structural Engineering, ASCE, 89:13-42 (1963).

[28] M. J. Frye, G. A. Morris, “Analysis of flexibly connected steel frames”, Can. J. civil Engineering 2 (1975).

[29] W. H. Sommer, “Behaviour of welded header plate connections”, Masters Thesis, University of Toronto (1969).

[30] D. J. L. Kennedy, “Moment-rotation characteristics of shear connections”, AISC Enana J. 6, (1969).

[31] M. G. Cox, “The numerical evaluation of B-splines”, J. Inst. Math. Applic. 10 (1972).

[32] S. W. Jones, P. A. Kirby, D. A. Nethercot, “Modelling of semi-rigid connection behaviour and its influence on steel column behaviour in joints in structural steelwork”, Pentech Press, London (1981).

[33] S. W. Jones, P: A. Kirby, D. A. Nethercot, “Columns with semi-rigid joints”, J. struct. Div. ASCE 108 (ST2) (1912).

[34] W. F. Chen, E. M. Lui, “Stability Design of Steel Frames”, CRC Press, New-York, NY, USA (1991).

[35] N. Krishnamurthy, H. T. Huang, P. K. Jeffrey, L. K. Avery, “Analytical M-Φ curves for end-plate connections”, J. struct. Div. ASCE. 105 (STI), (Proc. paper 14294) (1979).

[36] N. Kishi , W. F. Chen, “Moment-rotation relation of top- and seat-angle connections”, Structural Engineering Report no. CE-STR-87-4, School of Civil Engineering, Puidue University, West Lafayette, IN (1987).

[37] N. Kishi, W. F. Chen, “Moment-rotation of semi-rigid connections”, Structural Engineering Report no. CE-STR-87-29, School of Civil Engineering, Purdue University, West Lafayette, IN (1987).

[38] E. M. Lui, W. F. Chen, “Steel frame analysis with flexible joints”, Journal of Construction Steel Research 8 (1987).

[39] E. M. Lui, W. F. Chen, “Analysis and behavior of flexibly jointed frames”, Engineering Structures 8 (1986).

[40] Y. L. Yee, R. E. Melchers, “Moment-rotation curves for bolted connections", Journal of the Structural Division. ASCE 112 (ST3) (1986).

[41] European Committee for Standardization (CEN), EN 1993-1-8 “Design of steel structures – Design of joints”, Brussels (2005).

[42] R.T. Douty, W. McGuire, “High Strength Bolted Moment Connections”, Journal of the Structural Division, ASCE 91 (1965).

[43] H. Agerskov, “High-Strength Bolted Connections Subject to Prying”, Journal of the Structural Division, ASCE 102 (1976).

[44] P. Zoetemeijer, “A design method for the tension side of statically loaded, bolted beam-to-column connections”, Heron Vol. 20 (1) pp. 1-59, The Netherlands (1974).

[45] J. A. Packer, L. J. Morris, “A limit state design method for the tension region of bolted beam-column connections”, The structural Engineer Vol. 5 (10) pp. 446 - 458, United Kingdom (1977).

[46] L. S. da Silva, L. R. O. de Lima, P. C. G. da S. Vellasco, S. A. L. de Andrade, "Behaviour of flush end-plate beam-to-column joints under bending and axial force", Steel and Composite Structures vol. 4, 2 (2004).

[47] P. C. da L. Nunes, L. R. O. de Lima, J. G. S. da Silva, P. C. G. da S. Vellasco, S. A. L. de Andrade, "Parametrical analysis of extended end-plate semi-rigid joints subjected to bending moment and axial force", Latin American Journal of Solids and Structures 4 (2007).

[48] J.P. Jaspart, M. Braham, F. Cerfontaine, "Strength of joints subjected to combined action of bending moment and axial force", In Conference Eurosteel 99, CVUT Praha - Czech Republic (1999).

[49] F. Cerfontaine, “Étude analytique de l'interaction entre moment de flexion et effort normal dans les assemblages boulonnés", Construction Méttalique 4 (2001).

[50] F. Cerfontaine, "Etude de l'interaction entre moment de flexion et effort normal dans les assemblages boulonnés", Thèse de Docteur en Sciences Appliquées, Faculté des Sciences Appliquées, University of Liège, Belgium (2004).

[51] L. S. da Silva, A. M. G. Coelho, "An analytical evaluation of the response of steel joints under bending and axial force", Computer and Structures 79 (2001).

[52] L. S. da Silva, "Towards a consistent design approach for steel joints under generalized loading", Journal of Constructional Steel Research 64 (2008).

[53] K. Urbonas, A. Daniunas, “Component method extension to steel beam-to-beam and beam-to-column knee joints under bending and axial forces”, Journal of Civil Engineering and Management, XI (3) (2005).

[54] K. Urbonas, A. Daniunas, “Behaviour of semi-rigid beam-to-beam joints under bending and axial forces”, Journal of Constructional Steel Research, 62 (2006).

[55] D. Nethercot, A. Del Savio, P.C.G.S. Vellasco S.A.L. Andrade, L.F. Martha, "Developments in semi-rigid joint moment versus rotation curves to incorporate the axial versus moment interaction",ICSCS, Third International Conference on Steel and Composite Structures, Manchester (2007).

[56] W. František, M. Švarc, "Experiments with end-plate joints subjected to moment and normal force", Contributions to Experimental Investigation of Engineering Materials and Structures, CTU Reports No: 2-3, Prague (2001).

[57] U. Kuhlmann, J.-P. Jaspart, R. Zandonini et al., "Robust structures by joint ductility", Research Fund for Coal and Steel, Luxembourg (2009).

[58] Simulia Corp., "Abaqus v.6.8 user manual", Dassault Systèmes, Providence, USA (2008).

[59] E.H.Mansfield, “Studies in collapse analysis of rigid-plastic plates with a square yield diagram”, Royal Aircraft Establishment, Farnborough (1956).

[60] K. M. Abdalla, W. F. Chen, “Expanded Database of Semi-Rigid Steel Connections”, Computers and Structures, 56:553-564 (1995).

[61] W. F. Chen et Al., “Semi-rigid connections in Steel Frames”, McGraw-Hill Inc., USA (1992).

[62] K. M. Ang, G. A. Morris, “Analysis of three-dimensional frames with flexible beam-column connections”, Gun. J. civil Engrs 11 (1984).

[63] C. Faella, V. Piluso, G. Rizzano, “Structural steel semi-rigid connection: theory, design and software”, CRC Press (1999).

LIST OF FIGURES

LIST OF TABLES